PERFORMANCE ANALYSIS OF MULTIANTENNA AND COOPERATIVE COGNITIVE RADIO UNDER SPATIAL CORRELATION

A

Thesis submitted

in partial fulfillment of the requirements

for the degree of

DOCTOR OF PHILOSOPHY

By

Sikandar Kumar

DEPARTMENT OF ELECTRONICS AND ELECTRICAL ENGINEERING

INDIAN INSTITUTE OF TECHNOLOGY GUWAHATI

GUWAHATI - 781 039, ASSAM, INDIA

May, 2017

Certificate

This is to certify that the thesis entitled "**Performance Analysis of Multiantenna and Cooperative Cognitive Radio Under Spatial Correlation**", submitted by **Sikandar Kumar** (11610216), a research scholar in the *Department of Electronics and Electrical Engineering, Indian Institute of Technology Guwahati*, for the award of the degree of **Doctor of Philosophy**, is a record of an original research work carried out by him under my supervision and guidance. The thesis fulfills all requirements as per the regulations of the institute and in my opinion it meets the standard needed for submission. The results embodied in this thesis have not been submitted to any other University or Institute for the award of any degree or diploma.

Dated:

Guwahati.

Dr. Sonali Chouhan
Assistant Professor
Department of Electronics and Electrical Engineering
Indian Institute of Technology Guwahati
Guwahati - 781 039, Assam, India.

This work is dedicated to

MY PARENTS,

BROTHER

AND

SISTER-IN-LAW

for their love and encouragement

Acknowledgements

Many people have helped me during the course of my research and stay at IIT Guwahati. First of all, I would like to express my profound gratitude to my supervisor Dr. Sonali Chouhan for her continuous guidance and encouragement during this work. I would particularly like to thank her for her continuous effort and suggestions in improving the quality of all my manuscripts. Thank you madam for your deep concern in me and my works.

I wish to thank my doctoral committee members Prof. Rohit Sinha, Prof. Prabin Kumar Bora, and Dr. Tony Jacob for sparing their precious time to evaluate the progress of my work. My heartfelt thanks goes to you for your valuable feedbacks and suggestions. I would also like to thank Dr. Gaurav Trivedi, Dr. Samarajit Das, and Dr. Brijesh Kumar Rai for their friendly discussions on various issues during my stay at IIT Guwahati.

I would like to thank many of my seniors and colleagues, including but not limited to Samdarshi Khare, Brijesh Kumbhani, Rajib Jana, Atul Kumar, Ramesh Chandra Mishra, Santosh Kumar Yadav, Abhishek R Vahadane, Ankit Dalal, Saroj Mondal, Sandeep P, Kukil Khanikar, Saptarshi Pyne, Shivanshu Shrivastava, and Brajesh Rawat for their help and support in every possible aspects.

I would also like to thank MHRD, Government of India, for its financial support during the course of study. I would like to thank IIT Guwahati and Department of EEE for providing me the peaceful environment and resources to complete my works. I would also like to thank all staff members of IIT Guwahati who directly or indirectly helped me in my stay here.

Finally, my deepest gratitude goes to my family. The encouragement, love, and care from my parents, elder brother, and sister-in-law are always a powerful source of inspiration and energy for me.

Sikandar Kumar

Abstract

In cognitive radio, the transmitter behavior adapts according to the information about the surroundings in which it operates, thereby enhancing the spectrum utilization. Based on the available information, the spectrum-monitor decides the transmission strategies for the cognitive/secondary users (SUs)—whether to interweave, underlay, or overlay the SU signal. To improve the performance of the system multiantenna and cooperation strategies are introduced. Due to the size limitations of the devices the antennas separations may become very small which causes spatial correlation among signals. In this thesis, the performance of interweave- and underlay-paradigm based cognitive radio networks (CRNs) is analyzed under spatially correlated channels or noise. Firstly, an interweave paradigm based CRN is considered with multiantenna at SU receiver (SR) under spatially correlated noise. By exploiting the known spatial correlation information, two detectors—weighted cross-correlation absolute value detector and weighted energy detector—are proposed. The analytical expressions for decision threshold, probability of detection and false-alarm are derived. Secondly, an underlay paradigm based CRN is considered where interfering channels from secondary transmitter (ST) to licensed/primary receiver (PR) are spatially correlated. The performance of the system is analyzed with prewhitened interfering signals using outdated channel information at ST. The analytical expressions for the outage probability and the channel capacity are derived. Thirdly, the performance of a dual-hop relay-assisted cooperative underlay CRN is analyzed considering composite fading and shadowing channel model. In this scenario, the analysis is performed for single antenna users at both primary- and secondary-side. Further, this work is extended for multiantenna SR with spatially correlated channels. The analytical expressions for the out-

age probability and the ergodic capacity are derived for both the cases. All analytical results reported in this thesis are validated by Monte-Carlo simulations.

Contents

List of Figures xv

List of Tables xix

List of Acronyms xxi

List of Symbols xxv

List of Publications xxix

1 Introduction 1

1.1 Spectrum Sensing . . . 3

1.2 Multi-dimensional CRN . . . 6

1.3 Correlation in Multi-dimensional CRN . . . 8

1.4 Literature Survey . . . 9

1.4.1 Interweave Paradigm based CRN . . . 9

1.4.2 Underlay Paradigm based CRN . . . 11

1.5 Problem Formulation . . . 13

1.6 Thesis Contributions . . . 14

1.7 Thesis Organization . . . 15

2 Spectrum Sensing for Multiantenna Cognitive Radio Exploiting Spatial Correlation of Noise 17

2.1 System Model . . . 18

2.2 Neyman-Pearson Theorem . . . 20

2.3 Proposed Spectrum Sensing Schemes . . . 21

2.3.1 Weighted Cross-correlation Absolute Value Detector . . . 23

2.3.2 Weighted Energy Detector . . . 24

2.4 Performance Analysis of Proposed Detectors . . . 25
2.4.1 Weighted Cross-correlation Absolute Value Detector . . . 25
2.4.2 Weighted Energy Detector . . . 29
2.5 Computational Complexity . . . 31
2.6 Results and Discussion . . . 31
2.6.1 Statistical Distribution . . . 32
2.6.2 Effect of Noise Correlation . . . 34
2.6.3 Effect of Number of Received Samples . . . 34
2.6.4 Comparison between Proposed WCCAVD and WED . . . 38
2.7 Applicability in Multi-dimensional CR Systems . . . 39
2.8 Summary . . . 39

3 Performance Analysis of Multiantenna Underlay Cognitive Radio under Spatially Correlated Interfering Signals 41

3.1 System Model . . . 43
3.2 Channel Capacity . . . 46
3.3 Outage Probability . . . 47
3.3.1 Outage Probability of PU System . . . 48
3.3.2 Outage Probability of SU System . . . 49
3.4 Results and Discussion . . . 50
3.5 Summary . . . 52

4 Performance Analysis of Dual-Hop Cognitive Cooperative Relay Networks over κ-μ Shadowed Channels 57

4.1 System Model . . . 59
4.1.1 Power Allocation and End-to-End SNR . . . 60
4.1.2 Channel Model . . . 61
4.2 Outage Probability . . . 62
4.3 Ergodic Capacity . . . 65
4.4 Results and Discussion . . . 69

4.5 Summary . . . 76

5 Performance Analysis of SIMO-based Cognitive Cooperative Relay Networks over Spatially Correlated κ-μ Shadowed Channels 77

5.1 System Model . . . 78

5.2 Channel Model . . . 79

5.3 Analysis of SIMO Underlay CRN . . . 80

5.3.1 Outage Probability . . . 81

5.3.2 Ergodic Capacity . . . 82

5.3.3 Results and Discussion . . . 84

5.4 Analysis of Dual-hop DF Relay-assisted Underlay CRN . . . 88

5.4.1 Outage Probability . . . 89

5.4.2 Ergodic Capacity . . . 90

5.4.3 Results and Discussion . . . 92

5.5 Summary . . . 96

6 Conclusions and Future Work 99

6.1 Research Contributions . . . 100

6.2 Future Directions of Research . . . 101

A Appendix 103

A.1 Calculation of Mean and Variance of g_{ij} . . . 104

A.2 Calculation of Mean and Variance of Real and Imaginary Parts of g_{ij} for $i \neq j$ . . . 106

A.3 Calculation of Eq. (2.29) . . . 108

A.4 Calculation of Power Margin Factor κ_m . . . 110

A.5 Proof of Lemma 1 . . . 112

A.6 Conditions for Interchangeability of Summation and Integration . . . 115

A.7 Derivation of Eq. (5.27) . . . 116

References 119

List of Figures

2.1 PDFs of binary hypothesis testing problem and decision regions. 21

2.2 CDF plots of the proposed (a) WCCAVD and (b) WED under both hypotheses $\mathcal{H}_0$ and $\mathcal{H}_1$, when $M = 2$, $N = 100, 200$, $P_{FA} = 0.01$, $\gamma = -15$ dB, and $\rho = 0.5$. . 33

2.3 Average detection probability comparison of various forms of (a) CCAVD and (b) ED with respect to the average SNR per antenna for different values of ρ, when $M = 2$, $N = 200$, and $P_{FA} = 0.01$. 35

2.4 Average detection probability comparison of (a) WCCAVD and (b) WED with corresponding detectors obtained after the matrix-inverse based prewhitening with respect to γ for various values of N, when $M = 2$, $P_{FA} = 0.01$, and $\rho = 0.95$. 36

2.5 The complementary ROC curves of the proposed WCCAVD and WED for (a) $\rho =$ 0.9 (b) $\rho =$ 0.5, when $M = 2,\ 4$, $N = 200$, and $\gamma = -10$ dB. 37

2.6 Decision threshold vs P_{FA} plots of the proposed WCCAVD and WED for various values of ρ, when $M = 2$, $N = 200$, and $\gamma = -10$ dB. 38

3.1 A typical diagram of an underlay paradigm based CRN with multiantenna at all nodes. 43

3.2 CDF plots for SU system with varying λ when $M = 2$ and 4. The magnified plots for $\lambda \leq 20$ are shown as the inset. 50

3.3 (a) Ergodic capacities and (b) average outage probabilities of the PU and SU systems versus P_M for various ρ_0, when $\eta_{SP} = -5$ dB and $\varepsilon_o = 1\%$. 53

3.4 (a) Ergodic capacities and (b) average outage probabilities of the PU and SU systems versus ρ_0 for various values of ε_o, when $\eta_{SP} = -5$ dB and $P_M = 8$ dBm. 54

3.5 (a) Ergodic capacities and (b) average outage probabilities of the SU system versus ρ_0 for various values of η_{SP} and ε_o when $P_M = 8$ dBm. 55

4.1 A typical diagram of a dual-hop relay-assisted underlay CRN with single antenna at all nodes. 59

4.2 Outage probability vs Q/N_0 plots when channels at all links are identically distributed and the outage threshold γ_{th} = –5 dB. (Solid lines: Analytical and Markers: Simulated). 71

4.3 Ergodic capacity vs Q/N_0 plots when channels at all links are identically distributed. (Solid lines: Analytical and Markers: Simulated). 71

4.4 Outage probability vs Q/N_0 plots when the channels at ST→relay and relay→SR links are Nakagami-m distributed (Special case I), and $\gamma_{th} = -5$ dB. (Solid lines: Analytical and Markers: Simulated). 73

4.5 Ergodic capacity vs Q/N_0 plots when the channels at ST→relay and relay→SR links are Nakagami-m distributed (Special case I). (Solid lines: Analytical and Markers: Simulated). 73

4.6 Outage probability vs Q/N_0 plots when the channels at ST→relay and relay→SR links are Rician shadowed distributed (Special case II), and $\gamma_{th} = -5$ dB. (Solid lines: Analytical and Markers: Simulated). 74

4.7 Ergodic capacity vs Q/N_0 plots when the channels at ST→relay and relay→SR links are Rician shadowed distributed (Special case II). (Solid lines: Analytical and Markers: Simulated). 74

4.8 Outage probability vs Q/N_0 plots for non-identical μ parameter, and $\gamma_{th} = -5$ dB. (Solid lines: Analytical and Markers: Simulated). 75

4.9 Ergodic capacity vs Q/N_0 plots for non-identical μ parameter. (Solid lines: Analytical and Markers: Simulated). 75

5.1 A typical diagram of a dual-hop relay-assisted underlay CRN with multiantenna at SR. 79

5.2 A typical diagram of a SIMO underlay CRN with multiantenna at SR. 80

5.3 (a) Outage probability and (b) ergodic capacity vs Q/N_0 plots for different ρ when M=2, (κ_{1i},μ_{1i},m_1)=(2.5,1.1,1), $i \in [1,2]$; (κ_2,μ_2,m_2)=(1.5,3,2); and $\bar{\gamma}_1 = \bar{\gamma}_2 = 1$. 85

5.4 (a) Outage probability and (b) ergodic capacity vs Q/N_0 plots when M=2 and 4, ρ=0.5, (κ_{1i},μ_{1i},m_1)=(2.5,1.1,1), $i = 1, .., M$; (κ_2,μ_2,m_2)=(1.5,3,2); and $\bar{\gamma}_1 = \bar{\gamma}_2 = 1$. 86

5.5 (a) Outage probability and (b) ergodic capacity vs Q/N_0 plots when ST→SR links are κ-μ shadowed distributed and ST→PR link is having various fading/shadowing severities with $M = 2$, $\bar{\gamma}_1 = \bar{\gamma}_2 = 1$, and $\rho = 0.5$. (Markers: Simulated and Lines: Analytical). 87

5.6 (a) Outage probability and (b) ergodic capacity vs Q/N_0 plots for different ρ when M=2, (κ_1,μ_1,m_1)=(2.5,1.1,1), (κ_{2i},μ_{2i},m_2)= (2.5,1.1,1), $i \in [1,2]$; (κ_I,μ_I,m_I)= (1.5,3,2), $I \in [3,4]$; and $\bar{\gamma}_1 = \bar{\gamma}_2 = \bar{\gamma}_3 = \bar{\gamma}_4 = 1$. 93

5.7 (a) Outage probability and (b) ergodic capacity vs Q/N_0 plots for different M when ρ=0.5, (κ_1,μ_1,m_1)=(2.5,1.1,1), (κ_{2i},μ_{2i},m_2)= (2.5,1.1,1), $i = 1, .., M$; (κ_I,μ_I,m_I)= (1.5,3,2), $I \in [3,4]$; and $\bar{\gamma}_1 = \bar{\gamma}_2 = \bar{\gamma}_3 = \bar{\gamma}_4 = 1$. 94

5.8 (a) Outage probability and (b) ergodic capacity vs Q/N_0 plots when channels at ST→relay and relay→SR links are κ-μ shadowed distributed and interfering channels at ST→PR and relay→PR links are having various fading/shadowing severities with $M = 2$, $\bar{\gamma}_1 = \bar{\gamma}_2 = \bar{\gamma}_3 = \bar{\gamma}_4 = 1$, and $\rho = 0.5$. 95

List of Tables

4.1 Classical fading distributions obtained from the κ-μ shadowed distribution . . . 70

List of Acronyms

AF	Amplify-and-Forward
AGM	Arithmetic-to-Geometric Mean
AOP	Average Outage Probability
AOP-PU	Average Outage Probability - Primary User
AOP-SU	Average Outage Probability - Secondary User
AWGN	Additive White Gaussian Noise
CAV	Covariance Absolute Value
CCAVD	Cross-correlation Absolute Value Detector
CDF	Cumulative Distribution Function
CFAR	Constant False-alarm Rate
CP	Cyclic Prefix
CR	Cognitive Radio
CRN	Cognitive Radio Network
CSCG	Circular Symmetric Complex Gaussian
CV	Coefficient of Variation
dB	Decibel
D2D	Device-to-Device
DF	Decode-and-Forward
DOF	Degree of Freedom
ED	Energy Detector
EME	Energy with Minimum Eigenvalue
EVD	Eigenvalue Decomposition

FCC	Federal Communications Commission
GLRT	Generalized Likelihood Ratio Test
GSC	Generalized Selection Combining
iid	Independent and Identically Distributed
LLR	Log-likelihood Ratio
LOS	Line-of-Sight
MA	Moving Average
MATLAB	Matrix Laboratory
MIMO	Multi-input Multi-output
MME	Maximum-to-Minimum Eigenvalue
MP	Marchenko-Pastur
MRC	Maximal Ratio Combining
MTPC	Maximum Transmission Power Constraint
NP	Neyman-Pearson
OFDM	Orthogonal Frequency Division Multiplexing
PDF	Probability Density Function
PIPC	Peak Interference Power Constraint
PT	Primary User Transmitter
PR	Primary User Receiver
PU	Primary User
QOS	Quality of Service
ROC	Receiver Operating Characteristic
RV	Random Variable
SC	Selection Combining
SCN	Standard Condition Number
SIMO	Single-input Multi-output
SINR	Signal-to-Interference-Plus-Noise Ratio
SNR	Signal-to-Noise Ratio

ST	Secondary User Transmitter
SR	Secondary User Receiver
SU	Secondary User
TAS	Transmit Antenna Selection
WCCAVD	Weighted Cross-correlation Absolute Value Detector
WED	Weighted Energy Detector

List of Symbols

P_{FA}	Probability of false-alarm
P_D	Probability of detection
P_{MD}	Probability of miss-detection
$a \rightarrow b$	From a to b
Boldface Lower-case Letters	Vectors
Boldface Upper-case Letters	Matrices
$\mathcal{H}_0$	Null hypothesis
$\mathcal{H}_1$	Alternate hypothesis
$a \times b$	Dimension of a matrix or a vector
$(\cdot)^T$	Transpose
$(\cdot)^*$	Complex conjugate
$(\cdot)^H$	Conjugate transpose
$\lvert \cdot \rvert$	Absolute value or modulus
$\forall$	For all
$\in$	Set membership
$\delta_{ij} = \begin{cases} 1, & i = j \\ 0, & \text{Otherwise} \end{cases}$	Kronecker delta function
$\text{tr}(\cdot)$	Trace
$\det(\cdot)$	Determinant
$\text{E}[\cdot]$	Expectation
$\text{var}[\cdot]$	Variance

$\text{cov}[\cdot]$	Covariance
$\|\cdot\|$	Euclidean norm
$\Re(\cdot)$	Real-part
$\Im(\cdot)$	Imaginary-part
$\sum_{i=1}^{n}$	Summation
$\prod_{i=1}^{n}$	Product
$exp(\cdot)$	Exponential
$erf(x) = \frac{2}{\sqrt{\pi}} \int_0^x \exp(-t^2)dt$	Error function
$\Pr(\cdot)$	Probability
$Q(x) = \frac{1}{\sqrt{2\pi}} \int_x^\infty \exp\left(-\frac{t^2}{2}\right)dt$	Q-function
$\Gamma(\cdot)$	Gamma function
$\gamma(a,x) = \int_0^x t^{a-1}\exp(-t)dt$	Lower incomplete gamma function
$O(\cdot)$	Order
$\otimes$	Kronecker product
$\mathcal{N}(m,\sigma^2)$	Gaussian with mean m and variance σ^2
$\mathcal{CN}(m,\sigma^2)$	Complex Gaussian with mean m and variance σ^2
$\mathcal{FN}(m,\sigma^2)$	Folded Gaussian with mean m and variance σ^2
$(\cdot)^{-1}$	Inverse
$\mathbf{I}_M$	Identity matrix of dimension $M \times M$
$\log_{10}(\cdot)$	Logarithm with base 10
$\ln(\cdot)$	Natural log
$\max\{\cdot,...,\cdot\}$	Maximum
$\min\{\cdot,...,\cdot\}$	Minimum
$f_X(x)$	PDF of X
$F_X(x)$	CDF of X
$P_O(\cdot)$	Outage probability
C_{er}	Ergodic capacity

$\eta - \mu$	Eta-Mu fading channel
$\kappa - \mu$ Shadowed	Kappa-Mu Shadowed channel
${}_1F_1(\cdot;\cdot;\cdot)$	Kummer confluent hypergeometric function
${}_2F_1(\cdot,\cdot;\cdot;\cdot)$	Gauss hypergeometric function
$F_1(\cdot,\cdot,\cdot;\cdot;\cdot,\cdot)$	Type-1 Appell hypergeometric function
$F_2(\cdot,\cdot,\cdot;\cdot,\cdot;\cdot,\cdot)$	Type-2 Appell hypergeometric function
$(\cdot)_k$	Pochhammer symbol

List of Publications

Journal Publications

1. S. Kumar and S. Chouhan, "Performance analysis of MIMO spectrum-sharing networks with pre-whitened interfering signals under outdated channel information," *IEEE Wireless Communications Letters*, vol. 5, no. 2, pp. 156 - 159, April 2016.

2. S. Kumar and S. Chouhan, "Performance analysis of cognitive decode-and-forward dual-hop relay networks over $\kappa - \mu$ shadowed channels," *AEÜ International Journal of Electronics and Communications*, vol. 70, no. 9, pp. 1241 - 1248, Sep. 2016.

3. S. Kumar and S. Chouhan, "Performance analysis of SIMO spectrum sharing networks over correlated $\kappa - \mu$ shadowed fading relying on MRC reception," Under Review.

Conference Publications

1. S. Kumar and S. Chouhan, "Spectrum sensing in MIMO cognitive radio with temporally and spatially correlated signal," *IEEE 11th International Symposium on Wireless Communications Systems (ISWCS)*, 26-29 Aug. 2014, Barcelona, Spain, pp. 664 - 669.

2. S. Kumar and S. Chouhan, "Outage probability analysis of cognitive decode-and-forward relay networks over $\kappa - \mu$ shadowed channels," *IEEE 21st Asia-Pacific Conference on Communications (APCC)*, 14-16 Oct. 2015, Kyoto, Japan, pp. 433 - 437.

1

Introduction

Contents

1.1 Spectrum Sensing 3
1.2 Multi-dimensional CRN 6
1.3 Correlation in Multi-dimensional CRN 8
1.4 Literature Survey 9
1.5 Problem Formulation 13
1.6 Thesis Contributions 14
1.7 Thesis Organization 15

The demand for radio spectrum is increasing day-by-day to fulfill the need for spectrum for high data-rate services in next-generation wireless communications systems. The radio spectrum is a limited natural resource like petroleum and mines. According to the conventional spectrum allocation policies, the spectrum bands are allocated to the standard wireless communication systems such that only incumbent/licensed/primary users (PUs) can access the spectrum—causes inefficient utilization of the radio spectrums. Various spectrum occupancy measurements [1–4] indicate that most of the allotted spectrums are under-utilized or partially-utilized. Thus, the real problem is not the spectrum scarcity but the fixed spectrum allocation policy and the limited coordination among networks. In this context, the concept of the cognitive radio network (CRN) has been proposed by J. Mitola III [5, 6]. The CRN has the capability to increase the spectrum utilization, thus can overcome the problem of apparent spectrum scarcity. Latter, various aspects of CRN have been elaborated by S. Haykin [7]. The cognitive radio (CR) is a radio technology that can access the licensed spectrum based on the information about the surroundings in which it operates. Based on the available information about the surroundings, the spectrum-monitor decides the transmission strategies for the cognitive/secondary users (SUs). According to the transmission strategy, the CRNs are broadly categorized into three paradigms [8]—interweave, underlay, and overlay. These three transmission paradigms of CRNs are briefly discussed as follows.

(a) ***Interweave***: In CRN based on this paradigm, the SUs can opportunistically access the PUs spectrums using the spectrum vacancies in time, frequency, and space dimensions. Other than these three common dimensions, polarization [9, 10] and angular dimensions are also exploited. Thus, in interweave paradigm based CRN, the spectrum-monitor needs the information about the presence or absence of the PUs in the spectrum. The detection about the presence or absence of PUs in the spectrum is known as spectrum sensing [11]. Various signal processing techniques have been investigated for spectrum sensing which is discussed in Section 1.1. Moreover, as it uses the available vacancies in spectrum, there is no constraint on the transmission power of SUs. However, the performance of SU system is limited by the range of available spectrum vacancies. Also, the SUs have to immediately vacate the spectrum

whenever PUs reappear, to avoid any harmful interference.

(b) ***Underlay***: In underlay paradigm based CRN, both PUs and SUs can simultaneously transmit using the same spectrum band such that the interference induced at the PUs by the SUs is within a certain tolerance limit [12]. This interference limit is also known as interference temperature, as defined by FCC in [13]. Thus, in this paradigm, the transmission power of the SU is constrained to avoid any harmful interference to the PUs. For the realization of underlay paradigm based CRN, the SU nodes require the information of the channels at links between PU nodes and them so that the interference constraint of PUs can be maintained.

(c) ***Overlay***: In this paradigm based CRN, both PUs and SUs can simultaneously transmit relying on interference mitigation and cancellation techniques. Both PU and SU nodes can overhear each-other's message and can mitigate/cancel-out them using advanced signal processing and coding schemes, e.g., dirty paper coding [14], Gel'fand-Pinsker binning [15], etc. The SUs can transmit at any power, and the interference induced at the PUs can be offset by relaying the PU signals by the SU nodes [8]. In this paradigm, the SU nodes require the knowledge of PU channel gains, code books, and may be the PU message signals. Practically, this paradigm demands high level of cooperation and collaboration between primary and secondary networks.

Other than these three distinct CR paradigms, it can also be combined to form a hybrid paradigm based CRN, thereby further enhancing the overall spectrum utilization [16–18]. In this thesis, the works are carried-out under interweave- and underlay-paradigm based CRNs. Furthermore, in interweave paradigm based CRN, the spectrum sensing is an important phenomenon. A brief background of the spectrum sensing schemes is given below.

1.1 Spectrum Sensing

In interweave paradigm based CRN, the spectrum-monitor needs to detect the presence or absence of PU in the spectrum. When it detects the absence of PU, it allows the SUs to access the spectrum. The SUs have to leave the spectrum or switch to the other vacant spectrum immediately whenever the PU needs it. Hence, the spectrum-monitor has to sense the spectrum repeatedly, with an interval, to avoid any possible interference with the PU. For

this reason, a fast and accurate spectrum sensing is highly desirable. Various spectrum sensing schemes have been investigated each has its own advantages and disadvantages [11, 19]. The classical spectrum sensing techniques are described in brief as follows.

(a) ***Energy Detection***: In this spectrum sensing scheme, the energy of the received signals at SU receiver (SR) is evaluated and is compared with a threshold to detect the presence of PU signal in the spectrum [20, 21]. This threshold is predetermined using known noise variance and probability of false-alarm (P_{FA}) constraint of the CRN. The energy detector (ED) has an optimal performance in the presence of known noise variance and is easy to implement. ED does not require any information about PU signal and channel gains. On the other hand, its performance is highly susceptible to noise variance uncertainty [22]. ED is also unable to distinguish PU signal, SU signal, interference, and noise.

(b) ***Matched-filter based Detection***: In matched-filter based sensing scheme, the received signal is convolved with PU signal to find the correlation [23]. Thus, the SU needs the knowledge of PU signal to detect its presence in the spectrum. In addition, it also needs perfect synchronization between transmitted and known PU signals for optimal performance. Thus, this spectrum sensing scheme is practically not viable in the context of cognitive radio as both PUs and SUs are controlled by different network administrators—thereby perfect synchronization is difficult to attain.

(c) ***Cyclostationary Feature based Sensing***: In cyclostationary feature based sensing scheme, the periodicity property of the modulated PU signal is used for the detection of PU in the spectrum [24]. Usually, the modulated signal accompanied with carrier sine waves, pulse trains, and cyclic prefix (CP) (in orthogonal frequency division multiplexing (OFDM) signal), causes periodicity of the transmitted signals [25]. This feature of the PU signal can be used for the detection as well as for distinguishing multiple PUs in the spectrum. This detection scheme is also capable of differentiating PU signal, SU signal, interference, and noise. It is robust to the noise variance uncertainty in contrast to ED. However, the complexity associated with cyclostationarity based sensing scheme is high as it requires a large number of samples to exploit cyclostationarity of the received signals. It is susceptible to the cyclic frequency offset

caused by the clock mismatch [26]. This detection scheme also requires a prior knowledge of the features of the PU signal.

(d) ***Autocorrelation based Sensing***: Autocorrelation based sensing exploits the autocorrelation of PU signal to detect its presence in the spectrum. Specifically, if the PU signal is present, the autocorrelation of received signal differs from the autocorrelation of noise. This detection scheme does not need the information of PU signal and channel gains. In [27], the autocorrelation based sensing scheme has been proposed for OFDM PU signal. In this detection scheme, the autocorrelation of CP present in OFDM signal is used to detect the presence of PU signals. In [28, 29], the autocorrelation based sensing schemes have been proposed for OFDM PU signal which exploit the periodic repetition of the pilot subcarriers. These detection schemes outperform the CP-based detection scheme proposed in [27]. The autocorrelation based detection schemes are robust to the noise variance uncertainty.

(e) ***Covariance based Detection***: The difference between statistical covariances of the received signals and the noise is exploited for the detection of PU signal in the spectrum. In [30], covariance absolute value (CAV) based detection and generalized covariance based detection schemes have been proposed. A weighted covariance based detection scheme has been proposed in [31] which performs better than the CAV based scheme. These detection schemes rely on the sample covariance matrix of the received signals at SR and do not require any prior information about the PU signal, channel gains, and noise variance.

(f) ***Eigenvalue based Detection***: The properties of eigenvalues of the sample covariance matrix of the signals received at SR are exploited for the detection of PU signal in the spectrum [32, 33]. These detection schemes utilize the inherent signal structure in covariance matrix of the received signals. Some of the eigenvalue based detection schemes perform better than ED especially in the presence of noise covariance uncertainty. Under this detection scheme, some of the classical methods are largest eigenvalue based detection, scaled largest eigenvalue based detection, maximum-to-minimum eigenvalue (MME) based detection, arithmetic-mean to geometric-mean (AGM) of eigenvalues based detection, and energy with minimum eigenvalue (EME) based detection, etc. These detection schemes do not require the knowledge of PU signal

and channel gains.

Furthermore, the performance of both interweave and underlay paradigms based CRNs are severely affected due to multipath fading and shadowing. The effect of shadowing can be overcome by applying cooperation among users [34, 35]. To cope with the effect of multipath fading, various diversity enhancing strategies are explored in CRNs, e.g., multiantenna [36, 37], cooperation, and oversampling [32, 38–40]. These networks may be called as multi-dimensional CRNs, and are briefly discussed in the following section.

1.2 Multi-dimensional CRN

To improve the performance of the system, multiantenna users, cooperation among various users, and oversampling of the received signals are considered in literature. In these scenarios, the received signals are usually represented in the form of a matrix. The spatial and the temporal dimensions of multi-dimensional CRN are represented by the rows and the columns, respectively. Various multi-dimensional CRNs and their benefits are discussed below.

(a) ***Multiantenna based CRN***: Multiantenna users are considered in CRN to exploit the available spatial diversity, thereby enhancing the performance of the system. Various advantages of multiantenna systems are given as follows.

- The capacity of the system is increased without any expansion in the system bandwidth.
- The co-channel interference can be suppressed effectively for the multiuser system.
- The transmission reliability can be improved using space-time coding.
- Improved performance can be obtained in deep fading condition.

(b) ***Cooperation based CRN***: Cooperation strategy is implemented to exploit the spatial diversity, thereby improving the system performance under deep fading and shadowing conditions. The cooperative CRNs are broadly categorized into centralized, distributed, and relay-assisted cooperative CRNs [41, 42]. In centralized cooperative CRN, a number of SU nodes in cooperation transmit its information to a fusion-center. The fusion-center takes the final decision based on the information from several SU nodes. This decision is broadcasted to all SUs. In distributed cooperative CRN, the SU nodes in cooperation share their informa-

tion through hand-shaking and make their own decisions. Distributed cooperative approach is more advantageous than the centralized cooperative approach since the former does not require any backbone infrastructure for making final decisions. In relay-assisted cooperative CRN, the relay nodes are used between SU transmitter (ST) and SR. The benefit of the relay-assisted cooperative networks lies in the fact that a number of relay nodes in cooperation form a virtual multi-input multi-output (MIMO) system to take advantage of the available spatial diversity. Various advantages of the cooperative systems are as follows.

- The performance of the system can be improved by forming cooperative groups under deep fading and shadowing conditions.
- High data-rate coverage of the network can be increased.
- Transmissions reliability can be improved, thereby improving the quality-of-service (QOS) of the system.
- The capacity of the network can be increased.

(c) ***Oversampling based CRN***: The signals received at SR can be sampled at the rate higher than the Nyquist-rate. This phenomenon is known as oversampling. It increases the efficiency of the system under fading channel condition. The oversampled samples at SR can be considered as a virtual multiple output with supposedly independent fading effects, thus introduces diversity to the system [43]. In addition, the oversampling operation increases the resolution of analog-to-digital and digital-to-analog conversions. It also assists in avoiding aliasing and phase-distortion by relaxing the design parameters of the anti-aliasing filter at the receiver. Moreover, the effect of noise can also be reduced using multiple copies of the same sample with uncorrelated noise added to each copy of a sample.

Furthermore, the spatial/row dimension of the received signal matrix may represent either the multiple antennas of a multiantenna user, cooperative users of a cooperation based CRN, or multiple copies of the same sample of an oversampling based CRN. The temporal/column dimension of the received signal matrix may contain either the signals received at different antennas of a multiantenna user, at different cooperating users in a cooperation based CRN, or at a single antenna of an oversampling based CRN. Due to the different reasons, correlation

among signals may exist at both spatial and temporal dimensions of the receive signal matrix, which are elaborated in the following section.

1.3 Correlation in Multi-dimensional CRN

In multi-dimensional CRNs, which may use multiantenna, cooperation, or oversampling, correlation may exist in spatial and/or temporal dimensions of the received signal matrix. In the following paragraphs, the reasons of correlations in both spatial and temporal dimensions are discussed.

(a) ***Spatial Correlation***: The channels as well as the noise may be spatially correlated at multiantenna SR. The channels at SR can be spatially correlated due to multipath fading, poor scattering, and/or antenna mutual coupling [39, 40, 42, 44]. Due to multipath fading and poor scattering, the channels at different antennas have small angular spread, which causes spatial correlation among them. The noise at multiantenna SR may also be spatially correlated because of antenna mutual coupling [45]. Basically, in multiantenna systems, when an electromagnetic signal impinges on an antenna element, it induces an electromagnetic field. The antenna elements lying within this electromagnetic field may be coupled due to small separation among them. This phenomenon is known as antenna mutual coupling [44], and causes spatially correlated channels and noise in multiantenna CRN. Antenna mutual coupling may also exit at transmitter side, thereby causing spatially correlated source signals [46, 47]. In cooperative CRN, the channels and the noise may be spatially correlated due to collocated users in the network [42]. In oversampling based CRN, the channels and the noise may be spatially correlated due to oversampling operation [40, 42].

(b) ***Temporal Correlation***: The channels as well as the noise may get temporally correlated due to filtering and oversampling operations [39, 40, 42, 48]. The signals received at SR are generally passed through a pulse shaping filter before further processing. In this process, the channels and the noise are affected by the autocorrelation function of the filter, which causes temporal correlation among samples at different time instances. The oversampling operation in temporal dimension may also cause temporal correlation in both the channels and the noise.

Moreover, the source signals of the primary system may also become temporally correlated due to pulse shaping filter at the PU transmitter (PT) [47].

1.4 Literature Survey

In this section, the overview of the existing literature is presented for both interweave- and underlay-paradigm based multi-dimensional CRNs.

1.4.1 Interweave Paradigm based CRN

Various spectrum sensing techniques have been investigated for multi-dimensional CRNs under spatially and temporally correlated signals. In [49,50], ED has been analyzed considering spatially correlated signals at multiantenna SR. Generalized likelihood ratio test (GLRT)-based spectrum sensing schemes have been proposed in [36, 37, 51–55] for multiantenna users based CRNs. The spectrum sensing algorithms obtained in [36,37,51,55] are based on the eigenvalues of the sample covariance matrix of the signals received at multiantenna SR, which exploit the correlation among signals received at different antennas of SR. In [52–54], the proposed spectrum sensing schemes are the different forms of eigenvalues obtained from GLRT. The difference between statistical covariance matrices of the received signal and the noise has been exploited to obtain the spectrum sensing schemes in [30, 31]. The spectrum sensing schemes have been derived in [56] using cross-correlation of the signals received at spatially correlated antennas of multiantenna SR. The spectrum sensing schemes have been proposed in [57] to detect the spatially and temporally correlated signals received at multiantenna SR. In [58], the spectrum sensing techniques have been investigated in the presence of spatial correlation at multiantenna SR and temporal correlation of source signal transmitted by PT. Moreover, the spectrum sensing schemes have also been studied considering cooperative CRNs [33,59–62] and oversampling based CRNs [32, 38]. The eigenvalue based sensing schemes proposed in [32,33,38,59–62] have exploited the correlation among signals received at different cooperative users and oversampled samples for cooperative CRN and oversampling based CRN, respectively. The spectrum sensing schemes discussed so far have been analyzed by considering a particular

multi-dimensional CRN scenario, however they can be analogously analyzed for other multi-dimensional CRN scenarios as well.

All the works mentioned above [30–33, 36–38, 49–62] have considered the spatially and temporally uncorrelated noise. A weighted ED has been proposed in [48] considering temporally correlated noise for single antenna users based CRN. The moving average (MA) of independent and identically distributed (iid) random variables (RVs) has been used to model the temporally correlated noise in [48]. However, the analysis of multi-dimensional CRN with MA or autoregressive model based spatially- or temporally-correlated noise is very complex. The performance of various classical eigenvalue based sensing schemes has been analyzed under spatially correlated noise in [39] for multi-dimensional CRN. Authors in [39] have shown that MME, EME, and Marchenko-Pastur (MP) bound based spectrum sensing schemes fail under spatially correlated noise. Further, the standard condition number (SCN)—defined as the ratio of maximum to minimum eigenvalues—based spectrum sensing scheme has been proposed. The drawback of this sensing scheme is that it does not allow to tune the threshold for a target probability of false-alarm (P_{FA}) or probability of miss (P_{MD}). Thus, this sensing scheme does not ensure the constant false-alarm rate (CFAR) property, and both P_{FA} and P_{MD} vary as decision threshold changes. Moreover, in [39, 48], the correlation information is assumed to be known at SR. In [48], the weight terms of the proposed weighted ED have been determined using correlation coefficient of the noise. The proposed weighted ED in [48] has outperformed the conventional ED. Further, SCN based sensing scheme proposed in [39] has not efficiently exploited the known correlation information. The performance of this detector has degraded rapidly for higher values of noise correlation coefficients. However, when correlation information is known to the receiver, it can decorrelate the received signals before applying any sensing scheme. In this context, the matrix-inverse based classical whitening scheme has been frequently used in literature [23]. The improved sensing schemes can be proposed by efficiently exploiting the known correlation information along with whitening of the correlated noise.

1.4.2 Underlay Paradigm based CRN

In underlay paradigm based CRN with multiantenna users, one of the preliminary works in [63] considered peak interference power constraint (PIPC) of PU receiver (PR). In [64], both PIPC of PR and maximum transmission power constraint (MTPC) of ST have been incorporated for multiantenna users based underlay CRN. Thus, in underlay paradigm based CRNs, the transmission power of ST is constrained by both primary and secondary networks. To implement PIPC of PR, ST needs the perfect knowledge of channel at link between PR and itself. This channel information can be feedbacked to the ST directly by the PR since some extent of cooperation and collaboration can be considered in underlay paradigm based CRN [65]. However, due to the feedback latencies and mobility of the users, channel information at ST may become outdated. The performance of underlay CRNs under outdated channel information has been analyzed in [66–69] with single antenna users, and with multiantenna users in [70]. All the works discussed so far have not considered any of the spatial/temporal correlations for any users. In [71], the spatial correlation has been considered with interfering channels at links between ST and PR for multiantenna users. Also, the prewhitening and postwhitening techniques have been analyzed to decorrelate the spatially correlated interfering signals at PR. It has been shown that using prewhitening scheme, the interference power at PR can be mitigated more efficiently than the postwhitening scheme. The prewhitening scheme considered in [71] is the classical matrix-inverse based whitening. Further, subspace based prewhitening scheme has been proposed in [72], which has similar performance as in [71] but with reduced complexity. In [71, 72], the channel information of the link between ST and PR is assumed to be perfectly known to the ST. The effect of outdated channel information on prewhitening of spatially correlated interfering channels can be analyzed for underlay CRN with multiantenna users.

Furthermore, another aspect of underlay CRN, the relay-assisted cooperative underlay CRNs, has been broadly investigated in literature. Both dual-hop and multi-hop relay-assisted underlay CRNs have been analyzed considerably. Here, our concern is in dual-hop relay-assisted underlay CRNs in the presence of both single and multiantenna users. Interested readers may

refer to [73] and recent references therein for multi-hop relay-assisted underlay CRNs. In dual-hop relay-assisted networks, the decode-and-forward (DF) and the amplify-and-forward (AF) protocols have been implemented at the relay nodes. In [74–76], the outage performance of a DF dual-hop CRN has been analyzed under PIPC of PR. The outage performance of a DF dual-hop CRN has also been investigated in [77–80] considering both PIPC of PR and MTPC of ST. In [81], both the outage probability and the ergodic capacity have been obtained for a DF dual-hop CRN under PIPC of PR and MTPC of ST. For an AF dual-hop CRN, a tight lower bound of outage probability has been derived in [82] under PIPC of PR and in [83] under both PIPC of PR and MTPC of ST. An exact outage probability has been obtained in [84] under PIPC of PR for an AF dual-hop CRN. A tight upper bound outage probability under PIPC of PR for an AF dual-hop CRN has been derived in [85] with and without direct-link between ST and SR. The selection combining (SC) has been used at SR to combine signals from ST and relay nodes. In [86], the approximate outage probability under PIPC of PR for an AF dual-hop CRN has been derived considering a direct-link between ST and SR. Both maximal ration combining (MRC) and SC have been analyzed to combine signals at SR in [86]. The multiuser diversity has been incorporated in [87] and the outage probability has been obtained for both the DF and the AF dual-hop CRNs under PIPC of PR.

All the works discussed so far for relay-assisted CRNs have considered the single antenna users. Further, multiantenna users have been introduced along with cooperative relay in underlay CRNs. In [88–91], the outage performance of the DF dual-hop CRNs has been analyzed considering transmit antenna selection (TAS) and MRC techniques under PIPC and MTPC. In [92], the outage probability for a DF dual-hop CRN has been determined for TAS/MRC and TAS/SC under PIPC and MTPC. The outage probability for a DF dual-hop CRN with TAS and generalized selection combining (GSC) has been investigated in [93] under PIPC and MTPC. Both outage probability and ergodic capacity for a DF dual-hop CRN have been derived in [94] considering TAS/GSC under PIPC and MTPC. The works discussed in [88–94] have not considered any spatial/temporal correlation of the signals. In [95, 96], the outage performance for DF dual-hop CRNs with multiantenna users has been analyzed in the presence

of spatially correlated channels under PIPC and MTPC.

All the works mentioned above for relay-assisted CRNs have been analyzed under Rayleigh and Nakagami-m distributed channel models. Very recently, in [97], the outage performance of an AF dual-hop CRN has been investigated considering η-μ fading channel under both PIPC and MTPC but with single antenna users. The Rayleigh, Nakagami-m, and η-μ distributions are used to model the small-scale fading scenario. Thus, the works discussed so far for relay-assisted CRNs have not incorporated the effect of large-scale shadowing to analyze the performance of the considered network. Recently, the κ-μ shadowed fading model is proposed in [98] which is a composite channel model for multipath fading and shadowing. It has been shown that this distribution is well fit into the land mobile satellite and the underwater acoustic channels data [98]. The κ-μ shadowed distribution unifies most of the classical fading models as its particular cases. Due to the versatility of the κ-μ shadowed distribution, researchers have started analyzing the performance of various systems under this channel model, e.g., [99–102]. The performance of ED for interweave paradigm based CRNs has been analyzed in [99, 100] under κ-μ shadowed channel model. In [101], the approximate outage probability and the channel capacity have been derived for the interference limited communication system in the presence of multiple co-channel interferers. The performance of MRC scheme has been analyzed considering correlated κ-μ shadowed channels in [102]. The analysis of dual-hop relay-assisted underlay CRNs under composite multipath fading and shadowing channel is an open research problem. In this thesis, we model the composite multipath fading and shadowing channel by the κ-μ shadowed distribution for the analysis of dual-hop relay-assisted underlay CRN.

1.5 Problem Formulation

Based on the literature review presented in the previous section, some of the potential research problems are recognized. In this thesis, the following problems are considered for analysis.

1. Derive spectrum sensing schemes by exploiting the spatial correlation information of noise at multiantenna SR for interweave paradigm based CRNs.

2. Performance analysis of underlay paradigm based CRN having multiantenna users with prewhitening of spatially correlated interfering signals using outdated channel information of link between ST and PR.

3. Performance analysis of underlay paradigm based CRN with dual-hop cooperative relay under κ-μ shadowed channels for (a) single antenna users and (b) multiantenna users with spatially correlated channels.

For the above stated problems, we stress in obtaining expressions for various performance measures of interweave- and underlay-paradigm based CRNs under spatial correlation.

1.6 Thesis Contributions

The important contributions of the thesis are stated below.

1. Two spectrum sensing schemes—Weighted Cross-correlation Absolute Value Detector (WCCAVD) and Weighted Energy Detector (WED)—are proposed under spatially correlated noise at multiantenna SR for interweave paradigm based CRNs.

(a) The knowledge of correlation information is exploited to derive improved spectrum sensing schemes.

(b) The analytical expressions for decision threshold, probability of false-alarm (P_{FA}), and probability of detection (P_D) are derived.

2. Performance of underlay paradigm based CRN having multiantenna users is analyzed for prewhitened interfering signals using outdated channel information of link between ST and PR.

(a) The analytical expressions for channel capacity and outage probability are derived for both primary and secondary systems.

(b) The effects of outdatedness in channel information and prespecified interference outage are analyzed on both primary and secondary systems performance.

3. Performance of a dual-hop DF relay-assisted underlay CRN with single antenna users is analyzed under κ-μ shadowed channels.

(a) The closed-form expressions for cumulative distribution function (CDF) of signal-

to-noise ratio (SNR) at relay and SR are derived. Using these expressions, the closed-form expression for outage probability is obtained.

(b) The analytical expression for ergodic capacity is determined.

4. Performance of a dual-hop DF relay-assisted underlay CRN with multiantenna at SR is analyzed under spatially correlated κ-μ shadowed channels. The analytical expressions for outage probability and ergodic capacity are derived.

1.7 Thesis Organization

There are six chapters in this thesis. Brief description of the content of each chapter is as follows.

Chapter 2 presents two proposed spectrum sensing schemes in the presence of spatially correlated noise at multiantenna SR for interweave paradigm based CRNs. The knowledge of correlation information is exploited to derive improved and practically implementable sensing schemes. The performance of the proposed schemes is compared with the classical matrix-inverse whitening based sensing schemes. The computational complexities involved with the proposed schemes are calculated and compared with the schemes obtained using matrix-inverse based whitening. We also derive the analytical expressions for decision threshold, P_{FA}, and P_D for the proposed sensing schemes. The analytical results are validated by the close matching of analytical plots with the corresponding simulation plots. The applicability of the proposed sensing schemes in centralized and distributed CRNs is also discussed.

In Chapter 3, we analyze the performance of underlay paradigm based CRN under prewhitened interfering signals using outdated channel information of the link between ST and PR. The effects of outdatedness in the channel information and prespecified interference outage probability on the performance of both primary and secondary systems are described. The analytical expressions for the channel capacity and the outage probability are derived for both primary and secondary systems, and are validated through Monte-Carlo simulations.

Chapter 4 presents the performance of a dual-hop DF relay-assisted underlay CRN with single antenna users under κ-μ shadowed channels. The closed-form expressions for the CDF

of received SNR at relay and SR are derived. Using this CDF expressions, the closed-form expression for outage probability is obtained for the considered system. The analytical expression for ergodic capacity is also determined. Two special cases are investigated when the links ST→relay and relay→SR are Nakagami-m and Rician/Rician-shadowed distributed. In both cases, the simpler forms of the outage probability and the ergodic capacity are obtained. The considered system is simulated for various fading and shadowing channel conditions. In each case, the analytical results are verified by the close matching of analytical plots with the corresponding simulation plots.

In Chapter 5, we analyze the performance of a dual-hop DF relay-assisted underlay CRN with multiantenna SR under spatially correlated κ-μ shadowed channels. The MRC scheme is used to combine the signals received at different antennas of SR. The analytical expressions for the outage probability and the ergodic capacity are derived and validated through its close matching with the simulation results.

Chapter 6 presents the conclusions of the thesis with a brief summary of the works presented. This chapter also includes some potential future research directions.

2

Spectrum Sensing for Multiantenna Cognitive Radio Exploiting Spatial Correlation of Noise

Contents

2.1 System Model 18
2.2 Neyman-Pearson Theorem 20
2.3 Proposed Spectrum Sensing Schemes 21
2.4 Performance Analysis of Proposed Detectors 25
2.5 Computational Complexity 31
2.6 Results and Discussion 31
2.7 Applicability in Multi-dimensional CR Systems 39
2.8 Summary 39

The spectrum sensing schemes for interweave CRN have been investigated in [39, 48] considering correlated noise at SR. Single antenna at all users has been considered in [48], and the noise at SR has been correlated in temporal dimension. For multi-dimensional CRN, the spectrum sensing scheme has been proposed in [39] where noise has been considered to be correlated in spatial dimension. The sensing schemes proposed in these works require the knowledge of correlation information. In the presence of correlation information, the correlated received signals at SR can be prewhitened before applying any sensing schemes. For prewhitening, the classical matrix-inverse based scheme has been frequently used in literature [23,103–105]. However, the improved sensing schemes can be obtained by efficiently exploiting the knowledge of correlation information.

In this chapter, we propose two spectrum sensing schemes by exploiting the knowledge of spatial correlation among noise for multiantenna CRN. The decision statistics for sensing is first derived using Neyman-Pearson (NP) theorem. Based on this decision statistics, two simplified and practically implementable detectors are proposed. The performance of the proposed detectors are compared with the corresponding detectors obtained after the classical matrix-inverse based prewhitening. For performance analysis, we derive the analytical expressions for the decision threshold, the P_{FA}, and the P_D. The exactness of the analytical results are validated by Monte-Carlo simulations. The proposed schemes ensure the constant false-alarm rate (CFAR) property, and the decision threshold can be calculated for a prespecified value of P_{FA}. The proposed schemes throughout this chapter are discussed for multiantenna CRN, however, these are also implementable for other multi-dimensional CRNs, e.g., cooperation and oversampling based CRNs. Based on the trade-off between performance and complexity, the applicability of the proposed schemes for other multi-dimensional CRNs scenarios are also discussed.

2.1 System Model

The spectrum sensing problem can be modeled as the binary hypothesis test where two hypotheses $\mathcal{H}_0$ and $\mathcal{H}_1$ denote the absence and the presence of PU signal in the spectrum, respectively. Under $\mathcal{H}_0$ hypothesis, when PU signal is not present in the spectrum, the received

signal at SU node is equal to the noise. Whereas, under $\mathcal{H}_1$ hypothesis, the received signal comprises of both faded PU signal and noise. According to the binary hypothesis test, we must choose between two hypotheses to detect the presence or absence of PU signal in the spectrum. We consider an SU node, equipped with M antennas, to monitor the given primary/licensed spectrum. The received signals by this node are downconverted to baseband, and sampled at the Nyquist-rate to obtain N samples at each antenna. The received samples at the nth instant of time from M antennas of SU node under both hypotheses are stacked in a column vector $\mathbf{y}(n)$, and is expressed as

$$\begin{aligned} \mathcal{H}_0 : \mathbf{y}(n) &= \hat{\mathbf{w}}(n), \qquad\qquad n = 1, 2, ..., N \\ \mathcal{H}_1 : \mathbf{y}(n) &= \widetilde{\mathbf{h}} s(n) + \hat{\mathbf{w}}(n), \quad n = 1, 2, ..., N \end{aligned} \tag{2.1}$$

where $\tilde{\mathbf{h}}$ is the $M \times 1$ channel vector with zero-mean iid complex Gaussian elements, $s(n)$ is the PU signal at the nth instant of time, and $\hat{\mathbf{w}}(n)$ is the $M \times 1$ zero-mean complex correlated Gaussian random noise vector at the nth instant of time. Moreover, we make the following assumptions about the signal model used in this work.

- The samples of the PU signal are assumed to be wide-sense stationary and zero-mean circular symmetric complex Gaussian (CSCG) RV. The power of the signal s(n) is ε_s, i.e., $\mathrm{E}[|s(n)|^2] = \varepsilon_s$.
- Assuming flat-fading Rayleigh channel, the channel fading coefficient $\tilde{h}$ is considered to be unknown and constant for each antenna in a sensing duration. We assume that the channels at SU node are richly scattered so that $\tilde{h}$ is uncorrelated at each antenna of the SU node [44], i.e., $\mathrm{E}[\widetilde{\mathbf{h}}\widetilde{\mathbf{h}}^H] = \mathrm{I}$. Thus, under $\mathcal{H}_1$ hypothesis, the noiseless received signals, i.e., $\tilde{\mathbf{h}}s$, at SU node are spatially uncorrelated.
- The noise is assumed to be correlated among SU antennas and uncorrelated in temporal dimension. The spatial correlation of noise may exist due to the antenna mutual coupling in a multiantenna CR system [44].
- The focus of this work is to obtain the sensing schemes which exploit the spatial correlation

information of noise. Thus, we are not considering the temporal correlation either with noiseless received signals or with noise.

- $\tilde{\mathbf{h}}$, $\{\mathrm{s}(n)\}_{n=1}^{N}$, and $\{\hat{\mathbf{w}}(n)\}_{n=1}^{N}$ are mutually independent and Gaussian distributed sequences, thus are mutually uncorrelated.

Further, under both hypotheses, the probability density functions (PDFs) of the received signals depend only upon their correlations since all signals are zero-mean. The autocorrelation function of the received signal vector $\mathbf{y}(n)$ under both hypotheses are determined as

$$\begin{aligned}\mathbf{R}_y[m|\mathcal{H}_\upsilon] &= \mathrm{E}[\mathbf{y}(n+m)\mathbf{y}^H(n)|\mathcal{H}_\upsilon] \\ &= \tilde{\mathbf{h}}\tilde{\mathbf{h}}^H \mathrm{E}[s(n+m)s^*(n)|\mathcal{H}_\upsilon] + \mathrm{E}[\hat{\mathbf{w}}(n+m)\hat{\mathbf{w}}^H(n)] \\ &= (\upsilon\varepsilon_s\tilde{\mathbf{h}}\tilde{\mathbf{h}}^H + \sigma_w^2\mathbf{C})\delta[m] \end{aligned} \tag{2.2}$$

where $\upsilon \in \{0,1\}$, $\mathcal{H}_\upsilon \in \{\mathcal{H}_0, \mathcal{H}_1\}$, and $\delta[m]$ is the Kronecker delta; $\delta[m] = 1$ if $m = 0$, and 0 otherwise. σ_w^2 is the variance of zero-mean CSCG noise, and $\mathbf{C}$ is the correlation matrix in spatial domain. Both σ_w^2 and $\mathbf{C}$ are assumed to be known to the SU node through experimental calibration [39, 48]. Let $\mathbf{Y} = [\mathbf{y}(1), \mathbf{y}(2), ..., \mathbf{y}(N)]$ be the $M \times N$ received signal matrix at SU. The columns of $\mathbf{Y}$ are independently Gaussian distributed with zero-mean and covariance matrix of $(\upsilon\varepsilon_s\tilde{\mathbf{h}}\tilde{\mathbf{h}}^H + \sigma_w^2\mathbf{C})$.

2.2 Neyman-Pearson Theorem

In discussing NP approach for binary hypothesis test, we firstly define P_{FA} and P_D using a Gaussian variate y. In Fig. 2.1, the PDFs of y are shown under both hypotheses $\mathcal{H}_0$ and $\mathcal{H}_1$, and compared with a threshold to decide between both. In this scenario, two types of error may occur. If we decide $\mathcal{H}_1$ but $\mathcal{H}_0$ is true, this error is known as P_{FA}. And, if $\mathcal{H}_0$ is decided where $\mathcal{H}_1$ is true, this type of error is known as probability of miss-detection, i.e., P_{MD}. P_D is defined as $1 - P_{MD}$, i.e., the probability that $\mathcal{H}_1$ is decided when $\mathcal{H}_1$ is true. Further, it is not possible to minimize both the error probabilities P_{FA} and P_{MD} simultaneously. In this case, an optimal decision scheme can be obtained by fixing an error probability while minimizing

the other. This approach is termed as NP theorem for the hypothesis test. NP theorem, as stated in [23]: *to minimize P_{MD} or equivalently maximize P_D for a fixed P_{FA}, decide $\mathcal{H}_1$ if the likelihood ratio (hitherto undefined) is greater than the threshold value where the threshold is determined by the fixed value of P_{FA} and the distribution under $\mathcal{H}_0$ hypothesis.*

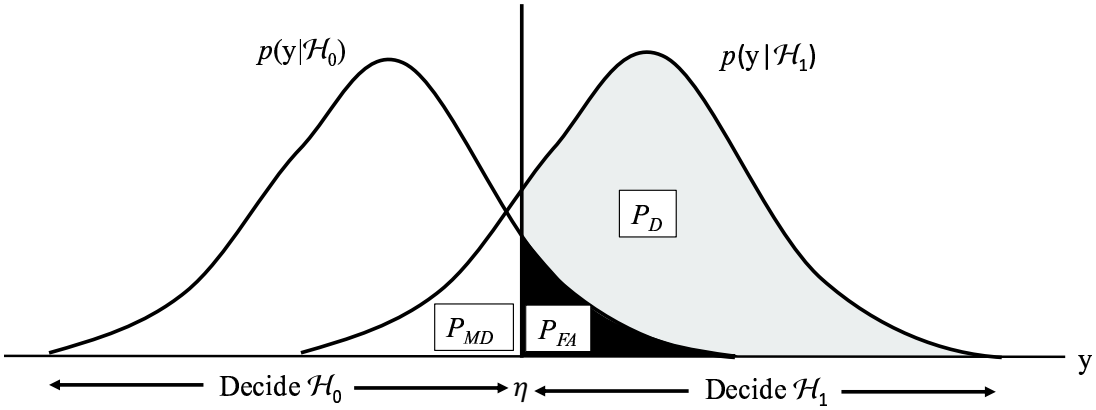

Figure 2.1: PDFs of binary hypothesis testing problem and decision regions.

2.3 Proposed Spectrum Sensing Schemes

In this section, we firstly obtain a decision statistics for the considered binary hypothesis test using NP theorem. The likelihood functions under both hypotheses $\mathcal{H}_0$ and $\mathcal{H}_1$ are multivariate complex Gaussian PDFs, which are denoted by $p(\mathbf{Y}|\mathcal{H}_0)$ and $p(\mathbf{Y}|\mathcal{H}_1)$, and are given by [23]

$$p(\mathbf{Y}|\mathcal{H}_0) = \frac{\exp\left(-\mathrm{tr}(\mathbf{Y}\mathbf{Y}^H(\sigma_w^2\mathbf{C})^{-1})\right)}{\pi^{MN}\{\det(\sigma_w^2\mathbf{C})\}^N} \tag{2.3}$$

$$p(\mathbf{Y}|\mathcal{H}_1) = \frac{\exp\left(-\mathrm{tr}(\mathbf{Y}\mathbf{Y}^H(\varepsilon_s\tilde{\mathbf{h}}\tilde{\mathbf{h}}^H + \sigma_w^2\mathbf{C})^{-1})\right)}{\pi^{MN}\{\det(\varepsilon_s\tilde{\mathbf{h}}\tilde{\mathbf{h}}^H + \sigma_w^2\mathbf{C})\}^N}, \tag{2.4}$$

respectively. The likelihood ratio is defined as $\frac{p(\mathbf{Y}|\mathcal{H}_1)}{p(\mathbf{Y}|\mathcal{H}_0)}$. In practice, it is easier to work with log of the likelihood ratio, without any loss, as logarithm is a strictly monotonically increasing function. Therefore, maximizing a function yields the same maximum as the logarithm of that function. Now, taking logarithm in (2.3) and (2.4), we have (2.5) and (2.6), respectively

$$\ln p(\mathbf{Y}|\mathcal{H}_0) = -MN\ln\pi - N\ln\det(\mathbf{C}) - MN\ln\sigma_w^2 - \mathrm{tr}(\mathbf{Y}\mathbf{Y}^H(\sigma_w^2\mathbf{C})^{-1}) \tag{2.5}$$

$$\ln p(\mathbf{Y}|\mathcal{H}_1) = -MN\ln\pi - N\ln\det(\varepsilon_s\tilde{\mathbf{h}}\tilde{\mathbf{h}}^H + \sigma_w^2\mathbf{C}) - \mathrm{tr}(\mathbf{Y}\mathbf{Y}^H(\varepsilon_s\tilde{\mathbf{h}}\tilde{\mathbf{h}}^H + \sigma_w^2\mathbf{C})^{-1}). \quad (2.6)$$

For further simplification, we perform eigenvalue decomposition (EVD) on $\mathbf{C}$ given by $\mathbf{C} = \mathbf{U}\Lambda\mathbf{U}^H$, where $\mathbf{U}$ is the $M \times M$ unitary matrix of the eigenvectors of $\mathbf{C}$, and Λ is the $M \times M$ diagonal matrix of the corresponding eigenvalues. Then, (2.5) and (2.6) can be written as

$$\ln p(\mathbf{Y}|\mathcal{H}_0) = -MN\ln\pi - N\ln\det(\Lambda) - MN\ln\sigma_w^2 - \mathrm{tr}(\mathbf{Z}\mathbf{Z}^H(\sigma_w^2\Lambda)^{-1}) \quad (2.7)$$

$$\ln p(\mathbf{Y}|\mathcal{H}_1) = -MN\ln\pi - N\ln\det(\varepsilon_s\mathbf{h}\mathbf{h}^H + \sigma_w^2\Lambda) - \mathrm{tr}(\mathbf{Z}\mathbf{Z}^H(\varepsilon_s\mathbf{h}\mathbf{h}^H + \sigma_w^2\Lambda)^{-1}), \quad (2.8)$$

respectively, where $\mathbf{Z} = \mathbf{U}^H\mathbf{Y}$ and $\mathbf{h} = \mathbf{U}^H\tilde{\mathbf{h}}$. The received signal matrix $\mathbf{Y}$ is linearly transformed to $\mathbf{Z}$. The effect of this linear transformation is that the received signals at SU node become spatially uncorrelated. Moreover, $\mathbf{h}$ has the same statistical properties as $\tilde{\mathbf{h}}$. From (2.7) and (2.8), the log-likelihood ratio (LLR) function can be determined as

$$\begin{aligned} LLR &= \ln p(\mathbf{Y}|\mathcal{H}_1) - \ln p(\mathbf{Y}|\mathcal{H}_0) \\ &= -N\ln\det(\varepsilon_s\mathbf{h}\mathbf{h}^H + \sigma_w^2\Lambda) - \mathrm{tr}(\mathbf{Z}\mathbf{Z}^H(\varepsilon_s\mathbf{h}\mathbf{h}^H + \sigma_w^2\Lambda)^{-1}) \\ &\quad + N\ln\det(\Lambda) + MN\ln\sigma_w^2 + \mathrm{tr}(\mathbf{Z}\mathbf{Z}^H(\sigma_w^2\Lambda)^{-1}). \end{aligned} \quad (2.9)$$

Using Sherman-Morrison formula [106], we obtain $\left(\Lambda + \frac{\varepsilon_s}{\sigma_w^2}\mathbf{h}\mathbf{h}^H\right)^{-1} = \left(\Lambda^{-1} - \frac{\Lambda^{-1}\mathbf{h}\mathbf{h}^H\Lambda^{-1}}{(\sigma_w^2/\varepsilon_s)+\mathbf{h}^H\Lambda^{-1}\mathbf{h}}\right)$. The decision statistics in NP sense can be determined by comparing the LLR function with respect to a threshold η'. If the LLR function in (2.9) found greater than η' then hypothesis $\mathcal{H}_1$ is decided, otherwise hypothesis $\mathcal{H}_0$ is decided. By incorporating the terms in (2.9) which are independent of $\mathbf{Z}$ with η' and after some simplifications, the decision statistics is obtained as

$$T = \mathrm{tr}\{\mathbf{h}\mathbf{h}^H\Lambda^{-1}\mathbf{Z}\mathbf{Z}^H\Lambda^{-1}\} \underset{\mathcal{H}_0}{\overset{\mathcal{H}_1}{\gtrless}} \eta. \quad (2.10)$$

The decision threshold η can be calculated for a prespecified value of P_{FA} using the distribution of decision statistics under $\mathcal{H}_0$ hypothesis [23]. The decision statistics T obtained in (2.10) can also be written as

$$T = \sum_{i=1}^{M}\sum_{j=1}^{M}\frac{\mathbf{z}_i^H\mathbf{z}_j h_i h_j^*}{\lambda_i\lambda_j} \underset{\mathcal{H}_0}{\overset{\mathcal{H}_1}{\gtrless}} \eta \quad (2.11)$$

where h_i denotes the channel coefficient at the ith antenna of SU node, $\mathbf{z}_i$ is the $N \times 1$ linearly transformed received signal vector at the ith antenna, and λ_i is the ith diagonal element of the eigenvalue matrix Λ. The decision statistics obtained in (2.11) depends upon unknown channel parameters, and hence cannot be directly implementable. In the sequel, two simple and implementable detection schemes are derived from (2.11) which do not need the channel information explicitly.

2.3.1 Weighted Cross-correlation Absolute Value Detector

We assume that all M SU antennas are clustered together as the separation between antennas is very small (which is also a valid reason for the spatial correlation in a multi-antenna CR system). In this case, all M SU antennas experience the same scale fading. We assume that all elements of channel gain vector $\mathbf{h}$ are of same magnitudes and expressing $h_i \approx \frac{\|\mathbf{h}\|}{\sqrt{M}} \exp(\mathbf{j} \arg\{h_i\})$, $\forall i$ where $\mathbf{j} = \sqrt{-1}$. Let us define $\phi_i = \arg\{h_i\}$ which is the phase term associated with the ith antenna of the SU node. Now, (2.11) can be written as

$$\begin{aligned} T &\approx \frac{\|\mathbf{h}\|^2}{M} \sum_{i=1}^{M} \sum_{j=1}^{M} \frac{\mathbf{z}_i^H \mathbf{z}_j}{\lambda_i \lambda_j} \exp\left(-\mathbf{j}(\phi_j - \phi_i)\right) \underset{\mathcal{H}_0}{\overset{\mathcal{H}_1}{\gtrless}} \eta \\ &= \sum_{i=1}^{M} \sum_{j=1}^{M} \frac{\mathbf{z}_i^H \mathbf{z}_j}{\lambda_i \lambda_j} \exp\left(-\mathbf{j}(\phi_j - \phi_i)\right) \underset{\mathcal{H}_0}{\overset{\mathcal{H}_1}{\gtrless}} \eta_{WCCAVD} \end{aligned} \tag{2.12}$$

where $\eta_{WCCAVD} = \frac{\eta M}{\|\mathbf{h}\|^2}$. The statistics in (2.12) is a function of phase difference introduced through all combinations of antennas, i.e., $\phi_{ji} = \phi_j - \phi_i$. The ϕ_{ji}, corresponding to the maximum value of the decision statistics, can be obtained as

$$\begin{aligned} \phi_{ji} &= \underset{\phi_{ji}, i,j \in \{1,..,M\}}{\arg\max} \sum_{i=1}^{M} \sum_{j=1}^{M} \frac{\mathbf{z}_i^H \mathbf{z}_j}{\lambda_i \lambda_j} \exp(-\mathbf{j}\phi_{ji}) \\ &= \sum_{i=1}^{M} \frac{\|\mathbf{z}_i\|^2}{\lambda_i^2} + \underset{\phi_{ji}, i,j \in \{1,..,M\}, i \neq j}{\arg\max} 2 \sum_{i=1}^{M} \sum_{j=i+1}^{M} \Re\left\{ \frac{\mathbf{z}_i^H \mathbf{z}_j}{\lambda_i \lambda_j} \exp(-\mathbf{j}\phi_{ji}) \right\}. \end{aligned} \tag{2.13}$$

It can be easily seen that the second term of right-hand side of (2.13) is maximized when $\phi_{ji} = \arg\{\mathbf{z}_i^H \mathbf{z}_j\}$. Hence, the decision statistics is obtained as

$$\begin{aligned} T_{WCCAVD} &= \sum_{i=1}^{M} \frac{\|\mathbf{z}_i\|^2}{\lambda_i^2} + 2\sum_{i=1}^{M}\sum_{j=i+1}^{M} \left|\frac{\mathbf{z}_i^H \mathbf{z}_j}{\lambda_i \lambda_j}\right| \\ &= \sum_{i=1}^{M}\sum_{j=1}^{M} \left|\frac{\mathbf{z}_i^H \mathbf{z}_j}{\lambda_i \lambda_j}\right| \underset{\mathcal{H}_0}{\overset{\mathcal{H}_1}{\gtrless}} \eta_{WCCAVD} \end{aligned} \tag{2.14}$$

where η_{WCCAVD} is the decision threshold for the detector. Note that, the decision statistics in (2.14) does not require the knowledge of channel gain, and also the need of phase information introduced by the channel coefficient at each antenna is sidestepped by the absolute values of cross-correlation terms.

Moreover, in conventional matrix-inverse based prewhitening, the received signal $\mathbf{Y}$ is multiplied by $\mathbf{C}^{-1/2}$ [23, 103], i.e., $\tilde{\mathbf{Y}} = \mathbf{C}^{-1/2}\mathbf{Y}$. The decision statistics of the conventional cross-correlation absolute value detector (CCAVD) is given by $\sum_{i=1}^{M}\sum_{j=1}^{M} \left|\tilde{\mathbf{y}}_i^H \tilde{\mathbf{y}}_j\right| \underset{\mathcal{H}_0}{\overset{\mathcal{H}_1}{\gtrless}} \eta$ where $\tilde{\mathbf{y}}_i$ is the $N \times 1$ prewhitened signal vector at the ith SU antenna. This decision statistics can be equivalently expressed as $\sum_{i=1}^{M}\sum_{j=1}^{M} \left|\frac{\mathbf{z}_i^H \mathbf{z}_j}{\sqrt{\lambda_i \lambda_j}}\right| \underset{\mathcal{H}_0}{\overset{\mathcal{H}_1}{\gtrless}} \eta$ where $\mathbf{z}_i$ is same as defined for (2.14). The argument of each term of the proposed decision statistics in (2.14) is $\frac{1}{\sqrt{\lambda_i \lambda_j}}$ times to each term of the conventional CCAVD. We consider $\frac{1}{\sqrt{\lambda_i \lambda_j}}$ as the weight factor associated with the cross-correlation of the prewhitened received signals at the ith and the jth antennas. Note that, the decision statistics derived in (2.14) is the sum of absolute value of the weighted cross-correlation between the prewhitened received signals at all pairs of antennas. Hence, we name it as a Weighted Cross-correlation Absolute Value Detector (WCCAVD).

2.3.2 Weighted Energy Detector

The simplest form of the decision statistics can be obtained from (2.11) when the cross-correlation terms are ignored. In addition, similar to WCCAVD, expressing $h_i = \frac{\|\mathbf{h}\|}{\sqrt{M}} \exp(\mathbf{j}\phi_i)$ $\forall i$. A new decision statistics is obtained as

$$T_{WED} = \sum_{i=1}^{M} \frac{\|\mathbf{z}_i\|^2}{\lambda_i^2} \underset{\mathcal{H}_0}{\overset{\mathcal{H}_1}{\gtrless}} \eta_{WED} \tag{2.15}$$

where $\eta_{WED} = \frac{\eta M}{\|\mathbf{h}\|^2}$. η_{WED} is the decision threshold for this detector. Note that, the decision statistics T_{WED} is the lower bound approximation of T_{WCCAVD}, i.e., $T_{WED} <= T_{WCCAVD}$.

Moreover, the decision statistics of the energy detector (ED) obtained after the matrix-inverse based prewhitening is given by $\sum_{i=1}^{M} \|\tilde{\mathbf{y}}_i\|^2 \underset{\mathcal{H}_0}{\overset{\mathcal{H}_1}{\gtrless}} \eta$ where $\tilde{\mathbf{y}}_i$ is same as defined in Subsection 2.3.1. This decision statistics can be equivalently expressed as $\sum_{i=1}^{M} \frac{\|\mathbf{z}_i\|^2}{\lambda_i} \underset{\mathcal{H}_0}{\overset{\mathcal{H}_1}{\gtrless}} \eta$. Each term of the proposed decision statistics in (2.15) is $\frac{1}{\lambda_i}$ times to each term of the conventional ED obtained after the matrix-inverse based prewhitening. We consider $\frac{1}{\lambda_i}$ as the weight factor associated with the energy of the prewhitened received signals at the ith antenna of SU. Note that, the decision statistics obtained in (2.15) is the sum of weighted energies of the prewhitened received signals at all antennas of SU. Hence, we name it as a Weighted Energy Detector (WED).

2.4 Performance Analysis of Proposed Detectors

In this section, we evaluate the performance of the proposed detectors. For this, the analytical expressions for P_{FA} and P_D are determined considering the asymptotic assumption in terms of a large number of samples received at the SU. The accuracy of the asymptotic assumptions and approximations used in the analysis are validated through Monte-Carlo simulations in Section 2.5.

2.4.1 Weighted Cross-correlation Absolute Value Detector

The decision statistics of WCCAVD in (2.14) can be equivalently expressed as

$$T_{WCCAVD} = \sum_{i=1}^{M} \sum_{j=1}^{M} \left| \frac{\mathbf{z}_i^H \mathbf{z}_j e^{\mathbf{j}\phi_{ij}}}{\lambda_i \lambda_j} \right| \tag{2.16}$$

where $\phi_{ij} = \phi_i - \phi_j = \arg\{h_i\} - \arg\{h_j\}$. Let us define $g_{ij} = \frac{\mathbf{z}_i^H \mathbf{z}_j e^{\mathbf{j}\phi_{ij}}}{\lambda_i \lambda_j}$.

Under $\mathcal{H}_0$ hypothesis: For $i = j$, $|g_{ii}| = g_{ii} = \frac{\|\mathbf{z}_i\|^2}{\lambda_i^2}$. For a large value of N, g_{ii} is assumed to be Gaussian distributed, and the mean and the variance are determined from (A.2) and (A.10) (Appendix A.1) for $|h_i| = 0$ and $|h_j| = 0$ given by $\mathrm{E}[g_{ii}|\mathcal{H}_0] = \frac{N\sigma_w^2}{\lambda_i}$ and $\mathrm{var}[g_{ii}|\mathcal{H}_0] = \frac{N\sigma_w^4}{\lambda_i^2}$, respectively. For $i \neq j$, g_{ij} is complex Gaussian distributed with independent real and imaginary

parts. The mean of the real and the imaginary parts is zero, and the variances are same. Hence, $|g_{ij}|$ is Rayleigh distributed with mean and variance given by $\mathrm{E}\left[|g_{ij}|\,|\mathcal{H}_0\right] = \frac{\sigma_w^2}{2}\sqrt{\frac{N\pi}{\lambda_i\lambda_j}}$ and $\mathrm{var}\left[|g_{ij}|\,|\mathcal{H}_0\right] = \left(1-\frac{\pi}{4}\right)\frac{N\sigma_w^4}{\lambda_i\lambda_j}$, respectively. The decision statistics T_{WCCAVD} is the sum of M Gaussian distributed and $\frac{M(M-1)}{2}$ (since $|g_{ij}| = |g_{ji}|$) Rayleigh distributed RVs. We assume that for a large value of N, T_{WCCAVD} is asymptotically Gaussian distributed with mean and variance given by

$$\mathrm{E}[T_{WCCAVD}|\mathcal{H}_0] = \sum_{i=1}^{M}\frac{N\sigma_w^2}{\lambda_i} + \sum_{i=1}^{M}\sum_{j=i+1}^{M}\sigma_w^2\sqrt{\frac{N\pi}{\lambda_i\lambda_j}} \tag{2.17}$$

$$\mathrm{var}[T_{WCCAVD}|\mathcal{H}_0] = \sum_{i=1}^{M}\frac{N\sigma_w^4}{\lambda_i^2} + \sum_{i=1}^{M}\sum_{j=i+1}^{M}\frac{(4-\pi)N\sigma_w^4}{2\lambda_i\lambda_j}, \tag{2.18}$$

respectively. The probability of false-alarm P_{FA}^{WCCAVD} can be determined for a given decision threshold η_{WCCAVD} as

$$\begin{aligned} P_{FA}^{WCCAVD} &= \Pr(T_{WCCAVD} > \eta_{WCCAVD}|\mathcal{H}_0) \\ &= Q\left(\frac{\eta_{WCCAVD} - \mathrm{E}\left[T_{WCCAVD}|\mathcal{H}_0\right]}{\sqrt{\mathrm{var}\left[T_{WCCAVD}|\mathcal{H}_0\right]}}\right) \\ &= Q\left(\frac{\eta_{WCCAVD} - \sum_{i=1}^{M}\frac{N\sigma_w^2}{\lambda_i} - \sum_{i=1}^{M}\sum_{j=i+1}^{M}\sigma_w^2\sqrt{\frac{N\pi}{\lambda_i\lambda_j}}}{\sqrt{\sum_{i=1}^{M}\frac{N\sigma_w^4}{\lambda_i^2} + \sum_{i=1}^{M}\sum_{j=i+1}^{M}\frac{(4-\pi)N\sigma_w^4}{2\lambda_i\lambda_j}}}\right) \end{aligned} \tag{2.19}$$

where $\Pr(\cdot)$ represents the probability. $Q(\cdot)$ denotes the Q-function and is defined as [23] $Q(x) = \frac{1}{\sqrt{2\pi}}\int_x^\infty \exp\left(-\frac{t^2}{2}\right)dt$. For a prespecified value of P_{FA}, the decision threshold η_{WCCAVD} can be directly calculated from (2.19) as

$$\eta_{WCCAVD} = N\sigma_w^2\left[Q^{-1}(P_{FA})\sqrt{\sum_{i=1}^{M}\frac{1}{N\lambda_i^2} + \sum_{i=1}^{M}\sum_{j=i+1}^{M}\frac{(4-\pi)}{2N\lambda_i\lambda_j}} + \sum_{i=1}^{M}\frac{1}{\lambda_i} + \sum_{i=1}^{M}\sum_{j=i+1}^{M}\sqrt{\frac{\pi}{N\lambda_i\lambda_j}}\right]. \tag{2.20}$$

Under $\mathcal{H}_1$ hypothesis: Similar to $\mathcal{H}_0$ hypothesis, for $i = j$, g_{ii} is asymptotically Gaussian distributed for a large value of N with mean and variance derived from (A.2) and (A.10) (Appendix A.1), and are given by $\mathrm{E}[g_{ii}|\mathcal{H}_1, \mathbf{h}] = \frac{N(|h_i|^2\varepsilon_s + \sigma_w^2\lambda_i)}{\lambda_i^2}$ and $\mathrm{var}[g_{ii}|\mathcal{H}_1, \mathbf{h}] = \frac{N(|h_i|^2\varepsilon_s + \sigma_w^2\lambda_i)^2}{\lambda_i^4}$,

respectively. For $i \neq j$, g_{ij} is asymptotically complex Gaussian distributed with independent real and imaginary parts. The mean and the variance of the real and imaginary parts are given by (for detail, refer to Appendix A.2)

$$\mathrm{E}\left[\Re\left\{g_{ij}\right\}|\mathcal{H}_1,\mathbf{h}\right] = \frac{N\varepsilon_s\left|h_i\right|\left|h_j\right|}{\lambda_i\lambda_j} \tag{2.21}$$

$$\mathrm{var}[\Re\{g_{ij}\}|\mathcal{H}_1,\mathbf{h}] = \frac{N}{2\lambda_i^2\lambda_j^2}\left[\left|h_i\right|^2\left|h_j\right|^2\varepsilon_s^2 + (\left|h_i\right|^2\varepsilon_s + \sigma_w^2\lambda_i)(\left|h_j\right|^2\varepsilon_s + \sigma_w^2\lambda_j)\right] \tag{2.22}$$

$$\mathrm{E}\left[\Im\left\{g_{ij}\right\}|\mathcal{H}_1,\mathbf{h}\right] = 0 \tag{2.23}$$

$$\mathrm{var}[\Im\{g_{ij}\}|\mathcal{H}_1,\mathbf{h}] = \frac{N}{2\lambda_i^2\lambda_j^2}\left[-\left|h_i\right|^2\left|h_j\right|^2\varepsilon_s^2 + (\left|h_i\right|^2\varepsilon_s + \sigma_w^2\lambda_i)(\left|h_j\right|^2\varepsilon_s + \sigma_w^2\lambda_j)\right] \tag{2.24}$$

From (2.21), (2.23), ((2.22), (2.24)), it is found that the mean (variance) of the real and the imaginary parts of g_{ij} is different. In this case, the distribution of $|g_{ij}|$ in simple closed-form is mathematically intractable. However, under some suitable conditions, an approximate distribution can be obtained as in [58]. We can write $|g_{ij}|$ as

$$|g_{ij}| = |\Re\{g_{ij}\}|\sqrt{1+a_{ij}^2} \tag{2.25}$$

where $a_{ij} = \frac{\Im\{g_{ij}\}}{\Re\{g_{ij}\}}$ is the ratio of two uncorrelated Gaussian random variables. It is known that if the coefficient of variation (CV) of the denominator of a_{ij} is less than 0.39, there exists a transformation $f(\cdot)$ such that the distribution of $f(a_{ij})$ can be approximated by a standard Gaussian distribution [107], i.e., $f(a_{ij}) \sim \mathcal{N}(0,1)$. The CV is a standardized measure of dispersion of the probability distribution and is defined as the ratio of the standard deviation to the mean. Here, the CV of the denominator $\Re\{g_{ij}\}$ is

$$\begin{aligned}\mathrm{CV}(\Re\{g_{ij}\}) &= \frac{\sqrt{\mathrm{var}[\Re\{g_{ij}\}|\mathcal{H}_1,\mathbf{h}]}}{\mathrm{E}[\Re\{g_{ij}\}|\mathcal{H}_1,\mathbf{h}]} \\ &= \frac{\sqrt{\left|h_i\right|^2\left|h_j\right|^2\varepsilon_s^2 + (\left|h_i\right|^2\varepsilon_s + \sigma_w^2\lambda_i)(\left|h_j\right|^2\varepsilon_s + \sigma_w^2\lambda_j)}}{\sqrt{2N}\varepsilon_s\left|h_i\right|\left|h_j\right|}\end{aligned} \tag{2.26}$$

which tends to zero as $N \to \infty$, provided $|h_i| \neq 0$ and $|h_j| \neq 0$. Hence, for large N, the random

variable

$$f(a_{ij}) = \frac{\mathrm{E}[\Re\{g_{ij}\}|\mathcal{H}_1,\mathbf{h}]a_{ij} - \mathrm{E}[\Im\{g_{ij}\}|\mathcal{H}_1,\mathbf{h}]}{\sqrt{\mathrm{var}[\Re\{g_{ij}\}|\mathcal{H}_1,\mathbf{h}]a_{ij}^2 + \mathrm{var}[\Im\{g_{ij}\}|\mathcal{H}_1,\mathbf{h}]}}$$
$$= \frac{\sqrt{2N}\,|h_i|\,|h_j|\,\varepsilon_s a_{ij}}{\sqrt{|h_i|^2\,|h_j|^2\,\varepsilon_s^2(a_{ij}^2-1) + (|h_i|^2\,\varepsilon_s + \sigma_w^2\lambda_i)(|h_j|^2\,\varepsilon_s + \sigma_w^2\lambda_j)(a_{ij}^2+1)}} \tag{2.27}$$

is approximately standard Gaussian distributed with zero-mean and unity variance [107]. Further, it can be easily determined that $\Pr(a_{ij}^2 > \tau) = 2Q(f(\sqrt{\tau}))$ which converges to zero for large N as $Q(\cdot)$ is a monotonically decreasing function. Hence, $|g_{ij}|$ in (2.25) can be approximated to $|\Re\{g_{ij}\}|$. Since $\Re\{g_{ij}\}$ is asymptotically Gaussian distributed for a large value of N, $|\Re\{g_{ij}\}|$ follows a folded normal distribution, i.e., $|\Re\{g_{ij}\}| \sim \mathcal{FN}\left(\mu_f(\mathbf{h}), \sigma_f^2(\mathbf{h})\right)$, with mean and variance given by

$$\mu_f(\mathbf{h}) = \sqrt{\frac{2\sigma^2(\mathbf{h})}{\pi}}\exp\left(-\frac{\mu^2(\mathbf{h})}{2\sigma^2(\mathbf{h})}\right) + \mu(\mathbf{h})erf\left(\frac{\mu(\mathbf{h})}{\sqrt{2\sigma^2(\mathbf{h})}}\right)$$

and

$$\sigma_f^2(\mathbf{h}) = \mu^2(\mathbf{h}) + \sigma^2(\mathbf{h}) - \mu_f^2(\mathbf{h})$$

where $\mu(\mathbf{h})$ and $\sigma^2(\mathbf{h})$ are given as (2.21) and (2.22), respectively. $erf(\cdot)$ denotes the error function [108]. The mean of T_{WCCAVD} under $\mathcal{H}_1$ hypothesis is sum of the mean of the normal (for $i=j$) and the folded normal (for $i \neq j$) distributions, and is given by

$$\mathrm{E}\left[T_{WCCAVD}|\mathcal{H}_1,\mathbf{h}\right] = \sum_{i=1}^{M}\frac{N\left(|h_i|^2\,\varepsilon_s + \sigma_w^2\lambda_i\right)}{\lambda_i^2} + 2\sum_{i=1}^{M}\sum_{j=i+1}^{M}\mu_f(\mathbf{h})$$
$$= \sum_{i=1}^{M}\frac{N(|h_i|^2\,\varepsilon_s + \sigma_w^2\lambda_i)}{\lambda_i^2} + \sum_{i=1}^{M}\sum_{j=i+1}^{M}\frac{2}{\lambda_i\lambda_j}$$
$$\left[\sqrt{\frac{N}{\pi}\left(|h_i|^2\,|h_j|^2\,\varepsilon_s^2 + (|h_i|^2\,\varepsilon_s + \sigma_w^2\lambda_i)(|h_j|^2\,\varepsilon_s + \sigma_w^2\lambda_j)\right)}\right.$$
$$\exp\left(-\frac{N\varepsilon_s^2\,|h_i|^2\,|h_j|^2}{|h_i|^2\,|h_j|^2\,\varepsilon_s^2 + (|h_i|^2\,\varepsilon_s + \sigma_w^2\lambda_i)(|h_j|^2\,\varepsilon_s + \sigma_w^2\lambda_j)}\right)$$
$$\left. + N\varepsilon_s\,|h_i|\,|h_j|\,erf\left(\sqrt{\frac{N\varepsilon_s^2\,|h_i|^2\,|h_j|^2}{|h_i|^2\,|h_j|^2\,\varepsilon_s^2 + (|h_i|^2\,\varepsilon_s + \sigma_w^2\lambda_i)(|h_j|^2\,\varepsilon_s + \sigma_w^2\lambda_j)}}\right)\right]. \tag{2.28}$$

The calculation of the variance of (2.16) under $\mathcal{H}_1$ hypothesis is not known as per our knowledge. Furthermore, to calculate an approximate variance, we assume $|\Re\{g_{ij}\}| \approx \Re\{g_{ij}\}$ as $\Pr(\Re\{g_{ij}\} < 0) = Q([\mathrm{CV}(\Re\{g_{ij}\})]^{-1})$ tends to zero for large N. Hence, an approximate expression of variance under $\mathcal{H}_1$ hypothesis is obtained as (for detail, refer to Appendix A.3)

$$\begin{aligned}
\mathrm{var}[T_{WCCAVD}|\mathcal{H}_1, \mathbf{h}] &\approx \sum_{i=1}^{M}\sum_{j=1}^{M}\sum_{k=1}^{M}\sum_{l=1}^{M} \mathrm{cov}[\Re\{g_{ij}\}, \Re\{g_{kl}\}] \\
&= \sum_{i=1}^{M}\sum_{j=1}^{M}\sum_{k=1}^{M}\sum_{l=1}^{M} \frac{1}{4}\left(\{\mathrm{E}[g_{ij}g_{kl}] - \mathrm{E}[g_{ij}]\mathrm{E}[g_{kl}]\} + \{\mathrm{E}[g_{ij}^* g_{kl}^*] - \mathrm{E}[g_{ij}^*]\mathrm{E}[g_{kl}^*]\}\right. \\
&\quad \left. + \{\mathrm{E}[g_{ij}^* g_{kl}] - \mathrm{E}[g_{ij}^*]\mathrm{E}[g_{kl}]\} + \{\mathrm{E}[g_{ij} g_{kl}^*] - \mathrm{E}[g_{ij}]\mathrm{E}[g_{kl}^*]\}\right) \\
&= \sum_{i=1}^{M}\sum_{j=1}^{M}\sum_{k=1}^{M}\sum_{l=1}^{M} \frac{1}{2\lambda_i\lambda_j\lambda_k\lambda_l}\left(2N\varepsilon_s^2 |h_i||h_j||h_k||h_l| + N\sigma_w^4\lambda_{i(=k)}\lambda_{j(=l)}\delta_{ik}\delta_{jl}\right. \\
&\quad + N\sigma_w^4\lambda_{j(=k)}\lambda_{i(=l)}\delta_{jk}\delta_{il} + N\varepsilon_s\sigma_w^2\left(|h_i||h_k|\,\lambda_{j(=l)}\delta_{jl} + |h_j||h_l|\,\lambda_{i(=k)}\delta_{ik}\right. \\
&\quad \left.\left. + |h_i||h_l|\,\lambda_{j(=k)}\delta_{jk} + |h_j||h_k|\,\lambda_{i(=l)}\delta_{il}\right)\right). \qquad (2.29)
\end{aligned}$$

Finally, using (2.28) and (2.29), the probability of detection $P_D^{WCCAVD}(\mathbf{h})$ can be determined as

$$\begin{aligned}
P_D^{WCCAVD}(\mathbf{h}) &= \Pr(T_{WCCAVD} > \eta_{WCCAVD}|\mathcal{H}_1, \mathbf{h}) \\
&= Q\left(\frac{\eta_{WCCAVD} - \mathrm{E}\left[T_{WCCAVD}|\mathcal{H}_1, \mathbf{h}\right]}{\sqrt{\mathrm{var}\left[T_{WCCAVD}|\mathcal{H}_1, \mathbf{h}\right]}}\right). \qquad (2.30)
\end{aligned}$$

2.4.2 Weighted Energy Detector

Under both hypotheses $\mathcal{H}_0$ and $\mathcal{H}_1$, for a large value of N, T_{WED} is assumed to be asymptotically Gaussian distributed.

Under $\mathcal{H}_0$ hypothesis: The mean and the variance of T_{WED} are determined from (A.2) and (A.10) (Appendix A.1), respectively, by keeping $i = j$ and $|h_i| = 0$, and are given by

$$\mathrm{E}[T_{WED}|\mathcal{H}_0] = \sum_{i=1}^{M} \frac{N\sigma_w^2}{\lambda_i} \qquad (2.31)$$

$$\text{var}[T_{WED}|\mathcal{H}_0] = \sum_{i=1}^{M} \frac{N\sigma_w^4}{\lambda_i^2}. \tag{2.32}$$

Using (2.31) and (2.32), the probability of false-alarm P_{FA}^{WED} can be determined for a given decision threshold η_{WED} as

$$\begin{aligned} P_{FA}^{WED} &= \Pr(T_{WED} > \eta_{WED}|\mathcal{H}_0) \\ &= Q\left(\frac{\eta_{WED} - \mathrm{E}\left[T_{WED}|\mathcal{H}_0\right]}{\sqrt{\text{var}\left[T_{WED}|\mathcal{H}_0\right]}}\right) \\ &= Q\left(\frac{\eta_{WED} - \sum_{i=1}^{M} \frac{N\sigma_w^2}{\lambda_i}}{\sqrt{\sum_{i=1}^{M} \frac{N\sigma_w^4}{\lambda_i^2}}}\right). \end{aligned} \tag{2.33}$$

For a prespecified value of P_{FA}, the decision threshold η_{WED} can be calculated from (2.33) as

$$\eta_{WED} = N\sigma_w^2 \left[\sum_{i=1}^{M} \frac{1}{\lambda_i} + Q^{-1}(P_{FA})\sqrt{\sum_{i=1}^{M} \frac{1}{N\lambda_i^2}}\right]. \tag{2.34}$$

Under $\mathcal{H}_1$ hypothesis: The mean of T_{WED} can be calculated from (A.2) (Appendix A.1) considering $i = j$, and is given by

$$\mathrm{E}[T_{WED}|\mathcal{H}_1, \mathbf{h}] = \sum_{i=1}^{M} \frac{N\left(|h_i|^2 \varepsilon_s + \sigma_w^2\lambda_i\right)}{\lambda_i^2}. \tag{2.35}$$

The variance of T_{WED} is determined as

$$\begin{aligned} \text{var}[T_{WED}|\mathcal{H}_1, \mathbf{h}] &= \sum_{i=1}^{M} \text{var}(g_{ii}) + 2\sum_{i=1}^{M}\sum_{k=i+1}^{M} \text{cov}(g_{ii}, g_{kk}) \\ &= \sum_{i=1}^{M} \frac{N\left(|h_i|^2 \varepsilon_s + \sigma_w^2\lambda_i\right)^2}{\lambda_i^4} + 2\sum_{i=1}^{M}\sum_{k=i+1}^{M} \frac{N\varepsilon_s^2 |h_i|^2 |h_k|^2}{\lambda_i^2\lambda_k^2}. \end{aligned} \tag{2.36}$$

The first term in the right-hand side of (2.36) is obtained from (A.10) (Appendix A.1) considering $i = j$. The second term is calculated from (A.26) (Appendix A.3) considering $i = j$ and

$k = l$. Using (2.35) and (2.36), the probability of detection $P_D^{WED}(\mathbf{h})$ can be obtained as

$$\begin{aligned} P_D^{WED}(\mathbf{h}) &= \Pr(T_{WED} > \eta_{WED}|\mathcal{H}_1) \\ &= Q\left(\frac{\eta_{WED} - \mathrm{E}[T_{WED}|\mathcal{H}_1, \mathbf{h}]}{\sqrt{\mathrm{var}[T_{WED}|\mathcal{H}_1, \mathbf{h}]}}\right) \\ &= Q\left(\frac{\sum\limits_{i=1}^{M} \frac{N\sigma_w^2}{\lambda_i} + Q^{-1}(P_{FA})\sqrt{\sum\limits_{i=1}^{M} \frac{N\sigma_w^4}{\lambda_i^2} - \sum\limits_{i=1}^{M} \frac{N\left(|h_i|^2\varepsilon_s + \sigma_w^2\lambda_i\right)}{\lambda_i^2}}}{\sqrt{\sum\limits_{i=1}^{M} \frac{N\left(|h_i|^2\varepsilon_s + \sigma_w^2\lambda_i\right)^2}{\lambda_i^4} + 2\sum\limits_{i=1}^{M}\sum\limits_{k=i+1}^{M} \frac{N\varepsilon_s^2|h_i|^2|h_k|^2}{\lambda_i^2\lambda_k^2}}}\right). \end{aligned} \tag{2.37}$$

2.5 Computational Complexity

The major computational complexity of the proposed WCCAVD and WED is involved in two terms: computation of EVD of the $M \times M$ correlation matrix $\mathbf{C}$ and the calculation of $\mathbf{Z}$. Thus, the total complexity of each of the proposed detection scheme is $\mathrm{O}(M^3)$+$\mathrm{O}(M^2N)$. Further, the major complexity involved in conventional CCAVD and ED is: computation of the inverse of $M \times M$ matrix $\mathbf{C}$ and the calculation of $\tilde{\mathbf{Y}}$. The resulting complexity involves with each of the conventional CCAVD and ED is $\mathrm{O}(M^3)$+$\mathrm{O}(M^2N)$. Hence, the order of computational complexity of the proposed detectors is same vis-a-vis the corresponding detectors obtained after the matrix-inverse based prewhitening.

2.6 Results and Discussion

In this section, the analytical and simulation results are presented to analyze the performance of the proposed detectors. The power of each PU sample is normalized to one, i.e., $\varepsilon_s = 1$. The average SNR per antenna at SU node is defined as $\gamma = \frac{\mathrm{E}[\|\tilde{\mathbf{h}}\|^2]}{M\sigma_w^2}$. For simulations, a simplified exponential correlation model [39] is considered to generate correlation matrix $\mathbf{C}$. The element of $\mathbf{C}$ at the ith row and the jth column is $\rho^{|i-j|}$, where $i, j \in \{1, ..., M\}$, and ρ is the correlation coefficient between noise samples at adjacent antennas, satisfying $0 \leq |\rho| \leq 1$. For each detection method 10^5 independent tests are performed under both hypotheses $\mathcal{H}_0$ and $\mathcal{H}_1$.

Calculation of decision-threshold for simulation plots: The decision statistics is calculated 10^5 independent times for each variable on horizontal axis under $\mathcal{H}_0$ hypothesis. A range of empirical decision threshold is considered based on the minimum and maximum values of decision statistics obtained 10^5 times. The decision statistics under $\mathcal{H}_0$ hypothesis is compared with the minimum value of empirical threshold, and subsequently compared with the desired P_{FA}. If the desired value of P_{FA} is not achieved, increase the chosen value of empirical threshold by a fixed amount–choose judiciously. This process is continued until the value of desired P_{FA} is achieved. Whenever the target value of P_{FA} is achieved, the value of empirical threshold at that instant will be the decision threshold. This value of decision threshold is used to compare the decision statistics under $\mathcal{H}_1$ hypothesis which finally gives the value of P_D. This process is repeated for each variable on horizontal axis for final simulation plot. For analytical plots, the decision-threshold is calculated using the expressions obtained in 2.20 and 2.34 for proposed WCCAVD and WED, respectively.

Moreover, the detection probabilities of both detectors are depending upon $\mathbf{h}$. Thus, the average detection probability is calculated through simulation. In each iteration, $\mathbf{h}$ is generated whose entries are complex Gaussian distributed. The detection probability is calculated for each iteration, and then mean is taken over all iterations to obtain the average P_D.

2.6.1 Statistical Distribution

The CDF of the decision statistics of the proposed WCCAVD and WED are shown in Figs. 2.2(a) and 2.2(b), respectively, to validate the asymptotic assumptions and approximations used in deriving the analytical results. Under $\mathcal{H}_0$ and $\mathcal{H}_1$, the analytical CDF are determined as $1 - P_{FA}$ and $1 - P_D$, respectively. Under $\mathcal{H}_0$ hypothesis, the analytical plots for CDF of both WCCAVD and WED are closely matched with the simulation plots. However, under $\mathcal{H}_1$ hypothesis, a marginal difference is observed between analytical and simulation plots of both WCCAVD and WED. This is due to the asymptotic assumptions considered in the presence of fading channels, and also, we must recall the additional approximations used to derive the detection probability of WCCAVD elaborated in Section 2.4.

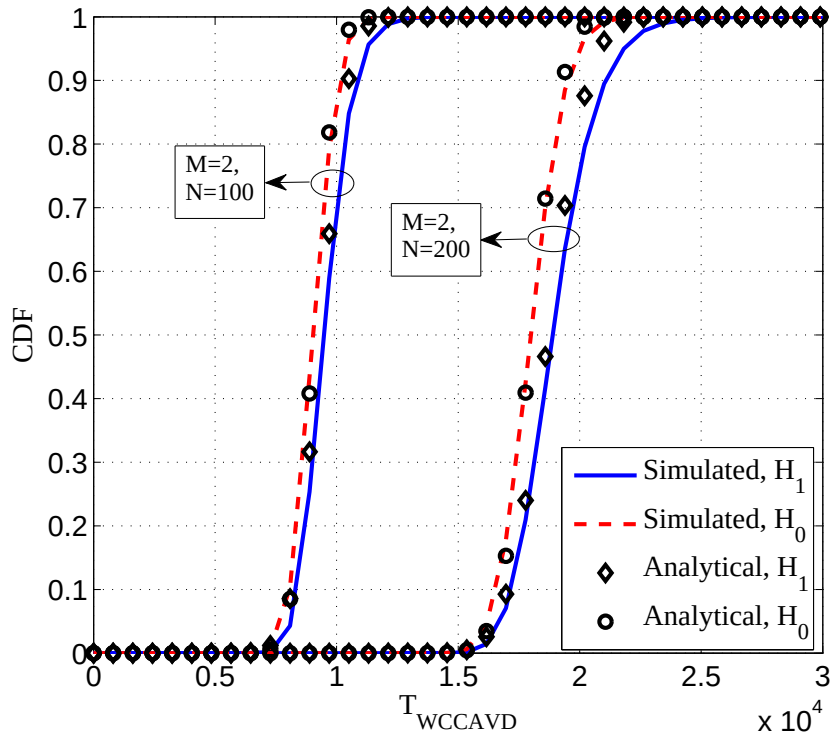

(a)

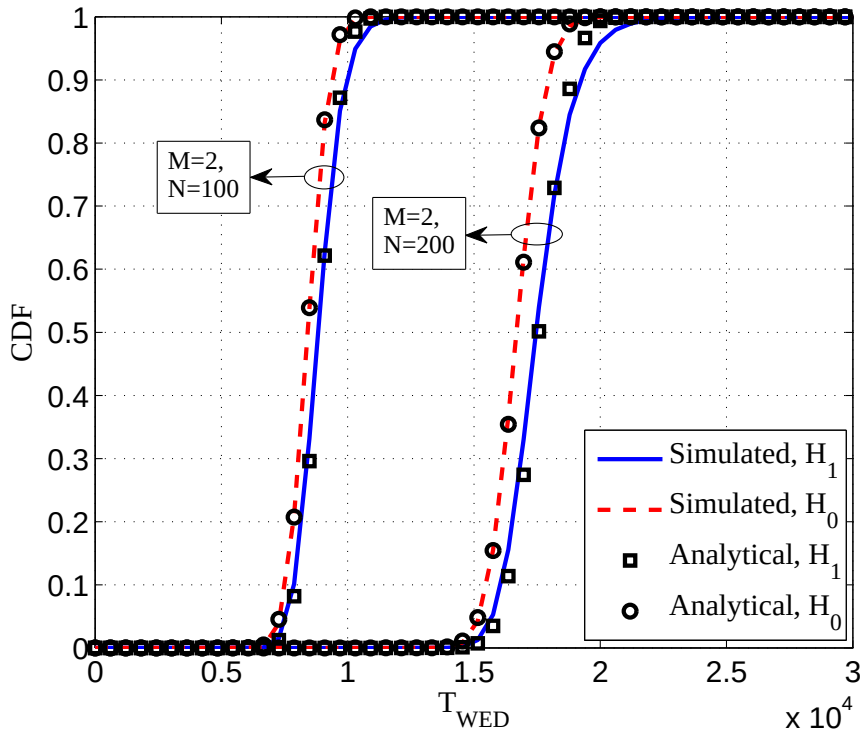

(b)

Figure 2.2: CDF plots of the proposed (a) WCCAVD and (b) WED under both hypotheses $\mathcal{H}_0$ and $\mathcal{H}_1$, when $M = 2$, $N = 100, 200$, $P_{FA} = 0.01$, $\gamma = -15$ dB, and $\rho = 0.5$.

2.6.2 Effect of Noise Correlation

In Figs. 2.3(a) and 2.3(b), the proposed WCCAVD and WED, respectively, are shown for various values of noise correlation coefficient ρ. The proposed detectors are also compared with the corresponding detectors obtained after the matrix-inverse based prewhitening and the detectors with spatially correlated noise. The decision statistics of the conventional CCAVD and ED with spatially correlated noise are given by $\sum_{i=1}^{M}\sum_{j=1}^{M}\left|\mathbf{y}_i^H\mathbf{y}_j\right| \underset{\mathcal{H}_0}{\overset{\mathcal{H}_1}{\gtrless}} \eta$ and $\sum_{i=1}^{M}\|\mathbf{y}_i\|^2 \underset{\mathcal{H}_0}{\overset{\mathcal{H}_1}{\gtrless}} \eta$, respectively, where $\mathbf{y}_i$ is the $N\times 1$ received signal vector at the ith antenna of SU. From the figures, it is observed that for high values of ρ, both the proposed WCCAVD and WED significantly outperform the corresponding detectors obtained after the matrix-inverse based prewhitening and the detectors with spatially correlated noise. It is noticed that, at low SNR, this performance gain is more than 1 dB with respect to the detectors obtained after the matrix-inverse based prewhitening. For $\rho < 0.5$, both the proposed detectors perform comparable to the corresponding detectors obtained after the matrix-inverse based prewhitening. The performance of both the proposed detectors converges to their corresponding conventional detectors with spatially correlated noise for the lower values of ρ. The performance gain in the proposed detectors is achieved due to the accumulated effect of the weight factors which is higher in the proposed detectors with respect to the detectors obtained after the matrix-inverse based prewhitening. Moreover, the analytical plots are closely matched with the simulation plots.

2.6.3 Effect of Number of Received Samples

In Figs. 2.4(a) and 2.4(b), the proposed WCCAVD and WED, respectively, are compared with the corresponding detectors obtained after the matrix-inverse based prewhitening for various values of received samples N when $\rho = 0.95$. From the figures, it can be seen that the improved performance of the proposed detectors with respect to the corresponding detectors obtained after the matrix-inverse based prewhitening is maintained with the increased values of N. Moreover, the analytical plots are observed to be more close to the simulation plots for higher values of N. This is due to the fact that the asymptotic assumptions and approximations used to derive the analytical results are more accurate for larger values of N.

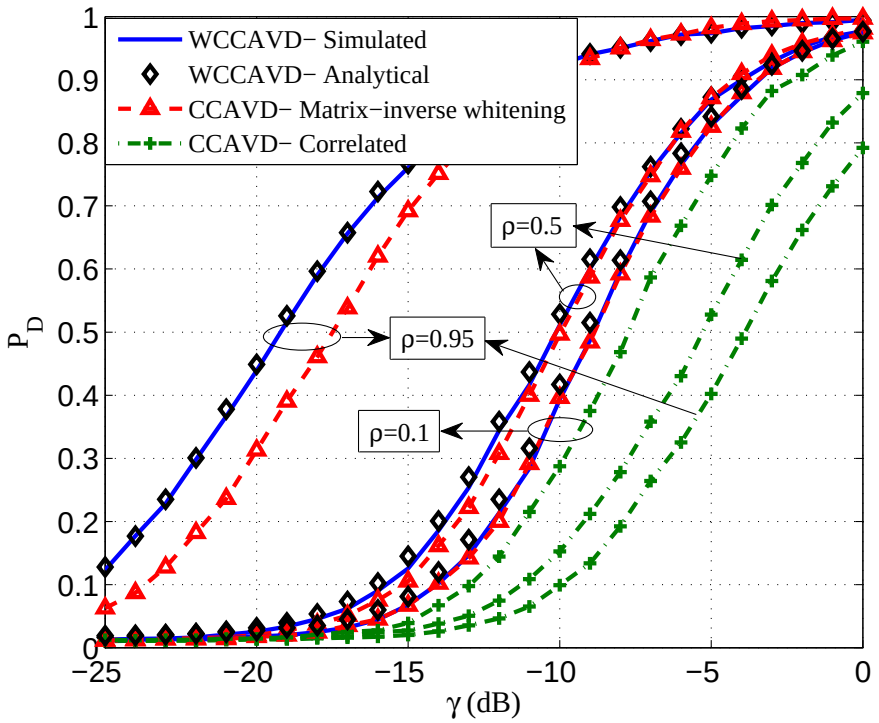

(a)

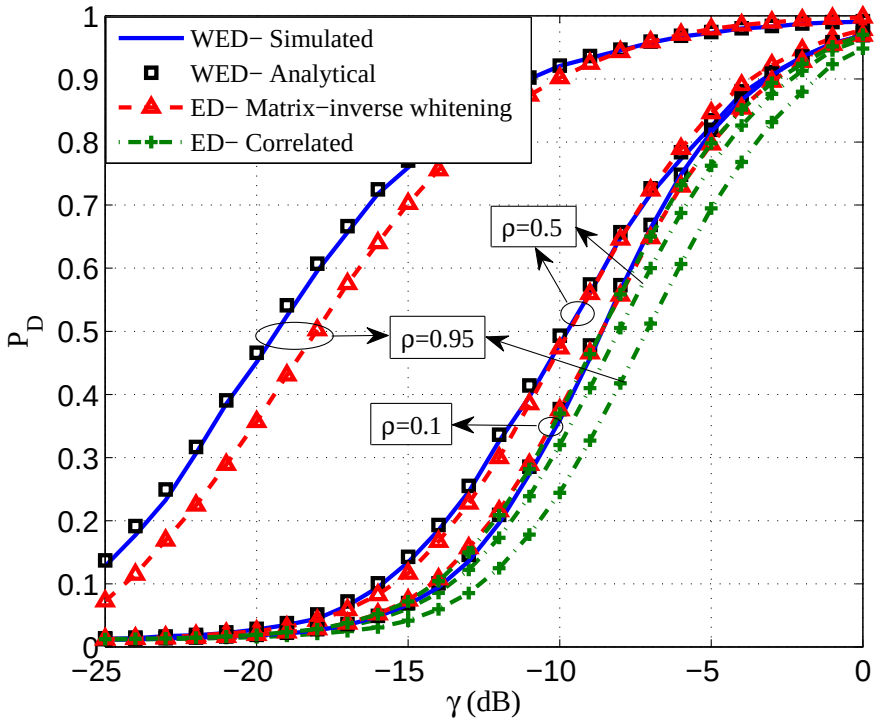

(b)

Figure 2.3: Average detection probability comparison of various forms of (a) CCAVD and (b) ED with respect to the average SNR per antenna for different values of ρ, when $M = 2$, $N = 200$, and $P_{fa} = 0.01$.

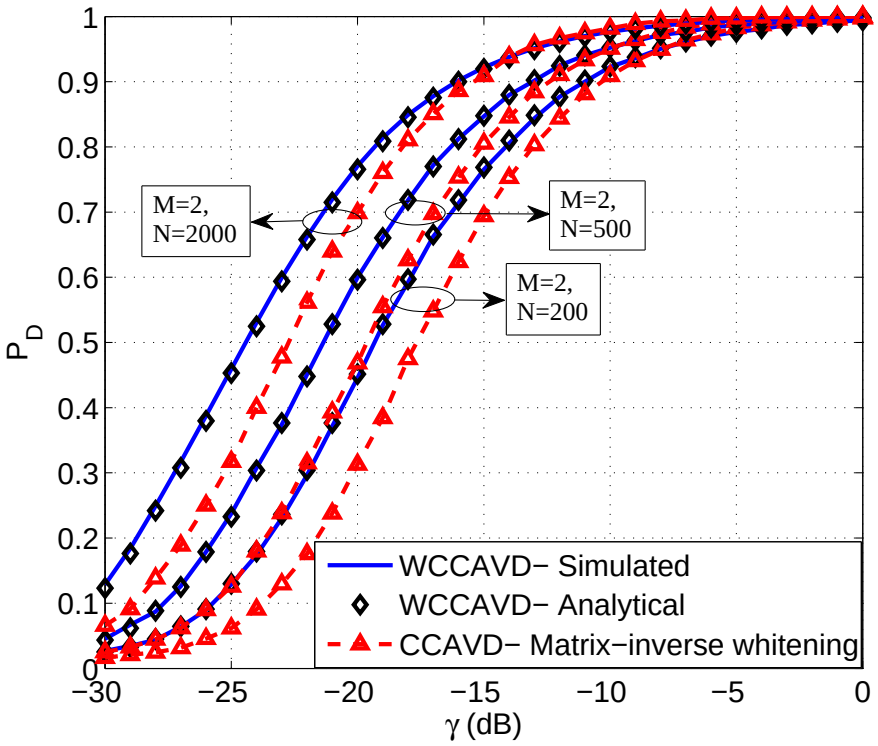

(a)

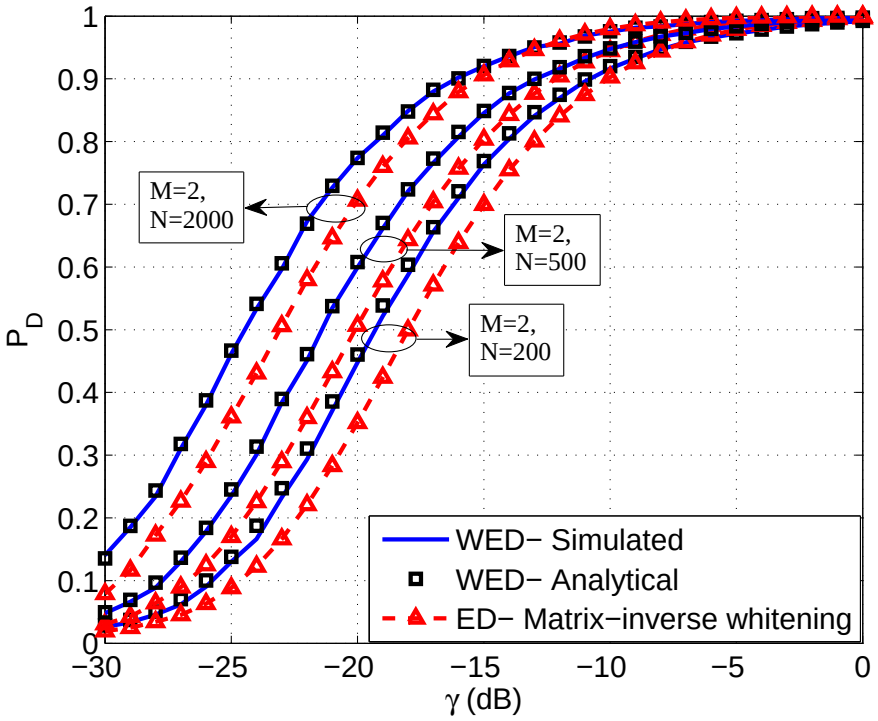

(b)

Figure 2.4: Average detection probability comparison of (a) WCCAVD and (b) WED with corresponding detectors obtained after the matrix-inverse based prewhitening with respect to γ for various values of N, when $M = 2$, $P_{FA} = 0.01$, and $\rho = 0.95$.

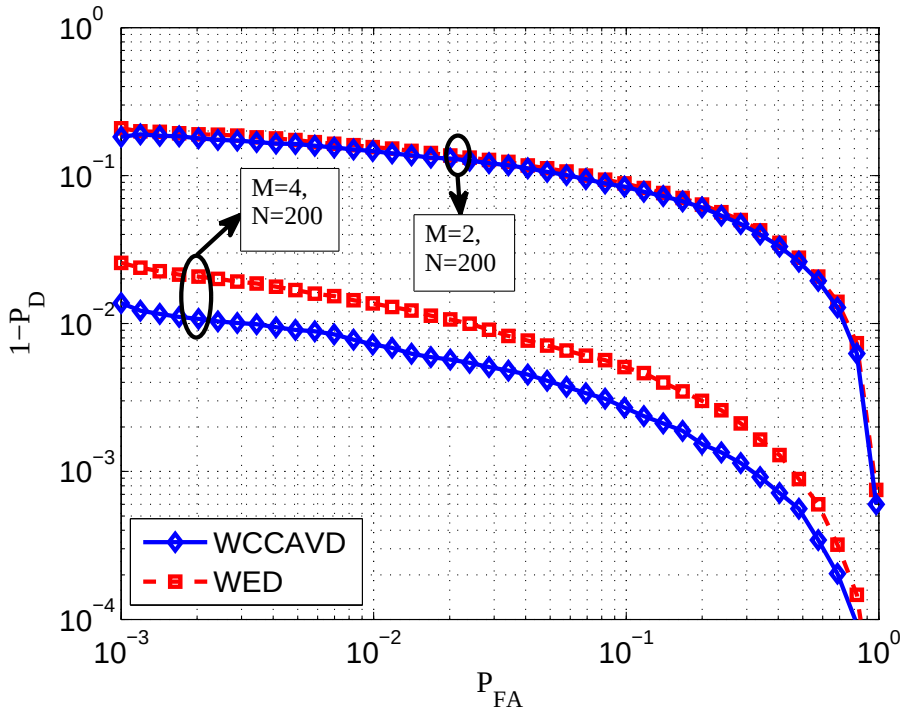

(a)

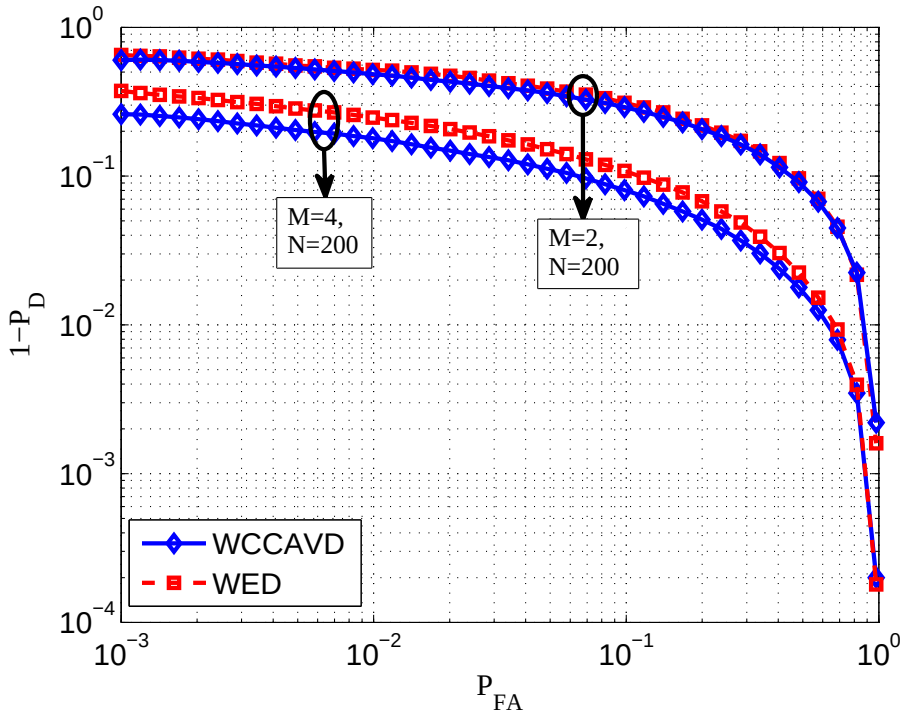

(b)

Figure 2.5: The complementary ROC curves of the proposed WCCAVD and WED for (a) $\rho =$ 0.9 (b) $\rho =$ 0.5, when $M = 2,\ 4$, $N = 200$, and $\gamma = -10$ dB.

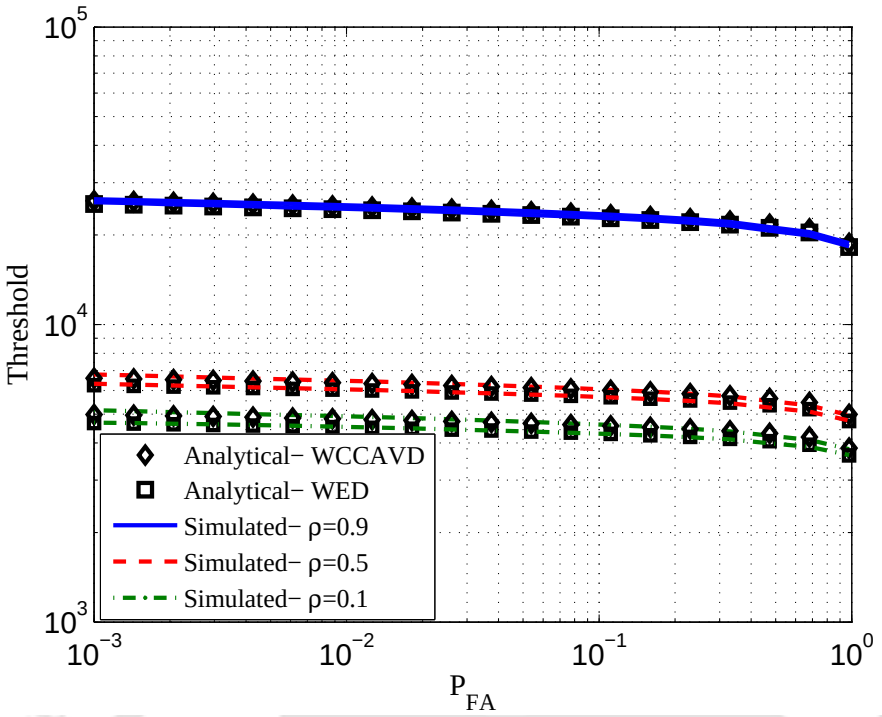

Figure 2.6: Decision threshold vs P_{FA} plots of the proposed WCCAVD and WED for various values of ρ, when $M = 2$, $N = 200$, and $\gamma = -10$ dB.

2.6.4 Comparison between Proposed WCCAVD and WED

The complementary receiver operating characteristic (ROC) curves of the proposed WCCAVD and WED are shown for $\rho = 0.9$ and 0.5 in Figs. 2.5(a) and 2.5(b), respectively. From the figures, it can be seen that the average miss-detection probability (defined as $1 - P_D$) of the proposed WCCAVD is lesser than the proposed WED. The performance gap between both detectors is observed to be more significant when the number of antennas at the SU node is increased from 2 to 4. The performance gain in WCCAVD with respect to WED is due to the fact that the decision statistics of WCCAVD includes the cross-correlation among signals received at different antennas of the SU node. However, the cross-correlation terms are relaxed in the decision statistics of the proposed WED which is aimed to produce a most simplified detector.

In Fig. 2.6, the decision threshold of both the proposed detectors is shown with respect to P_{FA}. It is observed that the value of decision threshold for both detectors decreases as

P_{FA} increases, consequently the performance improves. The improved performance can also be observed from Fig. 2.5, as the average miss-detection probability of both detectors decreases monotonically as P_{FA} increases. Moreover, the analytical plots are closely matched with the simulation plots.

2.7 Applicability in Multi-dimensional CR Systems

The proposed WCCAVD involves the cross-correlation terms among signals received at different antennas of the SU node. Hence, WCCAVD is suitable for the centralized multi-dimensional CR systems (for example, the multiantenna CR system, and the oversampling based CR system), and is used for the distributed multi-dimensional CR systems (for example, the cooperative CR system) at the cost of large handshake overhead. The proposed WED is suitable for the distributed multi-dimensional CR systems as it does not involve the cross-correlation terms among the received signals from different antennas. Moreover, both detectors can also be used in combination. In a cooperative cognitive network, when the SU nodes have multiple number of antennas (or oversampling is performed at the SU nodes having a single antenna), the WCCAVD can be used at each node to combine their received signals, and WED can be used at the fusion center to combine the decisions of several SU nodes.

2.8 Summary

In this chapter, we have proposed two spectrum sensing schemes, WCCAVD and WED, for multiantenna CR systems under spatially correlated noise. The knowledge of spatial correlation has been exploited to improve the performance of the proposed detectors with respect to the detectors obtained after classical matrix-inverse based prewhitening. It has been shown that in the presence of high spatial correlation and low SNR, the proposed detectors outperform the corresponding detectors obtained after the matrix-inverse based prewhitening by more than 1 dB. For the spatial correlation below 0.5, the performance of the proposed detectors is comparable to the corresponding detectors obtained after the matrix-inverse based prewhitening. The performance gain in the proposed detectors is achieved due to the accumulated effect of

the weight factor associated with each term of their decision statistics. It is also found that the order of computational complexity of the proposed detectors is same vis-a-vis the corresponding detectors obtained after the matrix-inverse based prewhitening. Further, we have derived the analytical expressions for the decision threshold, the P_{FA} and the P_D of the proposed detectors. The accuracy of the asymptotic assumptions and approximations used in analytical derivations has been validated through the closely matched analytical and simulation plots.

The detectors proposed in this chapter are analyzed considering multiantenna based multi-dimensional CRN, these are also implementable in cooperation and oversampling based multi-dimensional CRNs. Based on the trade-off between performance and complexity, we have discussed the applicability of the proposed detectors in different multi-dimensional CRNs. Moreover, the system model considered in this chapter assumed spatially correlated noise whereas signals are temporally white. Similar results can be obtained when one consider temporally correlated noise with spatially uncorrelated signals. There will be a modification in the latter case which is as follows: suppose $\hat{\mathbf{W}}$, $\mathbf{W}$, and $\mathbf{C}$ are correlated noise, white noise, and correlation matrix, respectively, then to generate spatially correlated noise $\hat{\mathbf{W}} = \mathbf{C}^{\frac{1}{2}}\mathbf{W}$ and for temporally correlated noise $\hat{\mathbf{W}} = \mathbf{W}\mathbf{C}^{\frac{1}{2}}$. Hence, considering temporally correlated noise in the presence of spatially uncorrelated signals is an easy extension of the work presented in this chapter.

3

Performance Analysis of Multiantenna Underlay Cognitive Radio under Spatially Correlated Interfering Signals

Contents

3.1 System Model 43
3.2 Channel Capacity 46
3.3 Outage Probability 47
3.4 Results and Discussion 50
3.5 Summary 52

In Chapter 2, the spectrum sensing schemes are proposed for interweave paradigm based CRNs considering spatially correlated noise at multiantenna SR. In this chapter, we consider an underlay paradigm based CRN with multiantenna users and spatially correlated interfering channels at link between ST and PR. Initial works in the literature have investigated various transmission schemes to optimize the performance of SUs under interference power limit of PR [12, 64]. With the introduction of multiantenna nodes, many factors such as antenna correlation, interference power, interference cancelation and mitigation schemes affect the performance of both primary and secondary systems. Performance analysis of underlay paradigm based multiantenna CRN under spatially correlated interfering signals is available in [71, 72]. The prewhitening of spatially correlated interfering signals is performed and its effect on the primary and secondary systems performance is analyzed in [71, 72]. The authors have proposed the prewhitening schemes of interfering channels between ST and PR and shown that it reduces the interfering signal power at PR. It has been claimed that the prewhitening of interfering channels is beneficial for underlay paradigm based underlay CRN. These analyses consider the perfect knowledge of channel information at ST about the link between PR and itself. Due to feedback latencies and mobility of the users the channel information may get outdated [66, 67]. Analysis of a CRN considering prewhitening of spatially correlated interfering signals with outdated channel information can provide actual performance of the primary and secondary systems from the implementation point view.

In this chapter, we analyze the performance of an underlay paradigm based CRN with multiantenna users under spatially correlated interfering channels between ST and PR. The classical matrix-inverse based prewhitening scheme is used to decorrelate the interfering signals received at PR. Performance of both primary and secondary systems is analyzed considering prewhitening scheme based on outdated channel information of the ST-PR link. We derive the analytical expressions for outage probability and channel capacity for both primary and secondary systems. The analytical results are validated by the closely matched analytical and simulation plots. The effect of outdatedness in channel information and prespecified interference outage probability on the performance of both primary and secondary systems are shown.

Moreover, we also compare the effect of outdated channel information and interference from primary transmissions on the performance of secondary system.

3.1 System Model

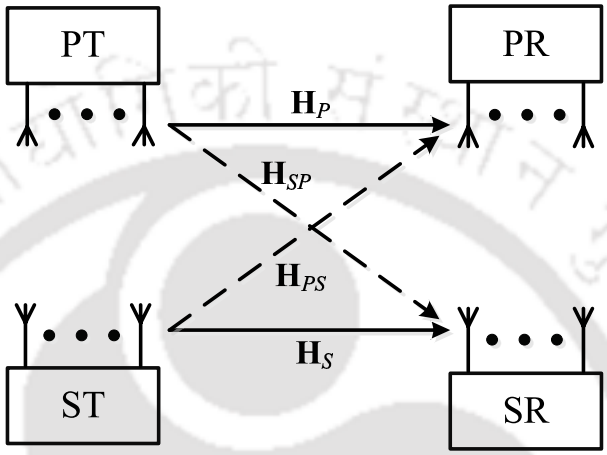

Figure 3.1: A typical diagram of an underlay paradigm based CRN with multiantenna at all nodes.

We consider an underlay paradigm based CRN which consists of a primary and a secondary networks as shown in Fig. 3.1. The primary and the secondary networks comprise of a PT, a PR, and an ST, an SR, respectively, with M number of antennas at all nodes. In underlay paradigm based CRN, the SU can transmit simultaneously with the PU such that the interference induced at the PU node falls within a certain limit. The peak interference power constraint (PIPC) of the primary network is denoted by Q. In addition, ST is also constrained by the maximum transmission power constraint (MTPC) which arises due to the non-linearity of the power amplifier of the transmitter. The MTPC of ST is represented by P_M. We also consider the harmful interference at PR and SR due to the SU and PU transmissions, respectively. In this scenario, the received signals at PR and SR, denoted by $\mathbf{y}_P$ and $\mathbf{y}_S$ (both are $M \times 1$), respectively, are given as

$$\mathbf{y}_P = \sqrt{\eta_P}\sqrt{P_P}\mathbf{H}_P\mathbf{s}_P + \sqrt{\eta_{PS}}\sqrt{P_S}\mathbf{H}_{PS}\mathbf{s}_S + \mathbf{w}_P \tag{3.1}$$

$$\mathbf{y}_S = \sqrt{\eta_S}\sqrt{P_S}\mathbf{H}_S\mathbf{s}_S + \sqrt{\eta_{SP}}\sqrt{P_P}\mathbf{H}_{SP}\mathbf{s}_P + \mathbf{w}_S \tag{3.2}$$

where η_P, η_S, η_{PS}, and η_{SP} are average channel gains of PT $\rightarrow$ PR, ST $\rightarrow$ SR, ST $\rightarrow$ PR, and PT $\rightarrow$ SR links, respectively. P_P and P_S are the transmission powers of PT and ST, respectively. $\mathbf{s}_P$ and $\mathbf{s}_S$ are the $M \times 1$ transmitted signal vector from PT and ST, respectively. $\mathbf{w}_P$ and $\mathbf{w}_S$ are the $M \times 1$ additive white Gaussian noise (AWGN) vector at PR and SR, respectively, whose entries independently belong to $\mathcal{CN}(0, N_0)$. $\mathbf{H}_P$, $\mathbf{H}_S$, $\mathbf{H}_{PS}$, and $\mathbf{H}_{SP}$ are the $M \times M$ channel matrices of PT $\rightarrow$ PR, ST $\rightarrow$ SR, ST $\rightarrow$ PR, and PT $\rightarrow$ SR links, respectively. The channel coefficients are assumed to be flat-fading Rayleigh distributed which are considered to be constant for the symbol duration.

We assume that the channel gains $\mathbf{H}_P$ and $\mathbf{H}_S$ are perfectly known to the PR and the SR but unknown to the PT and the ST, respectively. In this case, the optimal MIMO transmission scheme allocates equal transmission power to each antenna at PT and ST. Let us define a signal vector $\mathbf{u}_P$ of $M \times 1$ whose elements are independently Gaussian distributed with $\mathrm{E}[\mathbf{u}_P \mathbf{u}_P^H] = \mathbf{I}_M$ and the normalized signal transmitted from PT is $\mathbf{s}_P = \frac{\mathbf{u}_P}{\|\mathbf{u}_P\|}$. Thus, the covariance matrix of PT is $\mathrm{E}[\mathbf{s}_P \mathbf{s}_P^H] = \frac{1}{M}\mathbf{I}_M$. Similarly, the normalized signal transmitted from ST is $\mathbf{s}_S = \frac{\mathbf{u}_S}{\|\mathbf{u}_S\|}$ with $\mathrm{E}[\mathbf{u}_S \mathbf{u}_S^H] = \mathbf{I}_M$ and $\mathrm{E}[\mathbf{s}_S \mathbf{s}_S^H] = \frac{1}{M}\mathbf{I}_M$.

The interfering signals received by PR are assumed to be spatially correlated whereas the other received signals by PR and SR are considered to be spatially uncorrelated [71, 72]. This scenario may appear in several communication systems. For example, consider a two-tier macrocell-femtocell heterogeneous network where macrocell and femtocell deployments adopt licensed and unlicensed networks concept, respectively [109, 110]. All nodes of both networks consist of multiple antenna elements. In this scenario, it may happen that the transmitter at femtocell is located very near to the receiver at macrocell which may cause the poorly scattered signals received by the receiver at macrocell. Due to the poor scattering, the signals received by the macrocell-receiver have small angular spread at the adjacent antenna elements. This causes the spatially correlated signals received by the macrocell-receiver [44]. Whereas, the rich scattering between other links causes the spatially uncorrelated received signals. Another communication system, where this scenario may occur, can be a coexisting primary and secondary networks with multiple colocated SU nodes. In this scenario, the interfering signals received by

PR from multiple colocated SU nodes may get spatially correlated.

Motivated by the above mentioned scenarios, we assume the interfering signals at PR to be spatially correlated. Further, we consider a prewhitening scheme at ST so that the interfering signal at PR becomes uncorrelated. The prewhitening scheme uses the channel information of the ST-PR link which is considered to be outdated due to the feedback latencies and mobility of the users. We consider an outdated channel model as [68]

$$\mathbf{H}_{PS} = \rho_0 \hat{\mathbf{H}}_{PS} + \sqrt{1-\rho_0^2}\tilde{\mathbf{H}}_{PS} \tag{3.3}$$

where $\hat{\mathbf{H}}_{PS}$ is $M \times M$ outdated channel matrix of the ST-PR link which is known to the ST. The elements of $\hat{\mathbf{H}}_{PS}$ are iid complex Gaussian random variables. ρ_0 denotes the correlation coefficient between $\mathbf{H}_{PS}$ and $\hat{\mathbf{H}}_{PS}$, and assumed to be known. $\tilde{\mathbf{H}}_{PS}$ is the channel mismatch which is uncorrelated with $\hat{\mathbf{H}}_{PS}$. The elements of $\tilde{\mathbf{H}}_{PS}$ are complex Gaussian distributed with zero-mean and unit variance. The channel at PT-SR link is also considered to be known to SR through spectrum scanning by the SU nodes.

In the prewhitening scheme based on outdated channel information, the transmitted signal vector from ST is multiplied by $\hat{\mathbf{H}}_{PS}^{-1}$ to decorrelate the interfering signal vector received at PR. Thus, the normalized transmitted signal vector from ST is $\hat{\mathbf{s}}_S = \frac{\hat{\mathbf{H}}_{PS}^{-1}\mathbf{u}_S}{\sqrt{T_0}}$ where the normalizing term T_0 is defined as

$$T_0 = \mathrm{E}[||\hat{\mathbf{H}}_{PS}^{-1}\mathbf{u}_S||^2] = \mathrm{tr}\{\hat{\mathbf{H}}_{PS}^{-1}\mathrm{E}[\mathbf{u}_S\mathbf{u}_S^H](\hat{\mathbf{H}}_{PS}^{-1})^H\} = \mathrm{tr}\{(\hat{\mathbf{H}}_{PS}^H\hat{\mathbf{H}}_{PS})^{-1}\}. \tag{3.4}$$

Now, the signals received at PR and SR are given by

$$\mathbf{y}_P = \sqrt{\eta_P}\sqrt{P_P}\mathbf{H}_P\mathbf{s}_P + \sqrt{\eta_{PS}}\sqrt{P_S}\mathbf{H}_{PS}\frac{\hat{\mathbf{H}}_{PS}^{-1}\mathbf{u}_S}{\sqrt{T_0}} + \mathbf{w}_P \tag{3.5}$$

$$\mathbf{y}_S = \sqrt{\eta_S}\sqrt{P_S}\mathbf{H}_S\frac{\hat{\mathbf{H}}_{PS}^{-1}\mathbf{u}_S}{\sqrt{T_0}} + \sqrt{\eta_{SP}}\sqrt{P_P}\mathbf{H}_{SP}\mathbf{s}_P + \mathbf{w}_S, \tag{3.6}$$

respectively. Moreover, in case of outdated channel information of the ST-PR link, it is difficult to maintain the PIPC of PR. This is because it cannot be guaranteed that the interference power at PR will still fall within a prespecified interference limit. We consider an approach based on

the power margin in PIPC of PR as in [67–70] where ST adapts its transmission power such that the PR can maintain a predetermined interference outage probability. The interference outage probability is defined as the probability that the interference power at PR exceeds a prespecified limit and is denoted by ε_o. Thus, the transmission power of ST, constraint by both MTPC of ST and PIPC of PR with power margin factor κ_m which satisfies the predetermined interference outage probability, can be defined as [68, 70]

$$P_S = \min\left(P_M, \frac{\kappa_m Q}{\max\limits_{\{i,j\}\in\{1,..,M\}}\{|(\hat{H}_{PS})_{i,j}|^2\}}\right) \tag{3.7}$$

For a prespecified ε_o, κ_m can be calculated numerically using the expression given by (for detail, refer to Appendix A.4)

$$\begin{aligned}\varepsilon_o = &\exp\left(-\frac{Q}{P_M\eta_{PS}}\right) - \exp\left(-\frac{Q}{P_M\eta_{PS}}\right) Q_0\left(\sqrt{\frac{2\rho_0^2 Q}{(1-\rho_0^2)P_M\eta_{PS}}}, \sqrt{\frac{2\kappa_m Q}{(1-\rho_0^2)P_M\eta_{PS}}}\right) \\ &- \frac{t_0}{r_0}Q_0\left(\sqrt{\frac{(l_0-r_0)Q}{2P_M}}, \sqrt{\frac{(l_0+r_0)Q}{2P_M}}\right) + \frac{t_0+r_0}{2r_0}\exp\left(-\frac{l_0 Q}{2P_M}\right) I_0\left(\frac{2\rho_0 Q\sqrt{\kappa_m}}{(1-\rho_0^2)P_M\eta_{PS}}\right).\end{aligned} \tag{3.8}$$

Here, $l_0 = \frac{2(1+\kappa_m)}{(1-\rho_0^2)\eta_{PS}}$, $r_0 = \frac{2\sqrt{(1+\kappa_m)^2-4\kappa_m\rho_0^2}}{(1-\rho_0^2)\eta_{PS}}$, and $t_0 = \frac{2(1-\kappa_m)}{(1-\rho_0^2)\eta_{PS}}$.

3.2 Channel Capacity

The channel capacity is the maximum of the mutual information with respect to the input distribution. It defines the maximum achievable rate at which information can be reliably transmitted over a communication channel [111, 112]. Capacity per unit bandwidth of a MIMO system with channel information at the receiver and deterministic channel gain, denoted by $\mathbf{H}$, is given by [112]

$$\frac{C}{B} = \log_2 \det\left(\mathbf{I}_M + \frac{E_s}{MN_0}\mathbf{H}\mathbf{R}_s\mathbf{H}^H\right) \quad \text{bits/s/Hz} \tag{3.9}$$

where B and E_s denote the channel bandwidth and the energy of transmitted signals, respectively. $\mathbf{R}_s$ is the autocorrelation matrix of transmitted signal vector $\mathbf{s}$, defined as $\mathbf{R}_s = \mathrm{E}[\mathbf{s}\mathbf{s}^H]$.

Further, when channels vary randomly, i.e., $\mathbf{H}$ is a random matrix, then the channel capacity is also time-varying. In this case, the ergodic MIMO channel capacity can be evaluated by its time average. In practice, it is assumed that the time-varying channel is an ergodic process and then the ergodic channel capacity is calculated as [112]

$$\frac{C_{er}}{B} = \mathrm{E}\left[\log_2 \det\left(\mathbf{I}_M + \frac{E_s}{MN_0}\mathbf{H}\mathbf{R}_s\mathbf{H}^H\right)\right] \quad \text{bits/s/Hz} \tag{3.10}$$

which is known as ergodic channel capacity. Moreover, the unit of the capacity is bits/s/Hz (also written as bps/Hz) when it is calculated in logarithm with base 2. When the capacity is measured in natural logarithm, the unit will be nats/s/Hz.

We derive the channel capacities of PU and SU systems for the considered underlay CRN as described below. Symbolic complexity is reduced by using C_P and C_S instead of C_P/B and C_S/B for the capacities per unit bandwidth of PU and SU systems, respectively.

Lemma 1: When prewhitening is performed at ST using outdated channel information of the ST-PR link, the channel capacities of the PU and SU systems are given by

$$C_P = \log_2 \det\left(\mathbf{I}_M + \frac{\eta_P P_P T_0}{M(\eta_{PS} P_S \beta + N_0 T_0)}\mathbf{H}_P\mathbf{H}_P^H\right) \tag{3.11}$$

$$C_S = \log_2 \det\left(\mathbf{I}_M + \frac{M\eta_S P_S}{T_0}\mathbf{H}_S(\hat{\mathbf{H}}_{PS}^H\hat{\mathbf{H}}_{PS})^{-1}\mathbf{H}_S^H(\eta_{SP}P_P\mathbf{H}_{SP}\mathbf{H}_{SP}^H + MN_0\mathbf{I}_M)^{-1}\right), \tag{3.12}$$

respectively, where $\beta = \rho_0^2 + T_0(1-\rho_0^2)$.

Proof. Refer to Appendix A.5. □

For $\rho_0 = 1$, i.e., when channel information about ST-PR link is perfect at ST, the channel capacity of the PU system derived in *Lemma 1* is similar to the expression derived in [71] except that P_S is not considered to be constrained by the MTPC of ST and the PIPC of PR in [71].

3.3 Outage Probability

The outage occurs when the instantaneous signal-to-interference-plus-noise ratio (SINR) at the receiver falls below a certain threshold. In the following subsections, we derive the outage

probabilities of both PU and SU systems.

3.3.1 Outage Probability of PU System

The instantaneous SINR at PR is given by

$$SINR_{PR} = \frac{\eta_P P_P \text{tr}\{\text{E}[(\mathbf{H}_{PS}\mathbf{s}_P)^H(\mathbf{H}_{PS}\mathbf{s}_P)]\}}{\eta_{PS} P_S \text{tr}\{\text{E}[(\mathbf{H}_{PS}\hat{\mathbf{s}}_S)^H(\mathbf{H}_{PS}\hat{\mathbf{s}}_S)]\} + MN_0} = \frac{T_0\eta_P P_P \text{tr}\{\mathbf{H}_P^H\mathbf{H}_P\}}{M^2(\eta_{PS}P_S\beta + N_0T_0)}. \tag{3.13}$$

The first term in the denominator of (3.13) can be calculated similar to (A.40) (Appendix A.5) which results in (A.47). The outage probability of the PU system, denoted by $P_{O,PU}$, is obtained when SINR at PR falls below an outage threshold λ' and is given by

$$P_{O,PU}(\lambda') = \Pr(SINR_{PR} < \lambda') = F_{\text{tr}\{\mathbf{H}_P^H\mathbf{H}_P\}}(\lambda) \tag{3.14}$$

where $\lambda = \frac{\lambda' M^2(\eta_{PS}P_S\beta + N_0T_0)}{T_0\eta_P P_P}$ and $F(\cdot)$ denotes the CDF. $\text{tr}\{\mathbf{H}_P^H\mathbf{H}_P\}$ is central chi-square distributed with $2M^2$ degree of freedom (DOF). The element of $\mathbf{H}_P$ is distributed as complex Gaussian zero-mean and unit variance. Thus, the mean and the variance of $\text{tr}\{\mathbf{H}_P^H\mathbf{H}_P\}$ can be calculated as [108]

$$\begin{aligned}\text{E}[\text{tr}\{\mathbf{H}_P^H\mathbf{H}_P\}] &= \text{DOF} \times \frac{\text{variance of each element of } \mathbf{H}_P}{2} = M^2 \\ \text{var}[\text{tr}\{\mathbf{H}_P^H\mathbf{H}_P\}] &= 2(\text{DOF}) \times \left(\frac{\text{variance of each element of } \mathbf{H}_P}{2}\right)^2 = M^2.\end{aligned} \tag{3.15}$$

This distribution can also be represented by the gamma distribution, denoted by $G(\alpha, \theta)$ where α and θ are the shape and the scale parameters, respectively, and are determined as [113]

$$\begin{aligned}\alpha &= \frac{\text{E}^2[\text{tr}\{\mathbf{H}_P^H\mathbf{H}_P\}]}{\text{var}[\text{tr}\{\mathbf{H}_P^H\mathbf{H}_P\}]} = M^2 \\ \theta &= \frac{\text{var}[\text{tr}\{\mathbf{H}_P^H\mathbf{H}_P\}]}{\text{E}[\text{tr}\{\mathbf{H}_P^H\mathbf{H}_P\}]} = 1.\end{aligned} \tag{3.16}$$

Using (3.16), the CDF of $\text{tr}\{\mathbf{H}_P^H\mathbf{H}_P\}$ can be determined as

$$F_{\text{tr}\{\mathbf{H}_P^H\mathbf{H}_P\}}(\lambda) = \frac{\gamma(\alpha, \lambda/\theta)}{\Gamma(k)} = \frac{\gamma(M^2, \lambda)}{\Gamma(M^2)} \tag{3.17}$$

which is also the expression of $P_{O,PU}$. Here, $\gamma(\cdot,\cdot)$ and $\Gamma(\cdot)$ denote the lower incomplete and the complete gamma functions, respectively.

3.3.2 Outage Probability of SU System

The instantaneous SINR at SR is given by

$$\begin{aligned} SINR_{SR} &= \frac{\eta_S P_S \mathrm{tr}\{\mathrm{E}[(\mathbf{H}_S\hat{\mathbf{s}}_S)^H(\mathbf{H}_S\hat{\mathbf{s}}_S)]\}}{\eta_{SP} P_P \mathrm{tr}\{\mathrm{E}[(\mathbf{H}_{SP}\mathbf{s}_P)^H(\mathbf{H}_{SP}\mathbf{s}_P)]\} + MN_0} \\ &= \frac{M\eta_S P_S \mathrm{tr}\{(\mathbf{H}_S\hat{\mathbf{H}}_{PS}^{-1})^H(\mathbf{H}_S\hat{\mathbf{H}}_{PS}^{-1})\}}{T_0(\eta_{SP} P_P \mathrm{tr}\{\mathbf{H}_{SP}^H\mathbf{H}_{SP}\} + M^2N_0)}. \end{aligned} \tag{3.18}$$

The outage probability of SU system, denoted as $P_{O,SU}$, is obtained as

$$P_{O,SU}(\lambda') = \Pr\left(SINR_{SR} < \lambda'\right) = F_{\mathrm{tr}\{(\mathbf{H}_S\hat{\mathbf{H}}_{PS}^{-1})^H(\mathbf{H}_S\hat{\mathbf{H}}_{PS}^{-1})\}}(\lambda) \tag{3.19}$$

where $\lambda = \frac{\lambda' T_0(\eta_{SP}P_P \mathrm{tr}\{\mathbf{H}_{SP}^H\mathbf{H}_{SP}\}+M^2N_0)}{M\eta_S P_S}$. The distribution of $\mathrm{tr}\{(\mathbf{H}_S\hat{\mathbf{H}}_{PS}^{-1})^H(\mathbf{H}_S\hat{\mathbf{H}}_{PS}^{-1})\}$ is analytically intractable as the elements of $\mathbf{H}_S\hat{\mathbf{H}}_{PS}^{-1}$ are non-identically distributed. We derive an approximate distribution when the elements of $\mathbf{H}_S\hat{\mathbf{H}}_{PS}^{-1}$ are assumed to be identically distributed. In Fig. 3.2, the CDFs of $\mathrm{tr}\{(\mathbf{H}_S\hat{\mathbf{H}}_{PS}^{-1})^H(\mathbf{H}_S\hat{\mathbf{H}}_{PS}^{-1})\}$ are plotted for both identically and non-identically distributed elements (denoted by approximated analytical and simulated, respectively, in Fig. 3.2). It is observed that the plots are closely matched in both scenarios when $M = 2$ and $M = 4$, which validates the assumption made for approximate analysis.

Further, the mean and the covariance of $\mathbf{H}_S\hat{\mathbf{H}}_{PS}^{-1}$ are determined as $\mathrm{E}[\mathbf{H}_S\hat{\mathbf{H}}_{PS}^{-1}] = \mathbf{0}$ and $\mathrm{cov}[\mathbf{H}_S\hat{\mathbf{H}}_{PS}^{-1}] = \mathrm{tr}\{(\hat{\mathbf{H}}_{PS}^H\hat{\mathbf{H}}_{PS})^{-1}\}\mathbf{I}_M = T_0\mathbf{I}_M$, respectively. Considering the identical distribution for each element of $\mathbf{H}_S\hat{\mathbf{H}}_{PS}^{-1}$, the mean and the variance of each element are zero and $\frac{T_0}{M}$, respectively. Now, $\mathrm{tr}\{(\mathbf{H}_S\hat{\mathbf{H}}_{PS}^{-1})^H(\mathbf{H}_S\hat{\mathbf{H}}_{PS}^{-1})\}$ is approximated to the central chi-square distributed with $2M^2$ DOF. Similar to (3.15), the mean and the variance of $\mathrm{tr}\{(\mathbf{H}_S\hat{\mathbf{H}}_{PS}^{-1})^H(\mathbf{H}_S\hat{\mathbf{H}}_{PS}^{-1})\}$ are determined as MT_0 and T_0^2, respectively. This can also be represented in the form of gamma distribution with parameters $\alpha = M^2$ and $\theta = \frac{T_0}{M}$, calculated similar to (3.16). Hence, the CDF of $\mathrm{tr}\{(\mathbf{H}_S\hat{\mathbf{H}}_{PS}^{-1})^H(\mathbf{H}_S\hat{\mathbf{H}}_{PS}^{-1})\}$ which is also an expression of $P_{O,SU}$ is approximated to the CDF

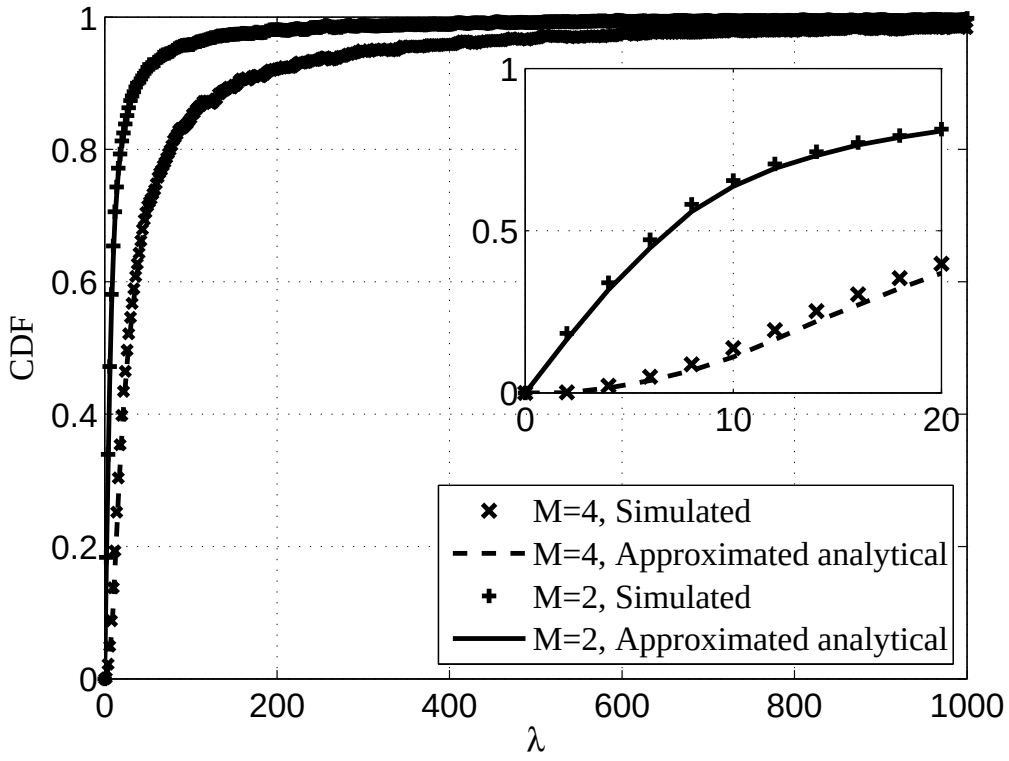

Figure 3.2: CDF plots for SU system with varying λ when $M = 2$ and 4. The magnified plots for $\lambda \leq 20$ are shown as the inset.

of a gamma variate [113] and is given by

$$F_{\mathrm{tr}\{(\mathbf{H}_S\hat{\mathbf{H}}_{PS}^{-1})^H(\mathbf{H}_S\hat{\mathbf{H}}_{PS}^{-1})\}}(\lambda) \approx \frac{\gamma\left(M^2, \frac{\lambda M}{T_0}\right)}{\Gamma(M^2)}. \tag{3.20}$$

3.4 Results and Discussion

The parameters used for simulations are $M = 2$, $P_P = 5$ dBm, $Q = 8$ dBm, $\eta_P = \eta_S = \eta_{PS} = 0$ dB, $\lambda' = 0$ dB and $N_0 = 1$. The ergodic capacities of SU and PU systems (denoted by E$[C_S]$ and E$[C_P]$, respectively) and the average outage probability (AOP) of SU and PU systems (denoted by AOP-SU and AOP-PU, respectively) are evaluated over 10^5 coherence time intervals of the channel.

In Fig. 3.3(a) (Fig. 3.3(b)), it is observed that as P_M increases, E$[C_S]$ (AOP-SU in Fig. 3.3(b)) and E$[C_P]$ (AOP-PU in Fig. 3.3(b)) improves and degrades, respectively, till $P_S = P_M$

as given in (3.7). For further increase in P_M, when $\rho_0 \neq 1$, E$[C_S]$ (AOP-SU in Fig. 3.3(b)) and E$[C_P]$ (AOP-PU in Fig. 3.3(b)) degrades and improves, respectively, and then attain a saturation for higher values of P_M. This trend in performances is due to the varying power margin factor κ_m with respect to varying P_M. For $\rho_0 = 1$, further increment in P_M causes a maximum and minimum capacities (AOPs in Fig. 3.3(b)) for the SU and PU systems, respectively. The performance limits in this case are controlled by the PIPC of PR and channel gain of ST-PR link. Moreover, E$[C_S]$ and AOP-SU degrade as ρ_0 decreases. This is due to the fact that as ρ_0 decreases, κ_m decreases to avoid any instantaneous violation of peak interference power at PR. For the PU system, E$[C_P]$ and AOP-PU degrade as ρ_0 decreases till $P_S = P_M$. This is because β increases as ρ_0 decreases. However, for further increase in P_M, E$[C_P]$ and AOP-PU improve as ρ_0 decreases. In this case, the effect of ρ_0 on the PU system is introduced through two factors: P_S and β. As ρ_0 decreases κ_m decreases, and hence P_S decreases which causes the degraded interfering signal power at PR. However, β increases as ρ_0 decreases which leads to the degraded performance of the PU system. β can be considered as the measure of quality of whitening of spatially correlated interfering signals where the smaller β implies the better whitening. Hence, as ρ_0 decreases, the effect of degraded interfering power at PR dominates over the effect of weak whitening which finally leads to the improved performance of the PU system. Moreover, it can be seen that the simulated plots are closely matched with the analytical plots. In Fig. 3.3(b), for the SU system, slight mismatch between approximate analytical and simulated plots is observed. This is due to the mismatch caused by the approximate analysis of outage probability in the lower region of $\lambda \leq 20$ shown as the inset of Fig. 3.2. For higher values of λ, mismatch is negligible.

From Figs. 3.4(a) and 3.4(b), it is observed that the ergodic capacities and the average outage probabilities of both SU and PU systems are sensitive to ρ_0, especially to high ρ_0. Hence, the performance of both systems are sensitive to the accuracy of channel information of the ST-PR link. Moreover, as ε_o increases, E$[C_S]$ and AOP-SU in Figs. 3.4(a) and 3.4(b), respectively, improve due to increased transmission power of ST for sufficiently higher P_M. Whereas, the degraded performance of the PU system can be observed from the figures as ε_o

increased. Thus, a suitable value of interference outage constraint must be chosen so that the performance of the PU system does not degrade much. Further, the effect of interfering signal power at SR is observed in Fig. 3.5. From the figures, it can be observed that performance degradation of the SU system is significant in case of outdated channel information when ε_o falls from 10% to 1% vis-a-vis the loss due to interference from PT. Hence, the effect of outdated channel information is more harmful than the interference induced by the PU system on the performance of the SU system.

3.5 Summary

In this chapter, we have analyzed the performance of an underlay paradigm based multiantenna CRN with prewhitened interfering signals using outdated channel information. We have derived the analytical expressions for channel capacity and outage probability for both PU and SU systems under PIPC of PR and MTPC of ST. The analytical results are validated by the simulation results. To avoid any instantaneous violation in PIPC of PR we have employed a power margin factor with PIPC so that a prespecified interference outage can be maintained at PR. We have shown the performance of both PU and SU systems for different ρ_0 and varying P_M. The variations in the performance of both systems are resulted from varying power margin factor as ρ_0 and P_M vary. It has shown that both PU and SU systems are sensitive to the accuracy of channel information of ST-PR link. It has also shown that, for the SU system, the effect of outdated channel information is more vulnerable with respect to the interference due to PU transmissions. Moreover, the work discussed in this chapter considered M number of antennas at all nodes, however, a more general scenario considering different number of antennas at different nodes can be analyzed likewise.

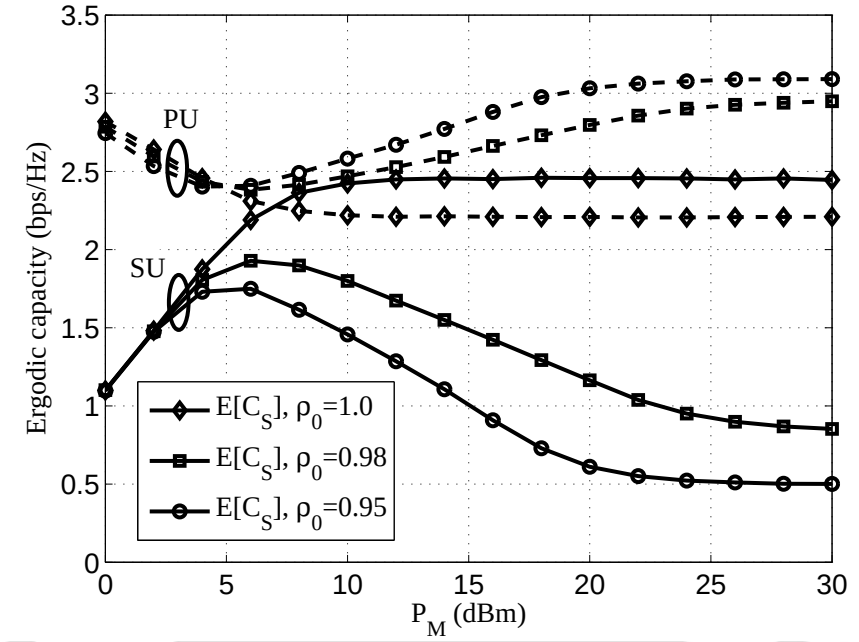

(a)

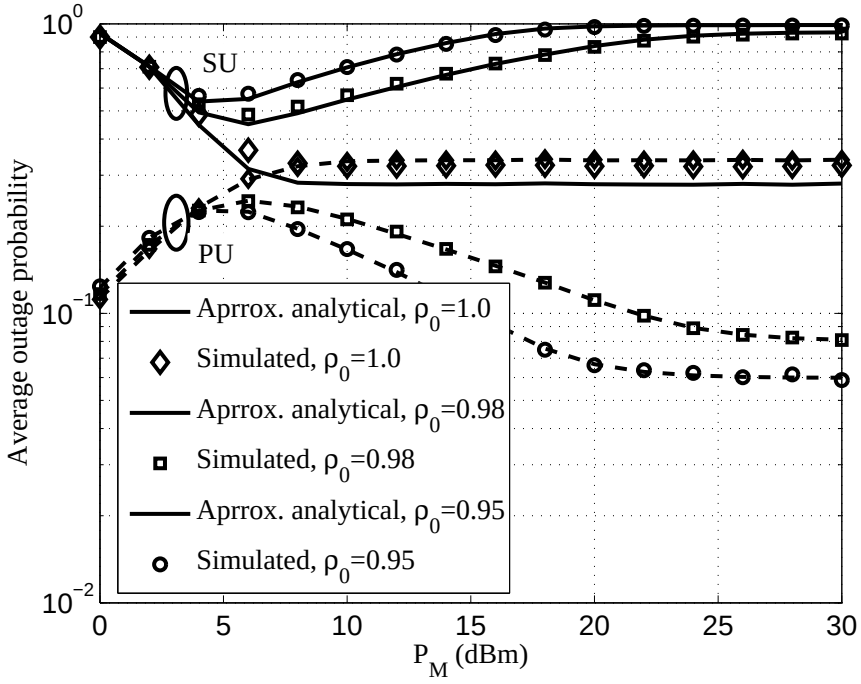

(b)

Figure 3.3: (a) Ergodic capacities and (b) average outage probabilities of the PU and SU systems versus P_M for various ρ_0, when $\eta_{SP} = -5$ dB and $\varepsilon_o = 1\%$.

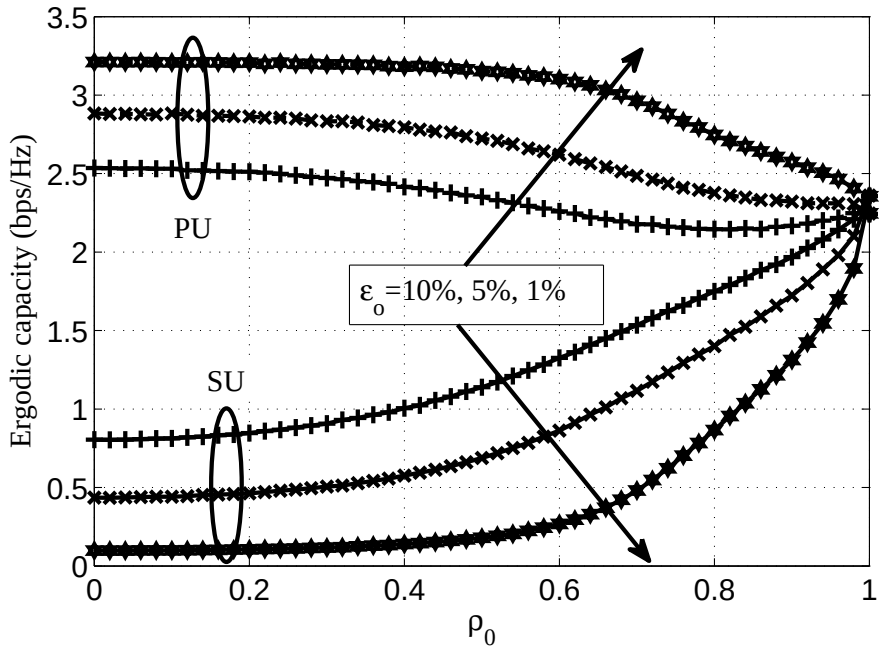

(a)

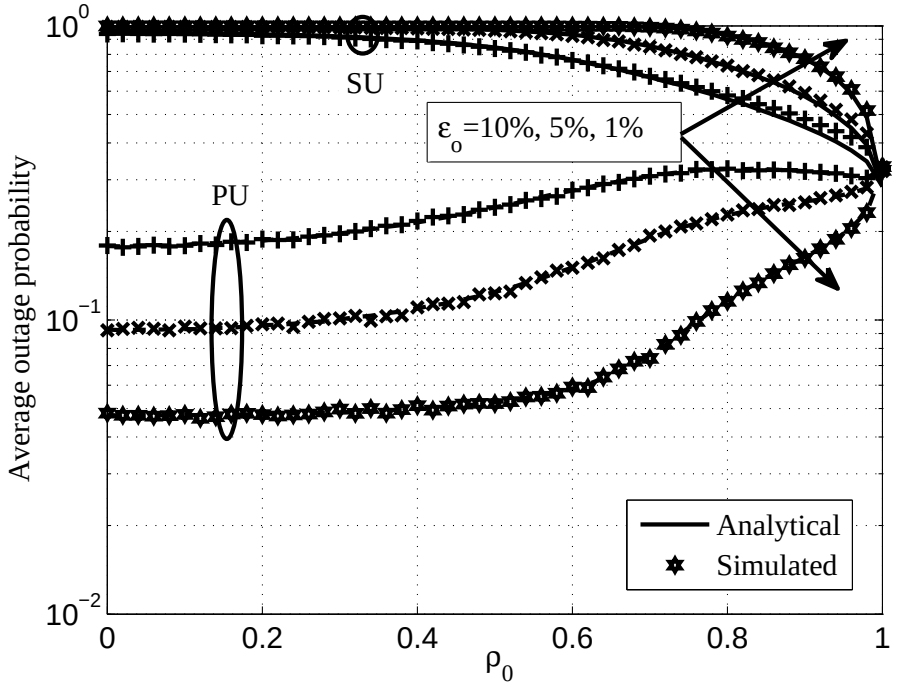

(b)

Figure 3.4: (a) Ergodic capacities and (b) average outage probabilities of the PU and SU systems versus ρ_0 for various values of ε_o, when $\eta_{SP} = -5$ dB and $P_M = 8$ dBm.

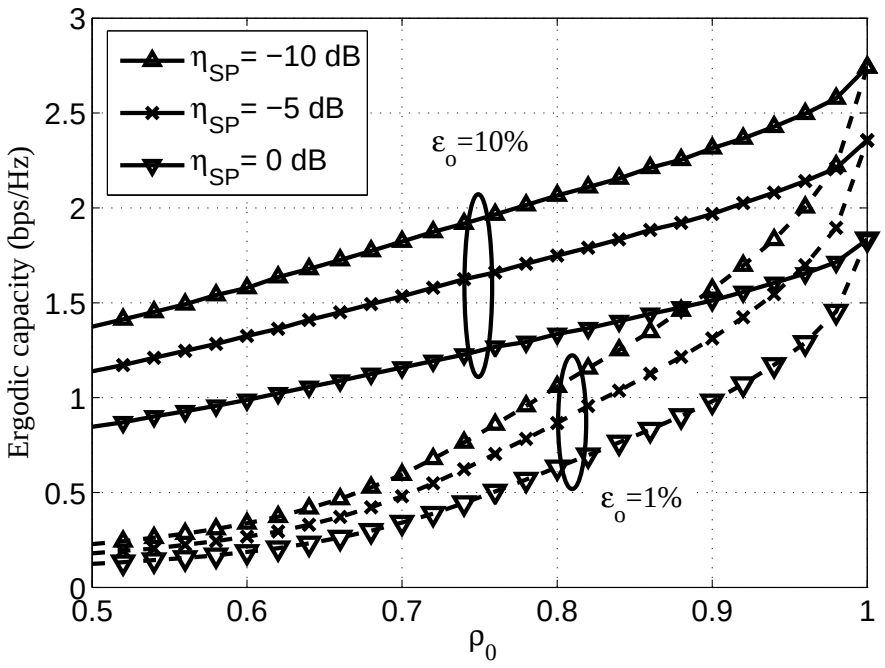

(a)

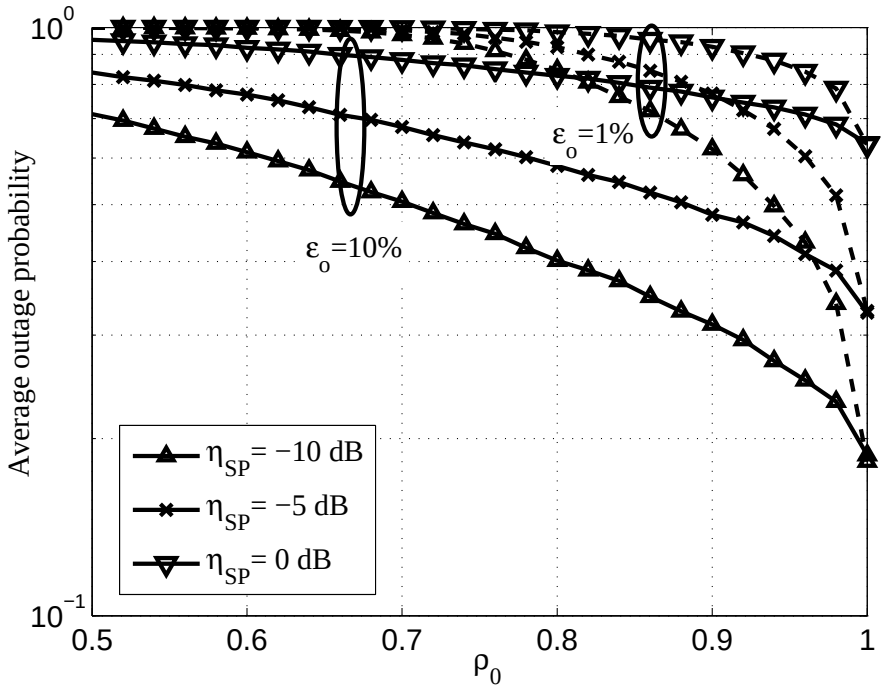

(b)

Figure 3.5: (a) Ergodic capacities and (b) average outage probabilities of the SU system versus ρ_0 for various values of η_{SP} and ε_o when $P_M = 8$ dBm.

4

Performance Analysis of Dual-Hop Cognitive Cooperative Relay Networks over κ-μ Shadowed Channels

Contents

4.1 System Model 59
4.2 Outage Probability 62
4.3 Ergodic Capacity 65
4.4 Results and Discussion 69
4.5 Summary 76

In Chapter 3, we have considered direct communication between ST and SR. However, when a direct link between ST and SR is not possible because of deep fading/shadowing or large distance between them, relay can be employed to setup a link between them. In this chapter, we consider a dual-hop cooperative relay-assisted underlay CRN unlike the direct communication between ST and SR in Chapter 3. The performance analyses of the dual-hop relay-assisted underlay CRNs are available in literature [74–97]. These analyses have considered Rayleigh, Nakagami-m, and η-μ distributions to model the small-scale fading scenario. The works discussed so far in literature for dual-hop relay-assisted underlay CRNs have not incorporated the effect of large-scale shadowing to analyze its performance. However, it has been shown that the real-world wireless channels can be accurately modeled by the composite multipath fading and shadowing channel models [98,114]. Hence, the analysis of cognitive cooperative relay networks under composite multipath fading and shadowing channels can provide actual performance of the considered system.

In this chapter, we consider a dual-hop cooperative relay-assisted underlay CRN which comprises a PR, an ST, an SR, and a secondary relay node with single antenna at all nodes. With multiantenna at SR and spatially correlated channels, the analysis is presented in the next chapter. The DF protocol is employed at the relay node. The physical channels among all nodes are considered to be multipath faded and shadowed and are compositely modeled by the κ-μ shadowed distribution. We assume the perfect knowledge of channel at ST-PR link unlike the outdated channel information as in Chapter 3 because of mathematical tractability. We derive the closed-form expressions for the CDFs of the received SNR at relay and SR under peak interference power constraint (PIPC) of PR. Using this CDF expressions, the closed-form expression for outage probability is obtained. The analytical expression for the ergodic capacity is also derived in the form of sum of infinite-series. Two special cases are investigated when the channels at links ST$\rightarrow$relay and relay$\rightarrow$SR are Nakagami-m and Rician/Rician-shadowed distributed. In both cases, simpler expressions for the outage probability and the ergodic capacity are obtained. The analytical derivations are validated by Monte-Carlo simulations. We have shown that the severity of fading/shadowing at interfering links is favorable to the

SUs communications up to a certain value of PIPC of PR. Beyond this value of PIPC, the SUs communications are benefited under less severe fading/shadowing at the interfering links.

4.1 System Model

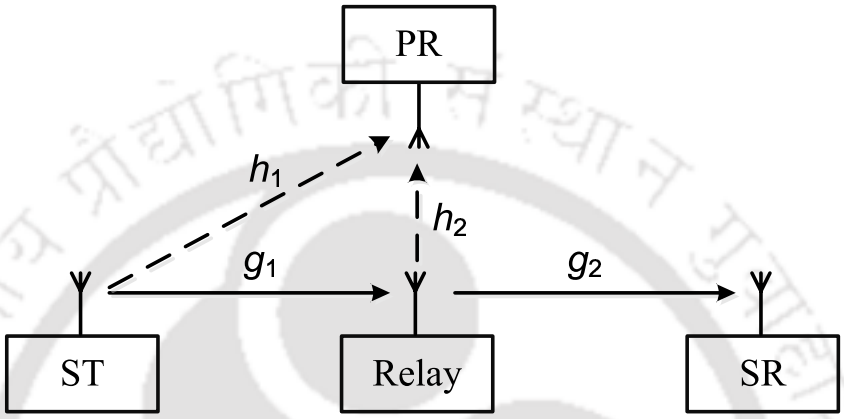

Figure 4.1: A typical diagram of a dual-hop relay-assisted underlay CRN with single antenna at all nodes.

We consider a dual-hop DF relay-assisted underlay CRN which comprises a secondary network and a PR as shown in Fig. 4.1. The secondary network consists of an ST, an SR, and a secondary DF relay. The SU nodes are considered to be located far away from PT. Thus, there exists a negligible interference from the PT to the SU nodes [78], [81], [86], [87], [94], [97], or this weak interference can be included with the noise terms of the SU nodes [115]. As in [78], [80], [81], [88], [94], [97], we assume that there is no direct link between the ST and the SR. This scenario may appear in the presence of severe fading/shadowing at ST-SR link or due to the large distance between ST and SR. All PU and SU nodes are equipped with a single antenna operating in half-duplex mode. The transmission of signals from ST to SR is executed in two different time frames. In the first time frame, ST broadcasts its signals to relay, and the relay node decodes the transmitted message based on the received signals. Then, the relay node re-encodes the message and forwards it to SR in the second time frame.

4.1.1 Power Allocation and End-to-End SNR

In an underlay paradigm based cognitive cooperative relay network, the ST and the relay nodes transmit its signals such that the interference induced at PR is within a certain limit. The peak interference power that can be tolerated by the PR is denoted by Q. For analytical tractability, we assume that there is no maximum transmission power constraint (MTPC) on the ST and the relay as considered in [52], [86], [87]. Thus, the transmission power of the ST and the relay, denoted by P_{ST} and P_R, respectively, is constrained only by the peak interference power of PR, and is given by $P_{ST}\left|h_1\right|^2 \leq Q$ and $P_R\left|h_2\right|^2 \leq Q$. Here, h_1 and h_2 are the channel coefficients of the ST→PR and the relay→PR links, respectively. Hence, the maximum allowable transmission powers of the ST and the relay are given by $P_{ST} = \frac{Q}{|h_1|^2}$ and $P_R = \frac{Q}{|h_2|^2}$, respectively. The instantaneous transmission power of the ST and the relay is constrained by Q rather the average transmission power for the purpose of restricting any instantaneous violation of the interfering power constraint of PR. Note that, to implement the PIPC of PR, the ST and the relay nodes require the knowledge of h_1 and h_2, respectively. This channel information can be exchanged between the PR and the SU nodes through collaboration where the PR directly feedbacked this channel information to the ST and the relay nodes [65], [67]. In this work, we assume that the ST and the relay nodes have perfect knowledge of the channel information of ST-PR and relay-PR links, respectively. Now, the instantaneous SNR at the relay and the SR is given by

$$\gamma_R = \frac{Q\left|g_1\right|^2}{N_0\left|h_1\right|^2}, \quad \gamma_{SR} = \frac{Q\left|g_2\right|^2}{N_0\left|h_2\right|^2}, \tag{4.1}$$

respectively. Here, g_1 and g_2 are the channel coefficients of the ST→relay and the relay→SR links, respectively. N_0 denotes the noise power both at the SR and the relay nodes. The end-to-end instantaneous SNR, denoted by γ_{e2e}, of the dual-hop DF relay-assisted underlay CRN is given by

$$\gamma_{e2e} = \min(\gamma_R, \gamma_{SR}). \tag{4.2}$$

4.1.2 Channel Model

We consider a physical channel which is assumed to have clusters of waves. In each cluster, multipath waves are considered which have scattered waves with identical power and a dominant component with arbitrary power. The dominant components of all clusters may fluctuate randomly due to shadowing. This physical channel can be modeled by the κ-μ shadowed distribution where the line-of-sight (LOS) multipath fading and the shadowing are modeled by the Rician and the Nakagami-m distributions, respectively [98]. The κ-μ shadowed distribution includes the one-sided Gaussian, Rayleigh, Nakagami- m, Rician, Rician shadowed, and κ-μ distributions as its particular cases. It has been shown that the κ-μ shadowed channel model is good-fit to describe the human body shadowing in body centric device-to-device (D2D) cellular communication where the users equipments are often located at the low elevation and in close proximity of the user's body [114]. The κ-μ shadowed fading model has also been shown to have good-fit to the land mobile satellite channel's experimental data and the underwater acoustic communication channels, as shown in [98].

Furthermore, the channels among all nodes are assumed to be independent. The power of the channel coefficients of all links is κ-μ shadowed distributed with arbitrary fading/shadowing parameters which is denoted by $\{|g_i|^2, |h_i|^2\} \sim S_{\kappa\mu}(\bar{\gamma}_i; \kappa_i, \mu_i, m_i)$. $\bar{\gamma}_i$ and (κ_i, μ_i, m_i) are the average channel power and the shaping parameters, respectively, where i$\in$[1,4] for the links ST$\rightarrow$relay, relay$\rightarrow$SR, ST$\rightarrow$PR, and relay$\rightarrow$PR, respectively. The PDF of the κ-μ shadowed distribution is given by [98], [101]

$$f_X(x) = \frac{\phi_1^{m-\mu} x^{\mu-1}}{\phi_2^m \Gamma(\mu)} e^{-\frac{x}{\phi_1}} {}_1F_1\left(m; \mu; \frac{(\phi_2 - \phi_1)\, x}{\phi_1 \phi_2}\right) \tag{4.3}$$

where $\phi_1 = \frac{\bar{\gamma}}{\mu(1+\kappa)}$, $\phi_2 = \frac{(\mu\kappa+m)\bar{\gamma}}{\mu(1+\kappa)m}$, and ${}_1F_1(\cdot)$ denotes the Kummer confluent hypergeometric function. Moreover, the κ-μ shadowed distribution is tightly approximated by the gamma distribution, denoted as $G(\alpha, \theta)$, with parameters given by [101] $\alpha = \frac{m\mu(1+\kappa)^2}{m+\mu\kappa^2+2m\kappa}$ and $\theta = \frac{\bar{\gamma}}{\alpha}$. The CDF of the gamma distribution is given by

$$F_X(x) = \frac{x^\alpha}{\theta^\alpha \Gamma(\alpha+1)} {}_1F_1\left(\alpha; \alpha+1; \frac{-x}{\theta}\right). \tag{4.4}$$

4.2 Outage Probability

The outage of a dual-hop DF relay-assisted underlay CRN occurs when the end-to-end SNR falls below a minimum threshold γ_{th}, and is given by

$$\begin{aligned} P_O(\gamma_{th}) &= \Pr(\min(\gamma_R, \gamma_{SR}) \leq \gamma_{th}) \\ &= 1 - (1 - F_{\gamma_R}(\gamma_{th}))(1 - F_{\gamma_{SR}}(\gamma_{th})) \end{aligned} \tag{4.5}$$

where $\Pr(\cdot)$ denotes the probability. $F_{\gamma_R}(\cdot)$ and $F_{\gamma_{SR}}(\cdot)$ are the CDFs of the SNR at relay and SR, respectively. γ_{th} is the outage threshold. Now, the CDF of the SNR at the relay can be calculated as

$$\begin{aligned} F_{\gamma_R}(\gamma_{th}) = \Pr(\gamma_R \leqslant \gamma_{th}) &= \Pr\left(\frac{Q|g_1|^2}{N_0|h_1|^2} \leqslant \gamma_{th}\right) \\ &= 1 - \Pr\left(\frac{|h_1|^2}{|g_1|^2} \leq \frac{Q}{\gamma_{th}N_0}\right) \\ &= 1 - \int_0^\infty F_{|h_1|^2}\left(\frac{Qy}{\gamma_{th}N_0}\right) f_{|g_1|^2}(y)dy. \end{aligned} \tag{4.6}$$

Using (4.3) and (4.4), (4.6) is written as

$$F_{\gamma_R}(\gamma_{th}) = 1 - A_1 \int_0^\infty e^{-\frac{y}{\phi_{11}}} y^{\alpha_3+\mu_1-1} {}_1F_1\left(\alpha_3; \alpha_3+1; -\frac{Qy}{\gamma_{th}N_0\theta_3}\right) {}_1F_1\left(m_1; \mu_1; \frac{\phi_{21}-\phi_{11}}{\phi_{21}\phi_{11}}y\right) dy \tag{4.7}$$

where $A_1 = \frac{\phi_{11}^{m_1-\mu_1}}{\phi_{21}^{m_1}\Gamma(\alpha_3+1)\Gamma(\mu_1)}\left(\frac{Q}{\gamma_{th}N_0\theta_3}\right)^{\alpha_3}$, $\phi_{11} = \frac{\bar{\gamma}_1}{\mu_1(1+\kappa_1)}$, $\phi_{21} = \frac{(\mu_1\kappa_1+m_1)\bar{\gamma}_1}{\mu_1(1+\kappa_1)m_1}$, $\alpha_3 = \frac{m_3\mu_3(1+\kappa_3)^2}{m_3+\mu_3\kappa_3^2+2m_3\kappa_3}$, $\theta_3 = \frac{\bar{\gamma}_3}{\alpha_3}$. To solve the integration involved in (4.7), the integral representation of Lauricella function $F_A^{(n)}$ is used, which is given by [116, Eq. 2.4.2]

$$F_A^{(n)}(a, b_1, .., b_n; c_1, .., c_n; x_1, .., x_n) = \frac{1}{\Gamma(a)} \int_0^\infty e^{-t} t^{a-1} {}_1F_1(b_1; c_1; x_1t) \cdots {}_1F_1(b_n; c_n; x_nt)dt, \ \mathrm{Re}(a) > 0. \tag{4.8}$$

Using (4.8) for $n = 2$, $F_A^{(2)} \equiv F_2$, and applying the variable transformation for $\frac{y}{\phi_{11}} = z$, the integration involved in (4.7) can be solved as

$$F_{\gamma_R}(\gamma_{th}) = 1 - \frac{\Gamma(\alpha_3+\mu_1)}{\Gamma(\alpha_3+1)\Gamma(\mu_1)} \left(\frac{Q\phi_{11}}{\gamma_{th}N_0\theta_3}\right)^{\alpha_3} \left(\frac{\phi_{11}}{\phi_{21}}\right)^{m_1} \times F_2\left(\alpha_3+\mu_1, \alpha_3, m_1; \alpha_3+1, \mu_1; -\frac{Q\phi_{11}}{\gamma_{th}N_0\theta_3}, 1-\frac{\phi_{11}}{\phi_{21}}\right) \tag{4.9}$$

where $F_2(\cdot)$ is the type-2 Appell hypergeometric function. The series form of $F_2(\cdot)$ converges when $|x_1|+|x_2| < 1$, i.e., $\frac{\gamma_{th}N_0}{Q} > \frac{\phi_{21}}{\theta_3}$, which may not be always satisfied. Hence, we use [116, Eq. 4.2.2]

$$F_2(a, b_1, b_2; c_1, c_2; x_1, x_2) = (1-x_1)^{-a} F_2\left(a, c_1-b_1, b_2; c_1, c_2; \frac{x_1}{x_1-1}, \frac{x_2}{1-x_1}\right) \tag{4.10}$$

for the convergent evaluation of $F_2(\cdot)$. The final expression of $F_{\gamma_R}(\gamma_{th})$ is obtained as

$$F_{\gamma_R}(\gamma_{th}) = 1 - A_2 F_2\left(\alpha_3+\mu_1, 1, m_1, \alpha_3+1, \mu_1; \frac{Q\phi_{11}}{Q\phi_{11}+\gamma_{th}N_0\theta_3}, \frac{(\phi_{21}-\phi_{11})\gamma_{th}N_0\theta_3}{\phi_{21}(Q\phi_{11}+\gamma_{th}N_0\theta_3)}\right) \tag{4.11}$$

where $A_2 = \frac{Q^{\alpha_3}\phi_{11}^{m_1+\alpha_3}(\gamma_{th}N_0\theta_3)^{\mu_1}\Gamma(\alpha_3+\mu_1)}{\phi_{21}^{m_1}(Q\phi_{11}+\gamma_{th}N_0\theta_3)^{\alpha_3+\mu_1}\Gamma(\alpha_3+1)\Gamma(\mu_1)}$. Similar expression is obtained in [101] for the outage probability analysis of the interference limited communication system in the presence of multiple co-channel interferers. Similarly, $F_{\gamma_{SR}}(\gamma_{th})$ can be determined by the appropriate replacement of the variables as $(\bar{\gamma}_1; \kappa_1, \mu_1, m_1) \to (\bar{\gamma}_2; \kappa_2, \mu_2, m_2)$, $(\bar{\gamma}_3; \kappa_3, \mu_3, m_3) \to (\bar{\gamma}_4; \kappa_4, \mu_4, m_4)$, $(\phi_{11}, \phi_{21}) \to (\phi_{12}, \phi_{22})$, $(\alpha_3, \theta_3) \to (\alpha_4, \theta_4)$, and $A_2 \to A_2'$ in (4.11). Finally, using (4.5), the outage probability is obtained, and is given by

$$\begin{aligned} P_O(\gamma_{th}) = 1 &- \frac{\Gamma(\alpha_3+\mu_1)\Gamma(\alpha_4+\mu_2)}{\Gamma(\alpha_3+1)\Gamma(\alpha_4+1)\Gamma(\mu_1)\Gamma(\mu_2)} \\ &\times \frac{Q^{\alpha_3+\alpha_4}\phi_{11}^{m_1+\alpha_3}\phi_{12}^{m_2+\alpha_4}\theta_3^{\mu_1}\theta_4^{\mu_2}(\gamma_{th}N_0)^{\mu_1+\mu_2}}{\phi_{21}^{m_1}\phi_{22}^{m_2}(Q\phi_{11}+\gamma_{th}N_0\theta_3)^{\alpha_3+\mu_1}(Q\phi_{12}+\gamma_{th}N_0\theta_4)^{\alpha_4+\mu_2}} \\ &\times F_2\left(\alpha_3+\mu_1, 1, m_1; \alpha_3+1, \mu_1; \frac{Q\phi_{11}}{Q\phi_{11}+\gamma_{th}N_0\theta_3}, \frac{(\phi_{21}-\phi_{11})\gamma_{th}N_0\theta_3}{\phi_{21}(Q\phi_{11}+\gamma_{th}N_0\theta_3)}\right) \\ &\times F_2\left(\alpha_4+\mu_2, 1, m_2; \alpha_4+1, \mu_2; \frac{Q\phi_{12}}{Q\phi_{12}+\gamma_{th}N_0\theta_4}, \frac{(\phi_{22}-\phi_{12})\gamma_{th}N_0\theta_4}{\phi_{22}(Q\phi_{12}+\gamma_{th}N_0\theta_4)}\right). \end{aligned} \tag{4.12}$$

The $F_2(\cdot)$ function can be evaluated using its integral representation in terms of the Gauss hypergeometric function ${}_2F_1(\cdot)$ given in [117, Eq. 20]. Note that, the Gauss hypergeometric

function is available in most of the common software. It can also be calculated using series representation in terms of ${}_2F_1(\cdot)$ [117, Eq. 82] up to N finite terms such that the error involved is less than 10^{-5}. Moreover, in the sequel, we derive outage probability expression in the simpler forms for some special cases.

Special case I: We consider a scenario when the channels at ST→relay and relay→SR links are Nakagami-m distributed. For further analysis, the $F_2(\cdot)$ function is represented by the sum of ${}_2F_1(\cdot)$ functions given by [117, Eq. 82]

$$F_2(a,b_1,b_2;c_1,c_2;x_1,x_2)=\sum_{k=0}^{\infty}\frac{(a)_k(b_2)_k}{(c_2)_k k!}x_2^k\ {}_2F_1(a+k,b_1;c_1;x_1),\quad |x_1|+|x_2|<1 \tag{4.13}$$

where $(\cdot)_k$ denotes the Pochhammer symbol, defined as [116, Eq. 1.1.3]

$$(y)_k=y(y+1)\cdots(y+k-1),\quad k\geq 0.$$

Using (4.13), $F_{\gamma_R}(\gamma_{th})$, obtained in (4.11), can be expressed as

$$F_{\gamma_R}(\gamma_{th})=1-A_2\sum_{j=0}^{\infty}\frac{(\alpha_3+\mu_1)_j(m_1)_j}{j!(\mu_1)_j}\left(\frac{\gamma_{th}N_0\theta_3}{Q\phi_{11}+\gamma_{th}N_0\theta_3}\right)^j \times\left(1-\frac{\phi_{11}}{\phi_{21}}\right)^j {}_2F_1\left(\alpha_3+\mu_1+j,1;\alpha_3+1;\frac{Q\phi_{11}}{Q\phi_{11}+\gamma_{th}N_0\theta_3}\right). \tag{4.14}$$

For this special case, as the channels at ST→relay and relay→SR links are Nakagami-m distributed: $\{\kappa_1,\kappa_2\}\to 0$ and $\{m_1,m_2\}\to\infty$. Thus, $\phi_{11}=\phi_{21}=\frac{\bar{\gamma}_1}{\mu_1}$ and $\phi_{12}=\phi_{22}=\frac{\bar{\gamma}_2}{\mu_2}$. Hence, $F_{\gamma_R}(\gamma_{th})$ in (4.14) can be simplified as

$$F_{\gamma_R}(\gamma_{th})=1-A_3\ {}_2F_1\left(\alpha_3+\mu_1,1;\alpha_3+1;\frac{Q\phi_{11}}{Q\phi_{11}+\gamma_{th}N_0\theta_3}\right) \tag{4.15}$$

where $A_3=\frac{Q^{\alpha_3}\bar{\gamma}_1^{\alpha_3}(\gamma_{th}N_0\theta_3\mu_1)^{\mu_1}\Gamma(\alpha_3+\mu_1)}{(Q\bar{\gamma}_1+\gamma_{th}N_0\theta_3\mu_1)^{\alpha_3+\mu_1}\Gamma(\alpha_3+1)\Gamma(\mu_1)}$. Similarly, $F_{\gamma_{SR}}(\gamma_{th})$ can be obtained simply by replacing the variables for the next hop between relay and SR. Finally, the outage probability in this scenario, denoted by $P_O^{C1}(\gamma_{th})$, is obtained as

$$P_O^{C1}(\gamma_{th})=1-A_3A_3'\ {}_2F_1\left(\alpha_3+\mu_1,1;\alpha_3+1;\frac{Q\phi_{11}}{Q\phi_{11}+\gamma_{th}N_0\theta_3}\right) \times {}_2F_1\left(\alpha_4+\mu_2,1;\alpha_4+1;\frac{Q\phi_{12}}{Q\phi_{12}+\gamma_{th}N_0\theta_4}\right) \tag{4.16}$$

which is simply the product of two ${}_2F_1(\cdot)$ functions. Here, A_3' is the constant analogous to A_3 and is obtained by replacing the variables for the next hop between relay and SR.

Special case II: For this case, we consider the channels at ST→relay and relay→SR links are Rician or Rician shadowed distributed, i.e., $\mu_1 = \mu_2 = 1$. The following property of the $F_2(\cdot)$ function is used [118, Sec 9.4, Eq. 107]

$$F_2(a, b_1, b_2; a, c; x_1, x_2) = (1 - x_1)^{-b_1} F_1\left(b_2, b_1, a - b_1; c; \frac{x_2}{1 - x_1}, x_2\right) \tag{4.17}$$

where $F_1(\cdot)$ is the type-1 Appell hypergeometric function. Using (4.17), $F_{\gamma_R}(\gamma_{th})$, obtained in (4.11), can be expressed as

$$F_{\gamma_R}(\gamma_{th}) = 1 - A_4\ F_1\left(m_1, 1, \alpha_3; 1; 1 - \frac{\phi_{11}}{\phi_{21}}, \frac{(\phi_{21} - \phi_{11})\gamma_{th} N_0 \theta_3}{\phi_{21}(Q\phi_{11} + \gamma_{th} N_0 \theta_3)}\right) \tag{4.18}$$

where $A_4 = \frac{Q^{\alpha_3} \phi_{11}^{m_1 + \alpha_3}}{\phi_{21}^{m_1} (Q\phi_{11} + \gamma_{th} N_0 \theta_3)^{\alpha_3}}$. Similarly, $F_{\gamma_{SR}}(\gamma_{th})$ can be obtained simply by replacing the variables for the next hop between relay and SR. Finally, the outage probability in this scenario, denoted by $P_O^{C2}(\gamma_{th})$, is obtained as

$$\begin{aligned} P_O^{C2}(\gamma_{th}) = 1 - A_4 A_4' F_1 &\left(m_1, 1, \alpha_3; 1; 1 - \frac{\phi_{11}}{\phi_{21}}, \frac{(\phi_{21} - \phi_{11})\gamma_{th} N_0 \theta_3}{\phi_{21}(Q\phi_{11} + \gamma_{th} N_0 \theta_3)}\right) \\ &\times F_1\left(m_2, 1, \alpha_4; 1; 1 - \frac{\phi_{12}}{\phi_{22}}, \frac{(\phi_{22} - \phi_{12})\gamma_{th} N_0 \theta_4}{\phi_{22}(Q\phi_{12} + \gamma_{th} N_0 \theta_4)}\right) \end{aligned} \tag{4.19}$$

which is simply the product of two $F_1(\cdot)$ functions. Note that, the $F_1(\cdot)$ function can be evaluated directly in Mathematica.

4.3 Ergodic Capacity

In this section, we derive expression for the ergodic capacity of the dual-hop DF relay-assisted underlay CRN. The ergodic capacity is defined as [111], $C_{er} = \mathrm{E}[\ln(1 + \gamma_{e2e})] = \int_0^\infty \Pr[\ln(1 + \gamma_{e2e}) > x]dx = \int_0^\infty \Pr[\gamma_{e2e} > (e^x - 1)]dx$, which leads to

$$C_{er} = \int_0^\infty [1 - P_O(e^x - 1)]dx. \tag{4.20}$$

Using (4.13) and [116, Eq. 1.2.2.2]

$$ {}_2F_1(a,b;c;x) = (1-x)^{c-a-b}\,{}_2F_1(c-a,c-b;c;x), $$

(4.20) can be obtained as

$$ \begin{aligned} C_{er} = A_5 \int_0^{\infty} & \frac{1}{(Q\phi_{11}+(e^x-1)N_0\theta_3)^{\alpha_3}(Q\phi_{12}+(e^x-1)N_0\theta_4)^{\alpha_4}} \\ & \times \sum_{j_1=0}^{\infty} A_6\ {}_2F_1\left(1-\mu_1-j_1,\alpha_3;\alpha_3+1;\frac{Q\phi_{11}}{Q\phi_{11}+(e^x-1)N_0\theta_3}\right) \\ & \times \sum_{j_2=0}^{\infty} A_7\ {}_2F_1\left(1-\mu_2-j_2,\alpha_4;\alpha_4+1;\frac{Q\phi_{12}}{Q\phi_{12}+(e^x-1)N_0\theta_4}\right) dx \end{aligned} \tag{4.21} $$

where $A_5 = \frac{Q^{\alpha_3+\alpha_4}\phi_{11}^{m_1+\alpha_3}\phi_{12}^{m_2+\alpha_4}\Gamma(\alpha_3+\mu_1)\Gamma(\alpha_4+\mu_2)}{\phi_{21}^{m_1}\phi_{22}^{m_2}\Gamma(\alpha_3+1)\Gamma(\alpha_4+1)\Gamma(\mu_1)\Gamma(\mu_2)}$, $A_6 = \frac{(\alpha_3+\mu_1)_{j_1}(m_1)_{j_1}}{j_1!(\mu_1)_{j_1}}\left(1-\frac{\phi_{11}}{\phi_{21}}\right)^{j_1}$, and $A_7 = \frac{(\alpha_4+\mu_2)_{j_2}(m_2)_{j_2}}{j_2!(\mu_2)_{j_2}}\left(1-\frac{\phi_{12}}{\phi_{22}}\right)^{j_2}$. Further, the series form of ${}_2F_1(\cdot)$ given by [116, Eq. 1.1.2]

$$ {}_2F_1(a,b;c;x) = \sum_{k=0}^{\infty} \frac{(a)_k(b)_k x^k}{k!(c)_k} $$

is used in (4.21). Then, (4.21) can be written as

$$ \begin{aligned} C_{er} = A_5 \int_0^{\infty} \sum_{j_1=0}^{\infty} A_6 \sum_{j_2=0}^{\infty} A_7 \sum_{j_3=0}^{\infty} A_8 & \frac{(Q\phi_{11})^{j_3}}{(Q\phi_{11}+(e^x-1)N_0\theta_3)^{\alpha_3+j_3}} \\ & \times \sum_{j_4=0}^{\infty} A_9 \frac{(Q\phi_{12})^{j_4}}{(Q\phi_{12}+(e^x-1)N_0\theta_4)^{\alpha_4+j_4}} dx \end{aligned} \tag{4.22} $$

where $A_8 = \frac{(1-\mu_1-j_1)_{j_3}(\alpha_3)_{j_3}}{j_3!(\alpha_3+1)_{j_3}}$ and $A_9 = \frac{(1-\mu_2-j_2)_{j_4}(\alpha_4)_{j_4}}{j_4!(\alpha_4+1)_{j_4}}$. For further simplification, the inner summations are interchanged with the integration (the conditions for interchangeability are satisfied, as shown in Appendix A.6). Thus, (4.22) is given by

$$ \begin{aligned} C_{er} = & A_5 \sum_{j_1=0}^{\infty} A_6 \sum_{j_2=0}^{\infty} A_7 \sum_{j_3=0}^{\infty} A_8 \sum_{j_4=0}^{\infty} A_9 \\ & \times \int_0^{\infty} \frac{Q^{j_3+j_4}\phi_{11}^{j_3}\phi_{12}^{j_4}}{(Q\phi_{11}+(e^x-1)N_0\theta_3)^{\alpha_3+j_3}(Q\phi_{12}+(e^x-1)N_0\theta_4)^{\alpha_4+j_4}} dx. \end{aligned} \tag{4.23} $$

The integration involves in (4.23) is solved in Mathematica in terms of F_1 function, and hence, the final expression of the ergodic capacity is obtained as

$$\begin{aligned} C_{er} =& \frac{Q^{\alpha_3+\alpha_4}\phi_{11}^{m_1+\alpha_3}\phi_{12}^{m_2+\alpha_4}\Gamma(\alpha_3+\mu_1)\Gamma(\alpha_4+\mu_2)}{\phi_{21}^{m_1}\phi_{22}^{m_2}\Gamma(\alpha_3+1)\Gamma(\alpha_4+1)\Gamma(\mu_1)\Gamma(\mu_2)} \sum_{j_1=0}^{\infty} \frac{(\alpha_3+\mu_1)_{j_1}(m_1)_{j_1}}{j_1!(\mu_1)_{j_1}} \left(1-\frac{\phi_{11}}{\phi_{21}}\right)^{j_1} \\ & \times \sum_{j_2=0}^{\infty} \frac{(\alpha_4+\mu_2)_{j_2}(m_2)_{j_2}}{j_2!(\mu_2)_{j_2}} \left(1-\frac{\phi_{12}}{\phi_{22}}\right)^{j_2} \sum_{j_3=0}^{\infty} \frac{(1-\mu_1-j_1)_{j_3}(\alpha_3)_{j_3}Q^{j_3}\phi_{11}^{j_3}}{j_3!(\alpha_3+1)_{j_3}(N_0\theta_3)^{\alpha_3+j_3}} \\ & \times \sum_{j_4=0}^{\infty} \frac{(1-\mu_2-j_2)_{j_4}(\alpha_4)_{j_4}Q^{j_4}\phi_{12}^{j_4}}{j_4!(\alpha_4+1)_{j_4}(N_0\theta_4)^{\alpha_4+j_4}(\alpha_3+\alpha_4+j_3+j_4)} \\ & \times F_1\left(\alpha_3+\alpha_4+j_3+j_4, \alpha_3+j_3, \alpha_4+j_4; 1+\alpha_3+\alpha_4+j_3+j_4; 1-\frac{Q\phi_{11}}{N_0\theta_3}, 1-\frac{Q\phi_{12}}{N_0\theta_4}\right). \end{aligned} \tag{4.24}$$

Each infinite series involved in (4.24) can be truncated to the sum of first N finite terms such that the error involve is less than 10^{-5}. Further, we derive the simple forms of the ergodic capacity expression for some special cases.

Special case I: Consider the channels at ST→relay and relay→SR links are Nakagami-m distributed. In this scenario, $\phi_{11} = \phi_{21} = \frac{\bar{\gamma}_1}{\mu_1}$ and $\phi_{12} = \phi_{22} = \frac{\bar{\gamma}_2}{\mu_2}$. The final form of the ergodic capacity, denoted by C_{er}^{C1}, is given by

$$\begin{aligned} C_{er}^{C1} =& \frac{Q^{\alpha_3+\alpha_4}\phi_{11}^{\alpha_3}\phi_{12}^{\alpha_4}\Gamma(\alpha_3+\mu_1)\Gamma(\alpha_4+\mu_2)}{\Gamma(\alpha_3+1)\Gamma(\alpha_4+1)\Gamma(\mu_1)\Gamma(\mu_2)} \sum_{j_3=0}^{\infty} \frac{(1-\mu_1)_{j_3}(\alpha_3)_{j_3}Q^{j_3}\phi_{11}^{j_3}}{j_3!(\alpha_3+1)_{j_3}(N_0\theta_3)^{\alpha_3+j_3}} \\ & \times \sum_{j_4=0}^{\infty} \frac{(1-\mu_2)_{j_4}(\alpha_4)_{j_4}Q^{j_4}\phi_{12}^{j_4}}{j_4!(\alpha_4+1)_{j_4}(N_0\theta_4)^{\alpha_4+j_4}(\alpha_3+\alpha_4+j_3+j_4)} \\ & \times F_1\left(\alpha_3+\alpha_4+j_3+j_4, \alpha_3+j_3, \alpha_4+j_4; 1+\alpha_3+\alpha_4+j_3+j_4; 1-\frac{Q\phi_{11}}{N_0\theta_3}, 1-\frac{Q\phi_{12}}{N_0\theta_4}\right). \end{aligned} \tag{4.25}$$

In this case, the expression of the ergodic capacity involves sum of only two infinite series.

Special case II: When channels at ST→relay and relay→SR links are considered to be Rician or Rician shadowed distributed. In this case, $\mu_1 = \mu_2 = 1$, and thus, $(1-\mu-j)$ is an integer. Using a property of Pochhammer's symbol [118, Sec 1.2, Eq. 12] $(-j)_k = \frac{(-1)^k j!}{(j-k)!}, 0 \le k \le j$ and $(-j)_k = 0, k > j$, the final form of the ergodic capacity in this case, denoted by C_{er}^{C2}, is

obtained as

$$C_{er}^{C2} = \frac{Q^{\alpha_3+\alpha_4}\phi_{11}^{m_1+\alpha_3}\phi_{12}^{m_2+\alpha_4}}{\phi_{21}^{m_1}\phi_{22}^{m_2}} \sum_{j_1=0}^{\infty} \frac{(\alpha_3+1)_{j_1}(m_1)_{j_1}}{(j_1!)^2}\left(1-\frac{\phi_{11}}{\phi_{21}}\right)^{j_1} \sum_{j_2=0}^{\infty} \frac{(\alpha_4+1)_{j_2}(m_2)_{j_2}}{(j_2!)^2}\left(1-\frac{\phi_{12}}{\phi_{22}}\right)^{j_2}$$
$$\times \sum_{j_3=0}^{j_1} \frac{(-j_1)_{j_3}(\alpha_3)_{j_3}Q^{j_3}\phi_{11}^{j_3}}{j_3!(\alpha_3+1)_{j_3}(N_0\theta_3)^{\alpha_3+j_3}} \sum_{j_4=0}^{j_2} \frac{(-j_2)_{j_4}(\alpha_4)_{j_4}Q^{j_4}\phi_{12}^{j_4}}{j_4!(\alpha_4+1)_{j_4}(N_0\theta_4)^{\alpha_4+j_4}(\alpha_3+\alpha_4+j_3+j_4)}$$
$$\times F_1\left(\alpha_3+\alpha_4+j_3+j_4, \alpha_3+j_3, \alpha_4+j_4; 1+\alpha_3+\alpha_4+j_3+j_4; 1-\frac{Q\phi_{11}}{N_0\theta_3}, 1-\frac{Q\phi_{12}}{N_0\theta_4}\right) \tag{4.26}$$

which also involves sum of only two infinite series.

Moreover, the series-form of F_1 function involved in (4.24), (4.25), and (4.26) converges when $\left|1-\frac{Q\phi_{11}}{N_0\theta_3}\right| < 1$ and $\left|1-\frac{Q\phi_{12}}{N_0\theta_4}\right| < 1$. This may not be satisfied for all values of parameters. In the following cases, we employ some transformations of F_1 function so that it becomes convergent.

Case I: When $\left|1-\frac{Q\phi_{11}}{N_0\theta_3}\right| \not< 1$ and $\left|1-\frac{Q\phi_{12}}{N_0\theta_4}\right| \not< 1$, we use a transformation given by [116, Eq. 4.2.4]

$$F_1(a, b_1, b_2; c; x_1, x_2) = (1-x_1)^{-b_1}(1-x_2)^{-b_2}F_1\left(c-a, b_1, b_2; c; \frac{x_1}{x_1-1}, \frac{x_2}{x_2-1}\right).$$

In this case, the F_1 function involved in (4.24), (4.25), and (4.26) is given by

$$F_1\left(\alpha_3+\alpha_4+j_3+j_4, \alpha_3+j_3, \alpha_4+j_4; 1+\alpha_3+\alpha_4+j_3+j_4; 1-\frac{Q\phi_{11}}{N_0\theta_3}, 1-\frac{Q\phi_{12}}{N_0\theta_4}\right)$$
$$= \frac{(N_0\theta_3)^{\alpha_3+j_3}(N_0\theta_4)^{\alpha_4+j_4}}{(Q\phi_{11})^{\alpha_3+j_3}(Q\phi_{12})^{\alpha_4+j_4}}F_1\left(1, \alpha_3+j_3, \alpha_4+j_4; 1+\alpha_3+\alpha_4+j_3+j_4; 1-\frac{N_0\theta_3}{Q\phi_{11}}, 1-\frac{N_0\theta_4}{Q\phi_{12}}\right). \tag{4.27}$$

Case II: When $\left|1-\frac{Q\phi_{11}}{N_0\theta_3}\right| \not< 1$ and $\left|1-\frac{Q\phi_{12}}{N_0\theta_4}\right| < 1$, we use a transformation given by [116, Eq. 4.2.4]

$$F_1(a, b_1, b_2; c; x_1, x_2) = (1-x_1)^{-a}F_1\left(a, c-b_1-b_2, b_2; c; \frac{x_1}{x_1-1}, \frac{x_1-x_2}{x_1-1}\right).$$

In this case, the F_1 function involved in (4.24), (4.25), and (4.26) is expressed as

$$F_1\left(\alpha_3+\alpha_4+j_3+j_4, \alpha_3+j_3, \alpha_4+j_4; 1+\alpha_3+\alpha_4+j_3+j_4; 1-\frac{Q\phi_{11}}{N_0\theta_3}, 1-\frac{Q\phi_{12}}{N_0\theta_4}\right)$$
$$= \left(\frac{N_0\theta_3}{Q\phi_{11}}\right)^{\alpha_3+\alpha_4+j_3+j_4}$$
$$\times F_1\left(\alpha_3+\alpha_4+j_3+j_4, 1, \alpha_4+j_4; 1+\alpha_3+\alpha_4+j_3+j_4; 1-\frac{N_0\theta_3}{Q\phi_{11}}, 1-\frac{\phi_{12}\theta_3}{\phi_{11}\theta_4}\right). \quad (4.28)$$

Case III: When $\left|1-\frac{Q\phi_{11}}{N_0\theta_3}\right| < 1$ and $\left|1-\frac{Q\phi_{12}}{N_0\theta_4}\right| \not< 1$, we use a transformation given by [116, Eq. 4.2.4]

$$F_1(a, b_1, b_2; c; x_1, x_2) = (1-x_1)^{c-a-b_1}(1-x_2)^{-b_2} F_1\left(c-a, c-b_1-b_2, b_2; c; x_1, \frac{x_2-x_1}{x_2-1}\right).$$

In this case, the F_1 function involved in (4.24), (4.25), and (4.26) is obtained as

$$F_1\left(\alpha_3+\alpha_4+j_3+j_4, \alpha_3+j_3, \alpha_4+j_4; 1+\alpha_3+\alpha_4+j_3+j_4; 1-\frac{Q\phi_{11}}{N_0\theta_3}, 1-\frac{Q\phi_{12}}{N_0\theta_4}\right)$$
$$= \frac{(N_0\theta_3)^{\alpha_3+j_3-1}(N_0\theta_4)^{\alpha_4+j_4}}{(Q\phi_{11})^{\alpha_3+j_3-1}(Q\phi_{12})^{\alpha_4+j_4}} F_1\left(1, 1, \alpha_4+j_4; 1+\alpha_3+\alpha_4+j_3+j_4; 1-\frac{Q\phi_{11}}{N_0\theta_3}, 1-\frac{\phi_{11}\theta_4}{\phi_{12}\theta_3}\right). \quad (4.29)$$

4.4 Results and Discussion

In this section, the analytical and the simulated plots are shown to get a better understanding of the effect of fading and shadowing on the considered system model. By varying three shape parameters of the κ-μ shadowed distribution, as shown below in the Table 4.1 [98], the one-sided Gaussian, Rayleigh, Nakagami-m, Rician, Rician shadowed, and κ-μ fading distributions are obtained. For simulations, we take κ=0.001 and m=100 to represent $\kappa\to 0$ and m$\to\infty$, respectively. Moreover, the type-2 Appell hypergeometric function $F_2(\cdot)$ involved in the outage probability expression in (4.12) is evaluated in accurate closed-form using its integral form [117, Eq. 20]. To evaluate the ergodic capacities in (4.24), (4.25), and (4.26), sum of infinite series is truncated to first N finite terms such that the error involved is less than 10^{-5}. The accuracy of the analytical results is validated by close matching of the analytical plots with the corresponding simulation plots. For simulations, 10^5 independent tests are performed, and

Table 4.1: Classical fading distributions obtained from the κ-μ shadowed distribution

Fading distribution	Parameters of the κ-μ shadowed distribution
One-sided Gaussian	$\kappa \to 0$, μ=0.5, m$\to\infty$
Rayleigh	$\kappa \to 0$, μ=1, m$\to\infty$
Nakagami-m	$\kappa \to 0$, μ=m, m$\to\infty$
Rician	κ=K, μ=1, m$\to\infty$
Rician shadowed	κ=K, μ=1, m=m
κ-μ	$\kappa=\kappa$, $\mu=\mu$, m$\to\infty$

finally, its average is taken.

Fig. 4.2 and Fig. 4.3 illustrate the outage probability and the ergodic capacity, respectively, with respect to the peak interference power to noise power ratio, i.e., Q/N_0, under different channel conditions. For both plots, it is considered that the channels at all links are identically distributed. It is observed that, up to a certain value of Q/N_0, the outage probability and the ergodic capacity of the SU system improve under severe channel conditions (this portion is magnified in both plots and shown as the inset of respective figures). The performance improvement in this scenario is achieved due to the fact that, when the peak interference power at PR is low, the severe fading/shadowing at the interference links is favorable to the SUs communication. Beyond this value of Q/N_0, the SU system shows improved performance under less severe channel conditions. In this case, even if the transmission power of the SU nodes is kept lower due to the less severe fading/shadowing at the interference links, the improved channel condition to the SU system causes its improved performance. This implies that when channels at all links are identically distributed, then the severe channel condition is beneficial for the SUs communication up to a certain value of Q/N_0. This value of Q/N_0 depends upon the outage threshold and the channel gains of different links. It is also observed that, beyond this value of Q/N_0, as the value of κ, μ, and m increases—can be seen in cases from Rayleigh to Rician, Rayleigh to Nakagami, and Rician shadowed to Rician, respectively—the performance of the SU system improves. However, the opposite is true for the lower region of Q/N_0.

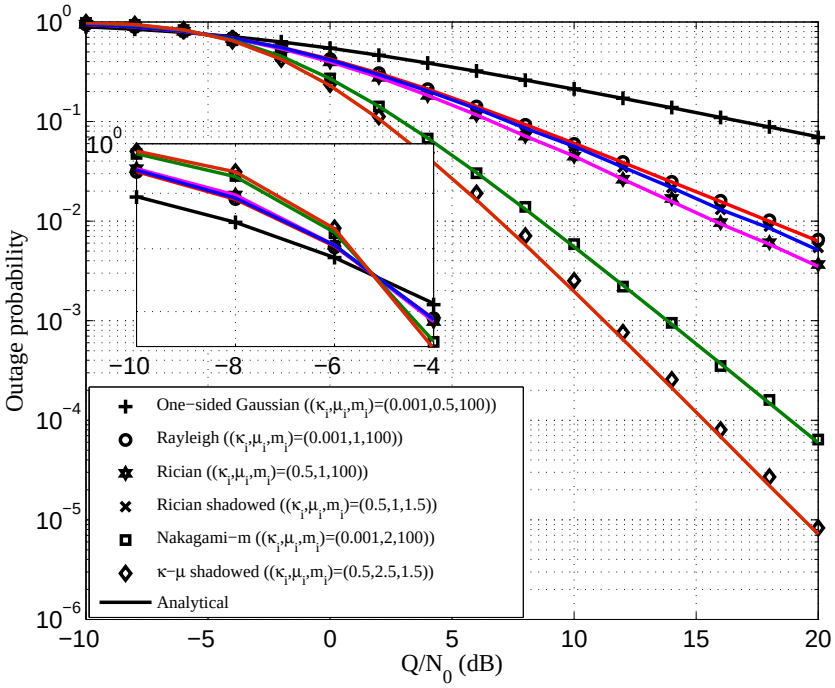

Figure 4.2: Outage probability vs Q/N_0 plots when channels at all links are identically distributed and the outage threshold $\gamma_{th} = -5$ dB. (Solid lines: Analytical and Markers: Simulated).

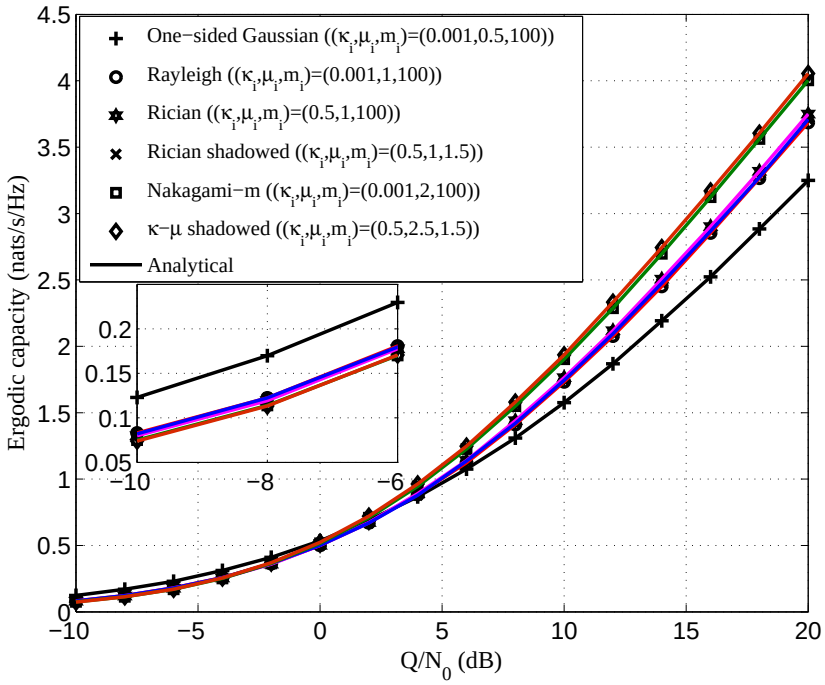

Figure 4.3: Ergodic capacity vs Q/N_0 plots when channels at all links are identically distributed. (Solid lines: Analytical and Markers: Simulated).

The outage probability and the ergodic capacity are shown in Fig. 4.4 and Fig. 4.5, respectively, when the channels at ST→relay and relay→SR links are Nakagami-m distributed (as discussed in Special case I). From the outage probability curve, similar to Fig. 4.2, it is seen that the severe fading/shadowing at the interference link is favorable for the SUs communication up to a certain value of Q/N_0. Beyond this value of Q/N_0, the outage probability improves under less severe fading/shadowing at the interference links. However, the ergodic capacity improves under severe fading/shadowing at the interference links for the given range of Q/N_0. This implies that in this case, the severe fading/shadowing at the interference links is favorable to the SU system both in terms of the outage probability and the ergodic capacity only up to a certain value of Q/N_0. The outage probability and the ergodic capacity are also shown in Fig. 4.6 and Fig. 4.7, respectively, when the channels at ST→relay and relay→SR links are Rician shadowed distributed (as discussed in Special case II). From both plots, it is observed that the severe fading/shadowing at the interference links is favorable to the SU system for the given range of Q/N_0. Moreover, in all scenarios, the analytical plots are closely matched with the simulation plots which validate analytical results obtained in Special cases I and II.

The plots for outage probability and the ergodic capacity are shown in Fig. 4.8 and Fig. 4.9, respectively, for non-identical μ parameters of the SUs communication and the interfering links of two hops. All links are κ-μ shadowed distributed with κ=0.5, m=2, and various μ parameters. From both the figures, it is observed that when the interfering links are severe than the SU's communication links at both hops, the SU system shows improved performance (as in the figures, compare the scenarios when ($\mu_1 = \mu_2 = 3,\ \mu_3 = \mu_4 = 2$) and ($\mu_1 = \mu_2 = 2,\ \mu_3 = \mu_4 = 3$)). This is because when interfering links are severe, the transmission power of the ST and relay nodes can be kept high for a certain PIPC of PR. Additionally, the improved channel conditions of the SUs communication links also encourage the performance improvement to the SU system. Moreover, both the outage probabilities and the ergodic capacities of the SU system are same when all channel parameters are interchanged between two hops (as in the figures, compare the scenarios when ($\mu_1 = \mu_3 = 2,\ \mu_2 = \mu_4 = 3$) and ($\mu_1 = \mu_3 = 3,\ \mu_3 = \mu_4 = 2$)). This implies that in a DF cooperative relay-assisted dual-hop CRN, all channel parameters of

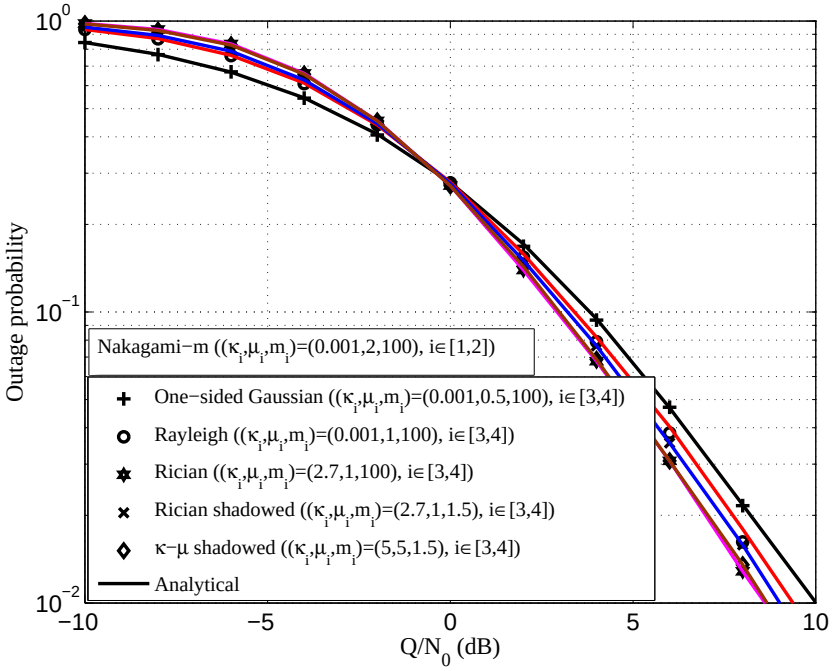

Figure 4.4: Outage probability vs Q/N_0 plots when the channels at ST→relay and relay→SR links are Nakagami-m distributed (Special case I), and $\gamma_{th} = -5$ dB. (Solid lines: Analytical and Markers: Simulated).

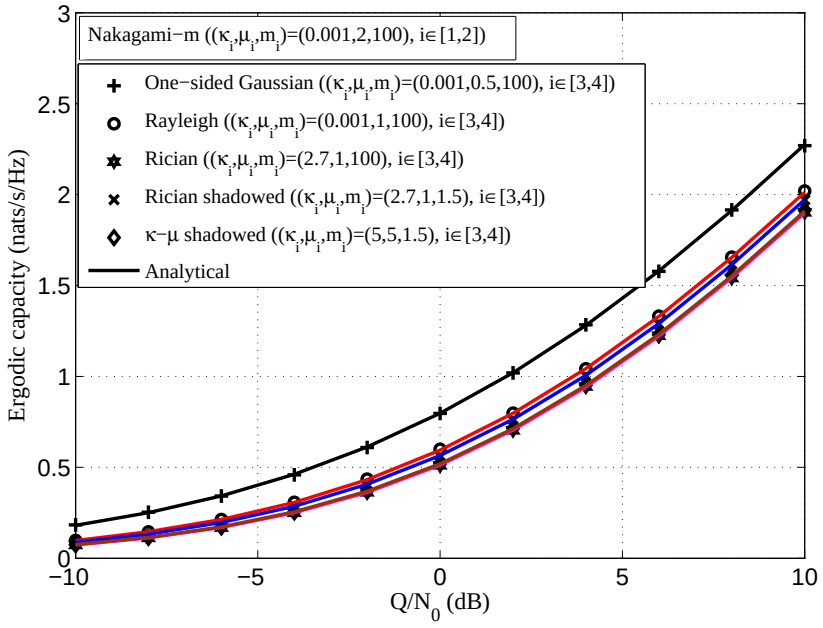

Figure 4.5: Ergodic capacity vs Q/N_0 plots when the channels at ST→relay and relay→SR links are Nakagami-m distributed (Special case I). (Solid lines: Analytical and Markers: Simulated).

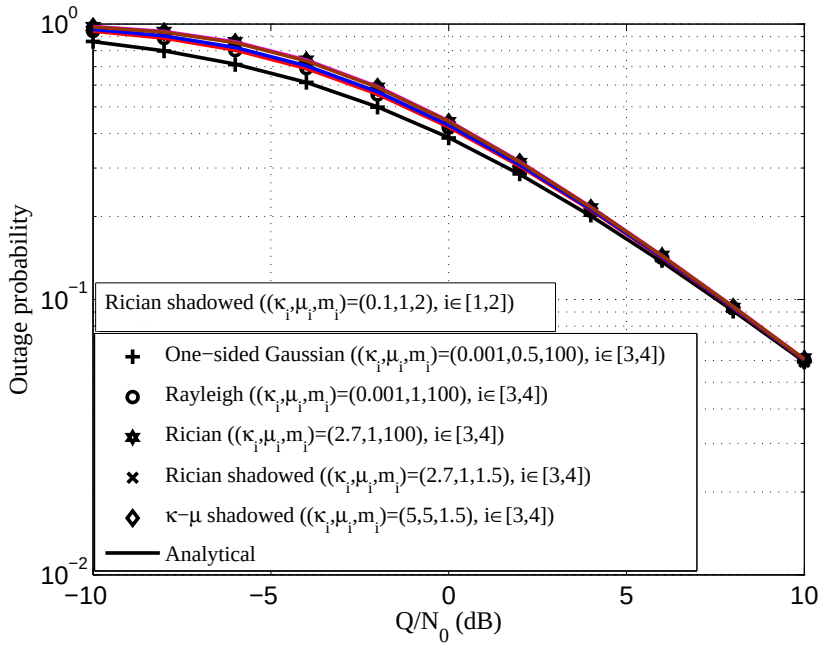

Figure 4.6: Outage probability vs Q/N_0 plots when the channels at ST→relay and relay→SR links are Rician shadowed distributed (Special case II), and $\gamma_{th} = -5$ dB. (Solid lines: Analytical and Markers: Simulated).

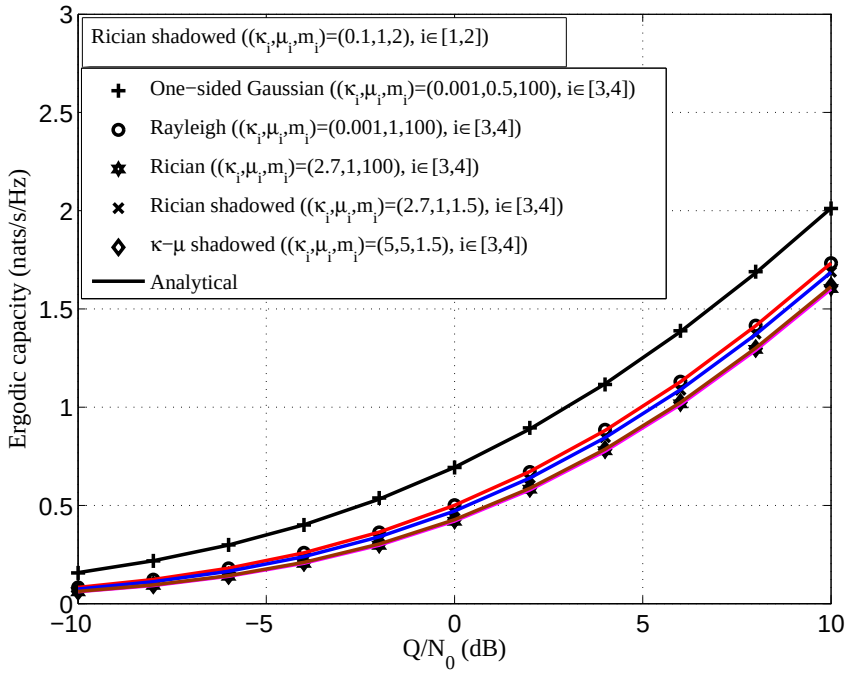

Figure 4.7: Ergodic capacity vs Q/N_0 plots when the channels at ST→relay and relay→SR links are Rician shadowed distributed (Special case II). (Solid lines: Analytical and Markers: Simulated).

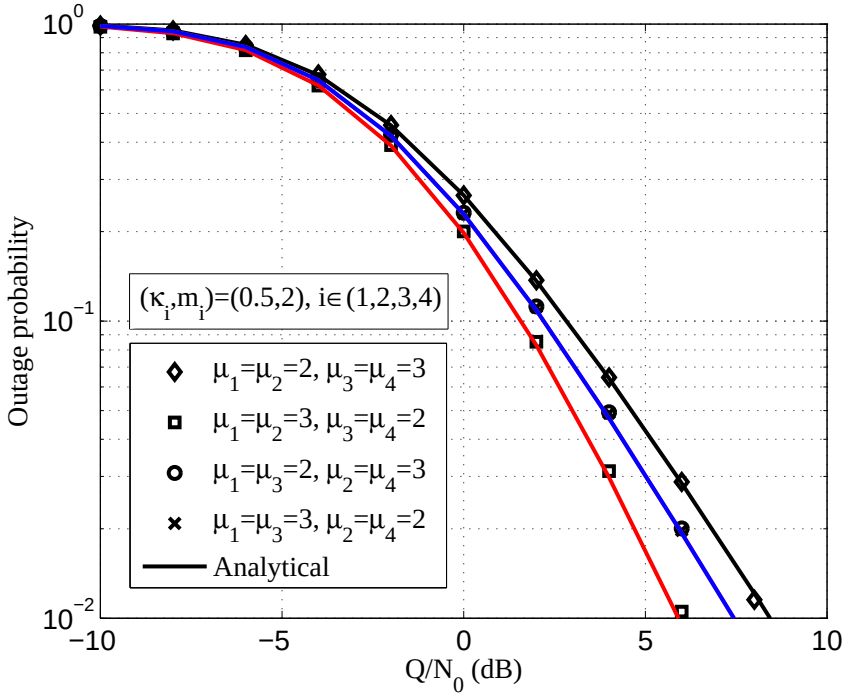

Figure 4.8: Outage probability vs Q/N_0 plots for non-identical μ parameter, and $\gamma_{th} = -5$ dB. (Solid lines: Analytical and Markers: Simulated).

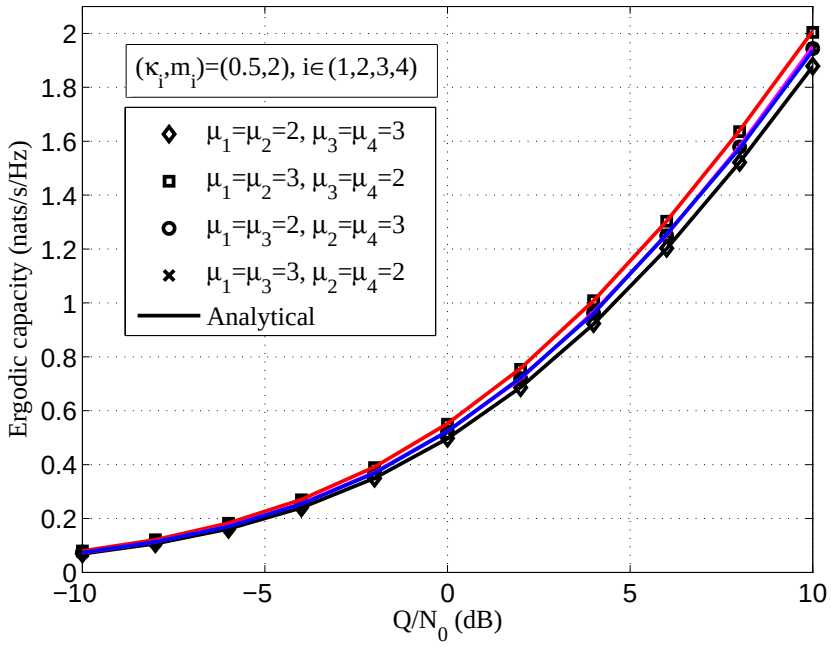

Figure 4.9: Ergodic capacity vs Q/N_0 plots for non-identical μ parameter. (Solid lines: Analytical and Markers: Simulated).

a hop can be interchanged with all channel parameters of the other hop without any loss in the performance of the SU system. This is because, in a dual-hop DF relay-assisted CRN, the end-to-end SNR is chosen to be the minimum SNR of the SR and relay nodes.

4.5 Summary

In this chapter, we have considered a dual-hop cooperative relay-assisted underlay CRN with single antenna at all nodes. We have analyzed the performance of the considered system in the presence of both fading and shadowing. The faded and shadowed channels at all links are compositely modeled by the κ-μ shadowed distribution. We have derived the analytical expressions for outage probability and ergodic capacity under PIPC of PR. Two special cases are also analyzed when the channels at links ST→relay and relay→SR are Nakagami-m and Rician/Rician-shadowed distributed. In both cases, the simpler forms for outage probability and ergodic capacity are deduced. In all scenarios, the analytical results are validated by the simulation results. Through this analysis, we have shown that the severity of fading/shadowing at the interfering links is favorable for the SUs communication up to a certain value of PIPC of PR. Beyond this value, the performance of the system improves under less severe fading/shadowing at the interfering links. Though, in this work, we have considered a single antenna at all users, this work can be further explored for multiantenna users to exploit the available spatial diversity. In the next chapter, we have discussed the extension of this work for multiantenna SR in the presence of spatially correlated channels.

5

Performance Analysis of SIMO-based Cognitive Cooperative Relay Networks over Spatially Correlated κ-μ Shadowed Channels

Contents

5.1 System Model 78
5.2 Channel Model 79
5.3 Analysis of SIMO Underlay CRN 80
5.4 Analysis of Dual-hop DF Relay-assisted Underlay CRN 88
5.5 Summary 96

In Chapter 4, we have considered a dual-hop DF relay-assisted underlay CRN with single antenna at all nodes. For performance analysis, the analytical expressions for outage probability and ergodic capacity have been derived under κ-μ shadowed channels. In this chapter, we consider the system model similar to Chapter 4 while incorporating multiantenna at the secondary receiver (SR). In addition, we consider that the channels at SR are spatially correlated. The performance analyses of relay-assisted underlay CRNs with multiantenna users are available in [88–96]. These analyses are carried-out under Rayleigh and Nakagami-m distributed channel models which do not include the effect of shadowing. The analysis of the considered system with spatially correlated channels at multiantenna SR under faded and shadowed channel condition can provide the actual performance of the system.

In this chapter, the scenario at first-hop—between ST and relay nodes—is same as the first-hop of the system considered in Chapter 4. Thus, the analytical expressions obtained in Chapter 4 for the first-hop can be directly used in this chapter. Sections 5.1 and 5.2 discuss the overall system and channel models for dual-hop cooperative relay-assisted underlay CRN with multiantenna at SR. In Section 5.3, we determine expressions for performance measures for single-input multi-output (SIMO)-based underlay CRN which are used for the analysis of second-hop—between relay and SR nodes—of the considered dual-hop DF relay-assisted CRN. Further, in Section 5.4, we combine the results obtained for both hops, and finally determine the expressions for the dual-hop DF relay-assisted CRN with multiantenna SR. We have also plotted the expressions obtained for the SIMO-based underlay CRN (analogous to the second-hop of the considered dual-hop CRN) in Section 5.3 and analyzed some important observations. In Section 5.4, we have plotted for the complete system model—the dual-hop DF relay-assisted underlay CRN with multiantenna SR—and deduce some key results.

5.1 System Model

In this chapter, we consider a dual-hop DF relay-assisted underlay CRN which comprises a PR, an ST, an SR, and a relay nodes as shown in Fig. 5.1. M number of antennas are considered at SR whereas other nodes are having a single antenna. The SR and the relay nodes

are considered to be located far away from the PU transmitter (PT). Thus, the interfering signals from PT to SR and relay nodes are assumed to be weak and can be considered with the noise terms at the respective nodes. Moreover, in an underlay paradigm based CRN, the ST and the relay nodes can transmit its signals such that the interference induced at PR is within a certain tolerance limit—known as the peak interference power constraint (PIPC) of PR and is denoted by Q. To maintain PIPC of PR, we assume that both ST and relay nodes have perfect knowledge of the channels at ST→PR and relay→PR links, respectively. We employ maximal ratio combining (MRC) at the SR to combine all signals received at different antennas.

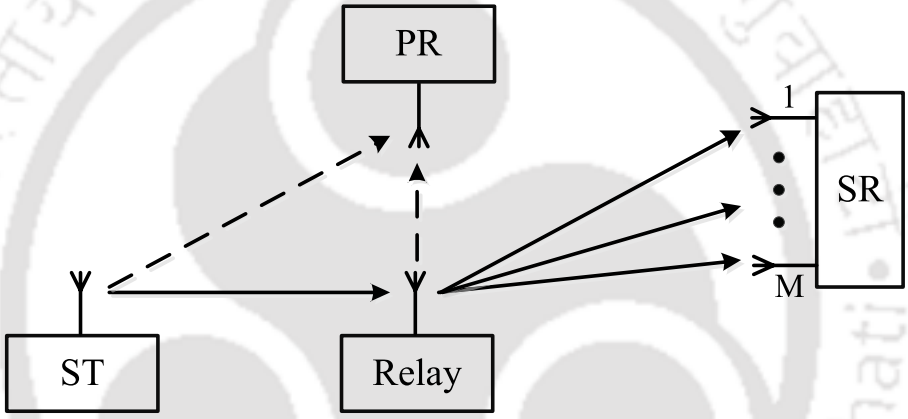

Figure 5.1: A typical diagram of a dual-hop relay-assisted underlay CRN with multiantenna at SR.

5.2 Channel Model

The faded and shadowed channels are considered at all links with arbitrary fading and shadowing parameters. The channels at all links are modeled by the κ-μ shadowed distribution—which compositely describes the LOS multipath fading and the shadowing of the links [98]. The κ-μ shadowed distribution encompasses most of the classical fading models—one-sided Gaussian, Rayleigh, Rician shadowed, Nakagami-m, and κ-μ—as its particular cases. Furthermore, the CDF of the squared κ-μ shadowed distribution is tightly approximated by the gamma distribution, denoted as $G(\alpha, \theta)$, with parameters given by [101] $\alpha = \frac{m\mu(1+\kappa)^2}{m+\mu\kappa^2+2m\kappa}$, $\theta = \frac{\bar{\gamma}}{\alpha}$ where $\{\kappa, \mu, m\}$ are the channel parameters of the κ-μ shadowed distribution, and $\bar{\gamma}$ is the average

channel power. The CDF of the gamma distribution is given by [101]

$$F_X(x) = \frac{x^\alpha}{\theta^\alpha \Gamma(\alpha+1)} {}_1F_1\left(\alpha; \alpha+1; \frac{-x}{\theta}\right) \tag{5.1}$$

where ${}_1F_1(\cdot)$ denotes the Kummer confluent hypergeometric function. Moreover, we consider that the channels at SR are spatially correlated. The PDF of the sum of M correlated squared κ-μ shadowed random variables, i.e., $Y = \sum_{i=1}^{M} Y_i$, is given by [102]

$$f_Y(y) = V_0 \left(\frac{\phi}{\bar{\gamma}}\right)^{\Omega} y^{\Omega-1} \exp\left(-\frac{\phi y}{\bar{\gamma}}\right) \sum_{j=0}^{\infty} U_{j1} F_1\left(mM+j; \Omega; \frac{\phi e_1 y}{\bar{\gamma}(1+e_1)}\right) \tag{5.2}$$

where $V_0 = \prod_{i=1}^{M} (e_1/e_i)^m$. $\{e_i\}_{i=1}^{M}$ are the eigenvalues of the matrix $\mathbf{WC}$, where $\mathbf{W}$ is a diagonal matrix with elements $\{\kappa_i \mu_i / m\}_{i=1}^{M}$, and $\mathbf{C}$ is the $M \times M$ correlation matrix with element at the ith-row and the jth-column is $\sqrt{\rho^{|i-j|}}$, $\{i, j\} = 1, .., M$ and ρ is the correlation coefficient. Other parameters in (5.2) are defined as $e_1 = \min_i\{e_i\}$, $\phi = \sum_{i=1}^{M} \mu_i(1+\kappa_i)$, $\Omega = \sum_{i=1}^{M} \mu_i$, and $U_j = \frac{\delta_j}{\Gamma(\Omega)(1+e_1)^{(mM+j)}}$. Here, δ_j is calculated recursively as

$$\delta_{j+1} = \frac{m}{j+1} \sum_{t=1}^{j+1} \left[\sum_{i=1}^{M} \left(1 - \frac{e_1}{e_i}\right)^t\right] \delta_{j+1-t} \tag{5.3}$$

where $j = 0, 1, ...,$ and $\delta_0 = 1$.

5.3 Analysis of SIMO Underlay CRN

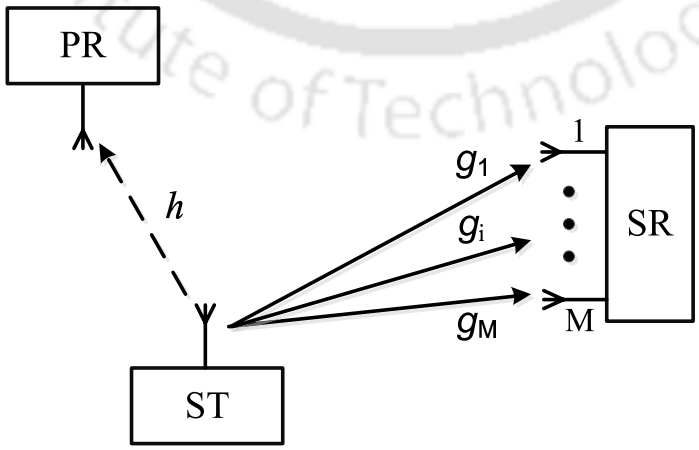

Figure 5.2: A typical diagram of a SIMO underlay CRN with multiantenna at SR.

In this section, we analyze for SIMO underlay CRN and the results are used in the analysis of the second-hop in dual-hop relay-assisted underlay CRN with multiantenna at SR. As shown in Fig. 5.2, the channels at links between ST and the ith antenna of SR, i.e., ST→SR$_i$, and ST→PR are denoted by g_i and h, respectively. The noise is zero-mean circular symmetric complex Gaussian (CSCG) with power N_0. The transmission power of ST is denoted by P_{ST}. To maintain PIPC of PR, $P_{ST}\,|h|^2 \leq Q$. Thus, the maximum allowable transmission power of ST is $P_{ST} = \frac{Q}{|h|^2}$. The instantaneous SNR at the ith antenna of SR, denoted by γ_i, is given by $\gamma_i = \frac{Q|g_i|^2}{N_0|h|^2}$. We employ MRC at SR to combine all signals received at different antennas. Hence, the combined SNR of the M antennas MRC receiver is given by

$$\gamma = \sum_{i=1}^{M} \gamma_i = \frac{Q}{N_0\,|h|^2} \sum_{i=1}^{M} |g_i|^2. \tag{5.4}$$

5.3.1 Outage Probability

The probability of outage is determined by the probability that the instantaneous SNR of the M antennas MRC-receiver falls below a specified threshold γ_{th}. Using (5.4), the outage probability, denoted by $P_O(\cdot)$, of a SIMO-based underlay CRN can be determined as

$$\begin{aligned} P_O(\gamma_{th}) &= \Pr\left(\frac{Q}{N_0\,|h|^2} \sum_{i=1}^{M} |g_i|^2 \leq \gamma_{th}\right) \\ &= 1 - \int_0^{\infty} F_{|h|^2}\left(\frac{Qx}{N_0\gamma_{th}}\right) f_{\sum_i |g_i|^2}(x)dx. \end{aligned} \tag{5.5}$$

Using (5.1) and (5.2), (5.5) can be written as

$$\begin{aligned} P_O(\gamma_{th}) = 1 - D_1 \sum_{j=0}^{\infty} U_j \int_0^{\infty} x^{\alpha+\Omega-1} \exp\left(-\frac{\phi x}{\bar{\gamma}_1}\right) \\ \times {}_1F_1\left(\alpha, \alpha+1, -\frac{Qx}{N_0\gamma_{th}\theta}\right) {}_1F_1\left(m_1M + j; \Omega; \frac{\phi e_1 x}{\bar{\gamma}_1(1+e_1)}\right) dx \end{aligned} \tag{5.6}$$

where $D_1 = \frac{V_0\phi^{\Omega}Q^{\alpha}}{\bar{\gamma}_1^{\Omega}(N_0\gamma_{th}\theta)^{\alpha}\Gamma(\alpha+1)}$, $U_j = \frac{\delta_j}{\Gamma(\Omega)(1+e_1)^{(m_1M+j)}}$, $\phi = \sum_{i=1}^{M} \mu_{1i}(1+\kappa_{1i})$, $\Omega = \sum_{i=1}^{M} \mu_{1i}$, $\alpha = \frac{m_2\mu_2(1+\kappa_2)^2}{m_2+\mu_2\kappa_2^2+2m_2\kappa_2}$, and $\theta = \frac{\bar{\gamma}_2}{\alpha}$. Here, the channel parameters of ST→SR and ST→PR links are denoted by $\{\kappa_{1i}, \mu_{1i}, m_1\}_{i=1}^{M}$ and $\{\kappa_2, \mu_2, m_2\}$, respectively. $\bar{\gamma}_1$ and $\bar{\gamma}_2$ denote the average

channel power at links ST→SR and ST→PR, respectively. Applying a change of variable as $z = \phi x/\bar{\gamma}_1$, and the integral representation of type-2 Appell hypergeometric function $F_2(\cdot)$ given by [116, Eq. 2.4.2]

$$F_2(a, b_1, b_2; c_1, c_2; y_1, y_2) = \frac{1}{\Gamma(a)} \int_0^\infty t^{a-1} \exp(-t) {}_1F_1(b_1; c_1; y_1 t) {}_1F_1(b_2; c_2; y_2 t) dt, \ \mathrm{Re}(a) > 0, \tag{5.7}$$

(5.6) is obtained as

$$P_O(\gamma_{th}) = 1 - \frac{V_0 \Gamma(\alpha + \Omega)}{\Gamma(\alpha + 1)} \left(\frac{Q\bar{\gamma}_1}{N_0 \gamma_{th} \theta \phi} \right)^\alpha \sum_{j=0}^{\infty} U_j \times F_2 \left(\alpha + \Omega, \alpha, m_1 M + j; \alpha + 1, \Omega; -\frac{Q\bar{\gamma}_1}{\phi \theta N_0 \gamma_{th}}, \frac{e_1}{1 + e_1} \right). \tag{5.8}$$

The series expression of $F_2(\cdot)$ converges when $|y_1| + |y_2| < 1$, where y_1 and y_2 symbols are used in (5.7). This condition may not be satisfied for all cases. Thus, for the convergent evaluation of F_2 function, we use a property given by [116, Eq. 4.2.2]

$$F_2(a, b_1, b_2; c_1, c_2; y_1, y_2) = (1 - y_1)^{-a} F_2 \left(a, c_1 - b_1, b_2; c_1, c_2; \frac{y_1}{y_1 - 1}, \frac{y_2}{1 - y_1} \right). \tag{5.9}$$

Hence, the final-form of outage probability for SIMO-based underlay CRN is obtained as

$$P_O(\gamma_{th}) = 1 - \frac{V_0 (Q\bar{\gamma}_1)^\alpha (\phi \theta N_0 \gamma_{th})^\Omega \Gamma(\alpha + \Omega)}{(Q\bar{\gamma}_1 + \phi \theta N_0 \gamma_{th})^{\alpha + \Omega} \Gamma(\alpha + 1)} \sum_{j=0}^{\infty} U_j \times F_2 \left(\alpha + \Omega, 1, m_1 M + j; \alpha + 1, \Omega; \frac{Q\bar{\gamma}_1}{Q\bar{\gamma}_1 + \phi \theta N_0 \gamma_{\mathrm{th}}}, \frac{e_1 \phi \theta N_0 \gamma_{\mathrm{th}}}{(1 + e_1)(Q\bar{\gamma}_1 + \phi \theta N_0 \gamma_{\mathrm{th}})} \right). \tag{5.10}$$

Note that, the F_2 function involved in (5.10) can be evaluated accurately using its integral form given by [117, Eq. 20] in terms of the Gauss hypergeometric function ${}_2F_1$—the ${}_2F_1$ function is defined in most of the common software.

5.3.2 Ergodic Capacity

The ergodic capacity is defined as the average maximum achievable rate and can be determined as $C_{er} = \mathrm{E}[\ln(1 + \gamma)] = \int_0^\infty \Pr[\ln(1 + \gamma) > x] dx$ which can be further simplified

to

$$C_{er} = \int_0^{\infty} [1 - P_O(e^x - 1)]dx. \tag{5.11}$$

Using series representation of F_2 function given by [116, Eq. 1.4.2]

$$F_2(a, b_1, b_2; c_1, c_2; y_1, y_2) = \sum_{j_1,j_2=0}^{\infty} \frac{(a)_{j_1+j_2}(b_1)_{j_1}(b_2)_{j_2} y_1^{j_1} y_2^{j_2}}{(c_1)_{j_1}(c_2)_{j_2} j_1! j_2!} \tag{5.12}$$

in (5.10), (5.11) can be obtained as

$$C_{er} = D_2 \sum_{j=0}^{\infty} U_j \sum_{j_1,j_2=0}^{\infty} D_3 \int_0^{\infty} \frac{(\phi\theta N_0(e^x - 1))^{\Omega+j_2}}{(Q\bar{\gamma}_1 + \phi\theta N_0(e^x - 1))^{\alpha+\Omega+j_1+j_2}} dx \tag{5.13}$$

where $D_2 = V_0(Q\bar{\gamma}_1)^{\alpha}$ and $D_3 = \frac{e_1^{j_2}(Q\bar{\gamma}_1)^{j_1}(m_1M+j)_{j_2}\Gamma(\alpha+\Omega+j_1+j_2)}{(1+e_1)^{j_2}(\Omega)_{j_2}\Gamma(\alpha+1+j_1)j_2!}$. Here, $(\cdot)_t$ represents the Pochhammer symbol, defined as $(a)_t = a(a+1)\cdots(a+t-1)$, $t \geq 0$ [116, Eq. 1.1.3]. The integration involved in (5.13) can be solved in Mathematica in terms of a single ${}_2F_1$ function, and then we use a property given by [116, Eq. 1.2.2.2]

$${}_2F_1(a, b; c; z) = (1 - z)^{c-a-b} {}_2F_1(c - a, c - b; c; z) \tag{5.14}$$

for further simplification. The final expression of the ergodic capacity for SIMO-based underlay CRN is obtained as

$$\begin{aligned} C_{er} =& D_4 \sum_{j=0}^{\infty} U_j \sum_{j_1,j_2=0}^{\infty} \frac{(\Omega + j_2)(m_1M + j)_{j_2} e_1^{j_2}}{(\alpha + j_1)(\alpha + \Omega + j_1 + j_2)(1 + e_1)^{j_2} j_2!} \\ & \times {}_2F_1\left(1, 1 + \Omega + j_2; 1 + \alpha + \Omega + j_1 + j_2; 1 - \frac{Q\bar{\gamma}_1}{\phi\theta N_0}\right) \end{aligned} \tag{5.15}$$

where $D_4 = \frac{Q\bar{\gamma}_1 V_0 \Gamma(\Omega)}{\phi\theta N_0}$. The ${}_2F_1$ function involved in (5.15) converges when $\left|1 - \frac{Q\bar{\gamma}_1}{\phi\theta N_0}\right| < 1$. Further, when $\left|1 - \frac{Q\bar{\gamma}_1}{\phi\theta N_0}\right| \geqslant 1$, we use a transformation given by [116, Eq. 1.2.2.2]

$${}_2F_1(a, b; c; z) = (1 - z)^{-a} {}_2F_1\left(a, c - b; c; \frac{z}{z - 1}\right). \tag{5.16}$$

In this case, (5.15) is obtained as

$$C_{er} = \sum_{j=0}^{\infty} U_j \sum_{j_1,j_2=0}^{\infty} \frac{V_0 \Gamma(\Omega)(\Omega + j_2)(m_1 M + j)_{j_2} e_1^{j_2}}{(\alpha + j_1)(\alpha + \Omega + j_1 + j_2)(1 + e_1)^{j_2} j_2!} \times {}_2F_1\left(1, \alpha + j_1; 1 + \alpha + \Omega + j_1 + j_2; 1 - \frac{\phi\theta N_0}{Q\bar{\gamma}_1}\right). \quad (5.17)$$

5.3.3 Results and Discussion

In this section, the outage probability and the ergodic capacity of SIMO-based underlay CRN are plotted with respect to the ratio of the peak interference power and the noise power, i.e., Q/N_0, for arbitrary fading/shadowing parameters. The sum of infinite series involved in the expressions are calculated by considering first N finite terms such that the error involved is less than 10^{-5}. From Figs. 5.3 - 5.5, it can be observed that the outage probability and the ergodic capacity improve as Q/N_0 increases. This is because of increased transmission power of the ST as Q/N_0 increases. From Figs. 5.3(a) and 5.3(b), it can be seen that both the outage probability and the ergodic capacity degrade as ρ increases. This is due to the decreased independent spatial directions of the signals received at SR as ρ increased. From Figs. 5.4(a) and 5.4(b), it can be observed that both the outage probability and the ergodic capacity improve as the value of M increases which is due to the increased spatial diversity at SR.

Figs. 5.5(a) and 5.5(b) show the effect of various fading and shadowing severities of the interfering channel at ST→PR link on the performance of the SU system. From Fig. 5.5(a), it is observed that, up to a certain value of Q/N_0, the outage probability improves as the severity of fading/shadowing at ST→PR link increases. Beyond this value of Q/N_0, the outage probability improves under less severe fading/shadowing at ST→PR link. For example, for the lower-region of Q/N_0, the outage probability improves when the channel at ST→PR link is one-sided Gaussian (the most severe faded/shadowed link with respect to other channels shown in Fig. 5.5(a)). However, for the upper-region of Q/N_0, the outage probability improves when the channel at ST→PR link is κ-μ (the least severe faded/shadowed link with respect to other channels shown in Fig. 5.5(a)). The value of Q/N_0, after which the outage probability

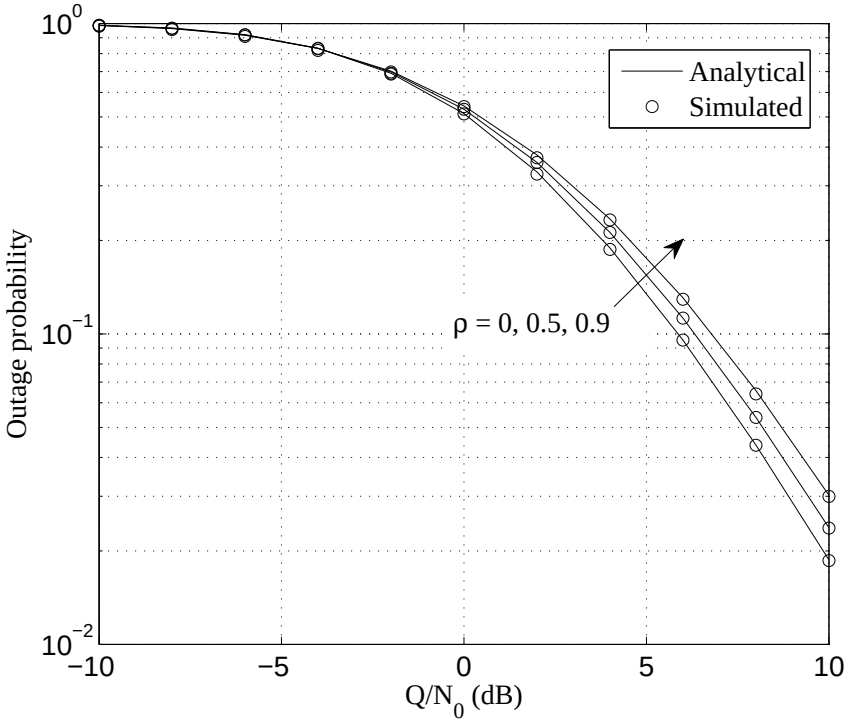

(a) When $\gamma_{th} = 0$ dB

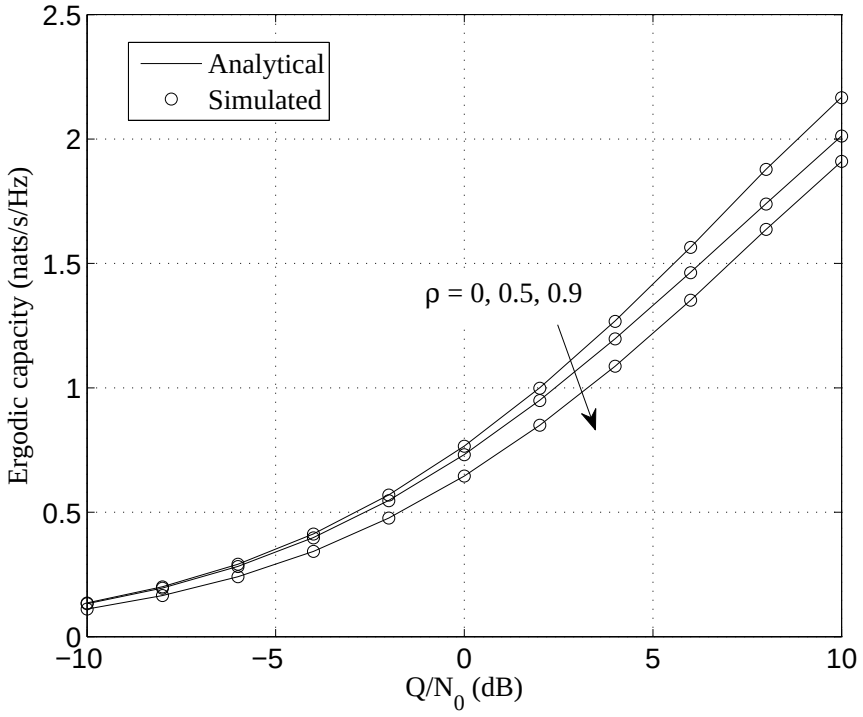

(b)

Figure 5.3: (a) Outage probability and (b) ergodic capacity vs Q/N_0 plots for different ρ when M=2, (κ_{1i},μ_{1i},m_1)=(2.5,1.1,1), $i \in [1, 2]$; (κ_2,μ_2,m_2)=(1.5,3,2); and $\bar{\gamma}_1 = \bar{\gamma}_2 = 1$.

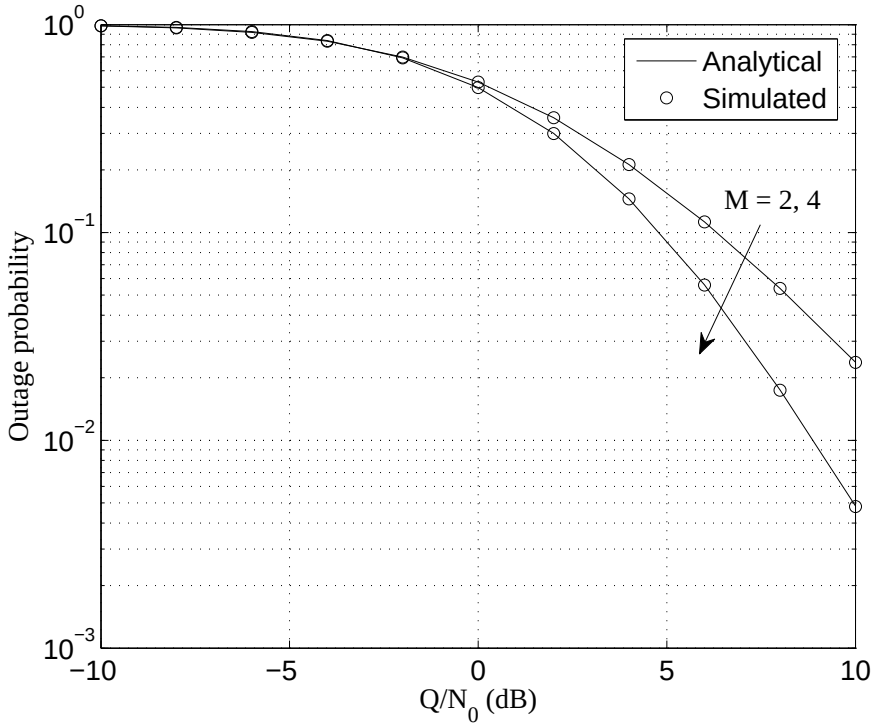

(a) When $\gamma_{th} = 0$ dB

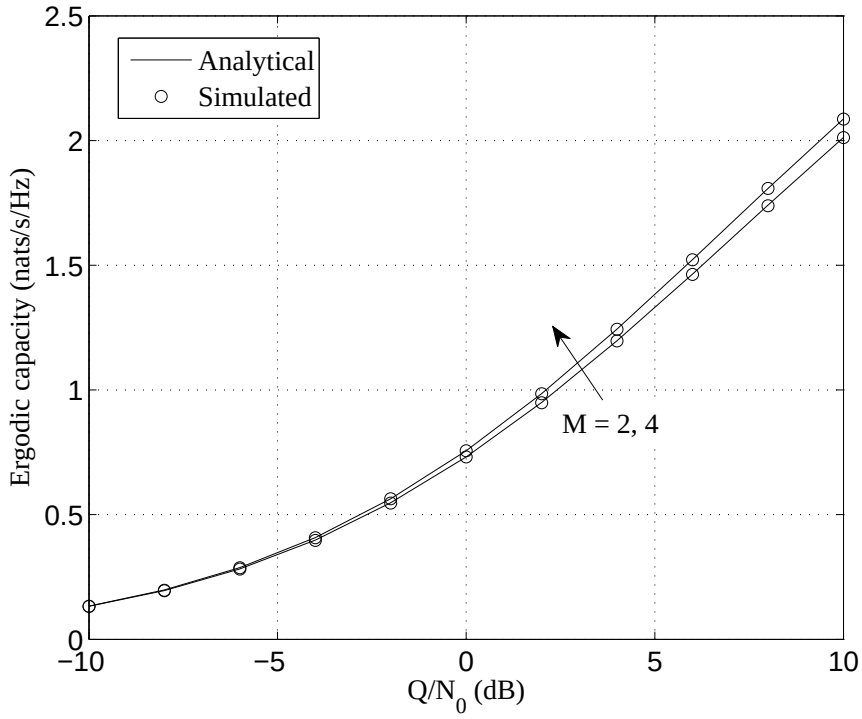

(b)

Figure 5.4: (a) Outage probability and (b) ergodic capacity vs Q/N_0 plots when M=2 and 4, ρ=0.5, (κ_{1i},μ_{1i},m_1)=(2.5,1.1,1), $i = 1, .., M$; (κ_2,μ_2,m_2)=(1.5,3,2); and $\bar{\gamma}_1 = \bar{\gamma}_2 = 1$.

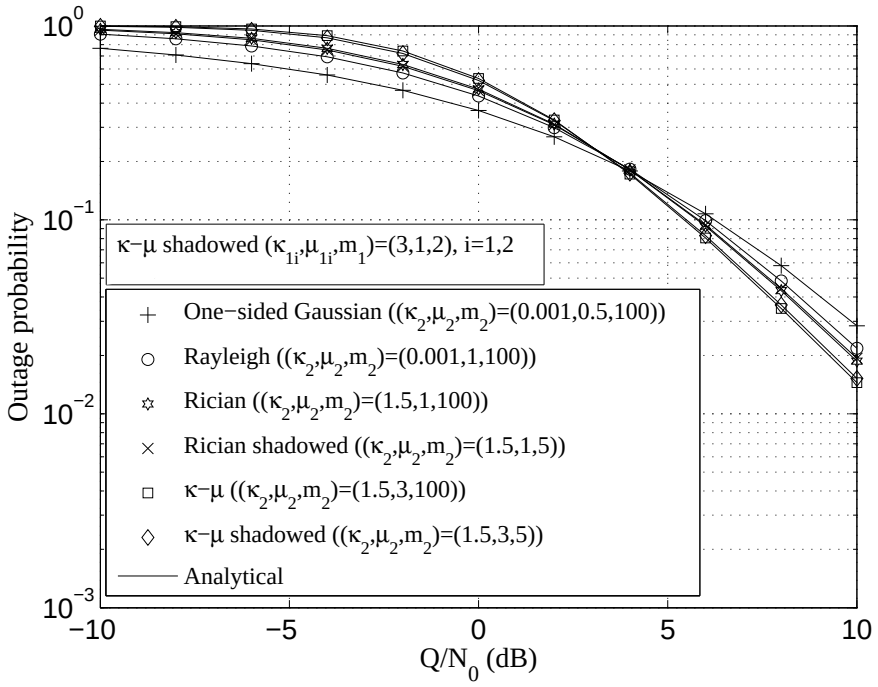

(a) When $\gamma_{th} = 0$ dB

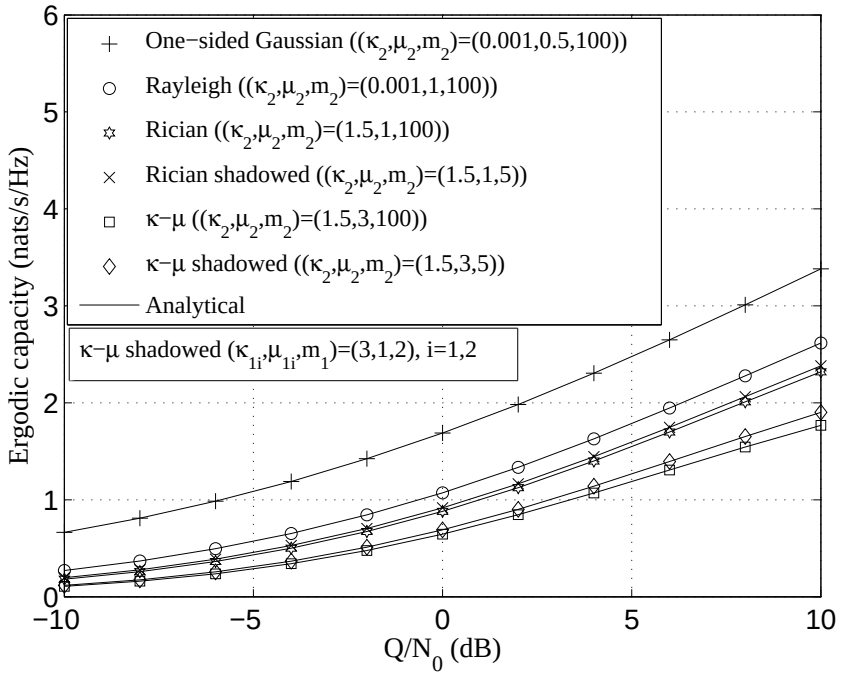

(b)

Figure 5.5: (a) Outage probability and (b) ergodic capacity vs Q/N_0 plots when ST→SR links are κ-μ shadowed distributed and ST→PR link is having various fading/shadowing severities with $M = 2$, $\bar{\gamma}_1 = \bar{\gamma}_2 = 1$, and $\rho = 0.5$. (Markers: Simulated and Lines: Analytical).

shows the opposite trend, depends upon the outage threshold and the channel parameters at ST→PR and ST→SR links. The ergodic capacity of the SU system improves under severe fading/shadowing at ST→PR link for the given range of Q/N_0. Hence, it can be concluded that the severe fading/shadowing at ST→PR link is favorable for the SUs communication, in terms of both the outage probability and the ergodic capacity, up to a certain value of Q/N_0.

5.4 Analysis of Dual-hop DF Relay-assisted Underlay CRN

In this section, the analytical expressions for performance measures of dual-hop DF relay-assisted underlay CRN with multiantenna at SR (shown in Fig. 5.1) are derived. The results obtained in Chapter 4 and Section 5.3 are used for the first-hop (between ST and relay) and the second-hop (between relay and SR), respectively, of the considered system model. The channels at links ST→relay, relay→SR$_i$, ST→PR, and relay→PR are denoted by g_1, g_{2i}, h_1, and h_2 with parameters $\{\bar{\gamma}_1; \kappa_1, \mu_1, m_1\}$, $\{\bar{\gamma}_2; \kappa_{2i}, \mu_{2i}, m_2\}_{i=1}^{M}$, $\{\bar{\gamma}_3; \kappa_3, \mu_3, m_3\}$, and $\{\bar{\gamma}_4; \kappa_4, \mu_4, m_4\}$, respectively. Here, $\bar{\gamma}_1$, $\bar{\gamma}_2$, $\bar{\gamma}_3$, and $\bar{\gamma}_4$ are the average channel power of the links at ST→relay, relay→SR, ST→PR, and relay→PR, respectively. The noise at both relay and SR nodes are zero-mean CSCG with power N_0. The transmission power of ST and relay are denoted by P_{ST} and P_R, respectively. To maintain PIPC of PR, $P_{ST}\left|h_1\right|^2 \leq Q$ and $P_R\left|h_2\right|^2 \leq Q$. Thus, the maximum allowable transmission power of ST and relay nodes are $P_{ST} = \frac{Q}{\left|h_1\right|^2}$ and $P_R = \frac{Q}{\left|h_2\right|^2}$, respectively. The instantaneous SNR at the relay and the ith antenna of SR, denoted by γ_R and γ_i, are given by $\gamma_R = \frac{Q\left|g_1\right|^2}{N_0\left|h_1\right|^2}$ and $\gamma_i = \frac{Q\left|g_{2i}\right|^2}{N_0\left|h_2\right|^2}$, respectively. We employ MRC at SR to combine all signals received at different antennas. Hence, the combined SNR of the M antennas MRC-based SR is given by

$$\gamma_{SR} = \sum_{i=1}^{M} \gamma_i = \frac{Q}{N_0\left|h_2\right|^2} \sum_{i=1}^{M} \left|g_{2i}\right|^2. \tag{5.18}$$

The end-to-end instantaneous SNR, denoted by γ_{e2e}, of the dual-hop DF relay-assisted underlay CRN can be determined as

$$\gamma_{e2e} = \min(\gamma_R, \gamma_{SR}). \tag{5.19}$$

5.4.1 Outage Probability

The outage occurs when the end-to-end SNR falls below a minimum threshold γ_{th}, and is determined as

$$\begin{aligned} P_O(\gamma_{th}) &= \Pr(\min(\gamma_R, \gamma_{SR}) \leq \gamma_{th}) \\ &= 1 - (1 - F_{\gamma_R}(\gamma_{th}))(1 - F_{\gamma_{SR}}(\gamma_{th})) \end{aligned} \tag{5.20}$$

where $F_{\gamma_R}(\cdot)$ and $F_{\gamma_{SR}}(\cdot)$ denote the CDFs of the SNR at relay and SR, respectively. Now, the CDF of the SNR at relay is calculated as

$$F_{\gamma_R}(\gamma_{th}) = \Pr\left(\gamma_R \leqslant \gamma_{th}\right) = \Pr\left(\frac{Q\left|g_1\right|^2}{N_0\left|h_1\right|^2} \leqslant \gamma_{th}\right). \tag{5.21}$$

The final expression of $F_{\gamma_R}(\gamma_{th})$ is same as (4.11) and is mentioned below for the sake of completeness

$$F_{\gamma_R}(\gamma_{th}) = 1 - A_2 F_2\left(\alpha_3+\mu_1, 1, m_1, \alpha_3+1, \mu_1; \frac{Q\phi_{11}}{Q\phi_{11}+\gamma_{th}N_0\theta_3}, \frac{(\phi_{21}-\phi_{11})\gamma_{th}N_0\theta_3}{\phi_{21}(Q\phi_{11}+\gamma_{th}N_0\theta_3)}\right) \tag{5.22}$$

where $A_2 = \frac{Q^{\alpha_3}\phi_{11}^{m_1+\alpha_3}(\gamma_{th}N_0\theta_3)^{\mu_1}\Gamma(\alpha_3+\mu_1)}{\phi_{21}^{m_1}(Q\phi_{11}+\gamma_{th}N_0\theta_3)^{\alpha_3+\mu_1}\Gamma(\alpha_3+1)\Gamma(\mu_1)}$, $\phi_{11} = \frac{\bar{\gamma}_1}{\mu_1(1+\kappa_1)}$, $\phi_{21} = \frac{(\mu_1\kappa_1+m_1)\bar{\gamma}_1}{\mu_1(1+\kappa_1)m_1}$, $\alpha_3 = \frac{m_3\mu_3(1+\kappa_3)^2}{m_3+\mu_3\kappa_3^2+2m_3\kappa_3}$, $\theta_3 = \frac{\bar{\gamma}_3}{\alpha_3}$. Further, the CDF of the SNR at SR is determined as

$$\begin{aligned} F_{\gamma_{SR}}(\gamma_{th}) &= \Pr\left(\frac{Q}{N_0\left|h_2\right|^2}\sum_{i=1}^{M}\left|g_{2i}\right|^2 \leq \gamma_{th}\right) \\ &= 1 - \int_0^{\infty} F_{|h_2|^2}\left(\frac{Qx}{N_0\gamma_{th}}\right) f_{\sum_i |g_{2i}|^2}(x)dx \end{aligned} \tag{5.23}$$

which is obtained in (5.10) and is given below for the sake of completeness

$$\begin{aligned} F_{\gamma_{SR}}(\gamma_{th}) =& 1 - \frac{V_0(Q\bar{\gamma}_2)^{\alpha_4}(\phi\theta_4 N_0\gamma_{th})^{\Omega}\Gamma(\alpha_4+\Omega)}{(Q\bar{\gamma}_2+\phi\theta_4 N_0\gamma_{th})^{\alpha_4+\Omega}\Gamma(\alpha_4+1)}\sum_{j=0}^{\infty}U_j \\ &\times F_2\left(\alpha_4+\Omega, 1, m_2M+j; \alpha_4+1, \Omega; \frac{Q\bar{\gamma}_2}{Q\bar{\gamma}_2+\phi\theta_4 N_0\gamma_{th}}, \frac{e_1\phi\theta_4 N_0\gamma_{th}}{(1+e_1)(Q\bar{\gamma}_2+\phi\theta_4 N_0\gamma_{th})}\right) \end{aligned} \tag{5.24}$$

where $\alpha_4 = \frac{m_4\mu_4(1+\kappa_4)^2}{m_4+\mu_4\kappa_4^2+2m_4\kappa_4}$, $\theta_4 = \frac{\bar{\gamma}_4}{\alpha_4}$, and $V_0 = \prod_{i=1}^{M}(e_1/e_i)^{m_2}$. $\{e_i\}_{i=1}^{M}$ are the eigenvalues of the matrix $\mathbf{WC}$, where $\mathbf{W}$ is a diagonal matrix with elements $\{\kappa_{2i}\mu_{2i}/m_2\}_{i=1}^{M}$, and $\mathbf{C}$ is the $M\times M$ correlation matrix with element at the ith-row and the jth-column is $\sqrt{\rho^{|i-j|}}$, $\{i,j\} = 1,..,M$ and ρ is the correlation coefficient. Other parameters in (5.24) are defined as $e_1 = \min_i\{e_i\}$, $\phi = \sum_{i=1}^{M}\mu_{2i}(1+\kappa_{2i})$, $\Omega = \sum_{i=1}^{M}\mu_{2i}$, and $U_j = \frac{\delta_j}{\Gamma(\Omega)(1+e_1)^{(m_2M+j)}}$ where δ_j is calculated recursively as (5.3). Using (5.22) and (5.24) in (5.20), the final expression of outage probability for the dual-hop DF relay-assisted underlay CRN with multiantenna SR is obtained as

$$\begin{aligned}P_O(\gamma_{th}) =& 1 - \frac{Q^{\alpha_3}\phi_{11}^{m_1+\alpha_3}(\gamma_{th}N_0\theta_3)^{\mu_1}\Gamma(\alpha_3+\mu_1)}{\phi_{21}^{m_1}(Q\phi_{11}+\gamma_{th}N_0\theta_3)^{\alpha_3+\mu_1}\Gamma(\alpha_3+1)\Gamma(\mu_1)} \\ &\times F_2\left(\alpha_3+\mu_1, 1, m_1, \alpha_3+1, \mu_1; \frac{Q\phi_{11}}{Q\phi_{11}+\gamma_{th}N_0\theta_3}, \frac{(\phi_{21}-\phi_{11})\gamma_{th}N_0\theta_3}{\phi_{21}(Q\phi_{11}+\gamma_{th}N_0\theta_3)}\right) \\ &\times \frac{V_0(Q\bar{\gamma}_2)^{\alpha_4}(\phi\theta_4N_0\gamma_{th})^{\Omega}\Gamma(\alpha_4+\Omega)}{(Q\bar{\gamma}_2+\phi\theta_4N_0\gamma_{th})^{\alpha_4+\Omega}\Gamma(\alpha_4+1)}\sum_{j=0}^{\infty}U_j \\ &\times F_2\left(\alpha_4+\Omega, 1, m_2M+j; \alpha_4+1, \Omega; \frac{Q\bar{\gamma}_2}{Q\bar{\gamma}_2+\phi\theta_4N_0\gamma_{th}}, \frac{e_1\phi\theta_4N_0\gamma_{th}}{(1+e_1)(Q\bar{\gamma}_2+\phi\theta_4N_0\gamma_{th})}\right).\end{aligned} \tag{5.25}$$

Moreover, the expression of outage probability for dual-hop DF relay-assisted underlay CRN with single antenna users, given in (4.12), can be deduced from (5.25) by considering M=1 along with the parameters given by $V_0 = 1$, $e_1 = \kappa_2\mu_2/m_2$, $\phi = \mu_2(1+\kappa_2)$, $\Omega = \mu_2$, and $U_0 = \frac{m_2^{m_2}}{\Gamma(\mu_2)(\kappa_2\mu_2+m_2)^{m_2}}$.

5.4.2 Ergodic Capacity

Ergodic capacity can be determined as

$$C_{er} = \int_0^{\infty}[1 - P_O(e^x - 1)]dx. \tag{5.26}$$

Using (5.25) in (5.26), the final-form of C_{er} for the dual-hop DF relay-assisted underlay CRN with multiantenna SR is determined as (for detail, refer to Appendix A.7)

$$C_{er} = B_1 B_3 \sum_{j_1=0}^{\infty} B_2 \sum_{j_2=0}^{\infty} B_5 \sum_{j=0}^{\infty} U_j \sum_{j_3=0}^{\infty} B_4 \sum_{j_4=0}^{\infty} B_6 \frac{1}{(N_0\theta_3)^{\alpha_3+j_2}(\phi N_0\theta_4)^{\alpha_4+j_4}(\alpha_3+\alpha_4+j_2+j_4)} \times F_1\left(\alpha_3+\alpha_4+j_2+j_4, \alpha_3+j_2, \alpha_4+j_4; 1+\alpha_3+\alpha_4+j_2+j_4; 1-\frac{Q\phi_{11}}{N_0\theta_3}, 1-\frac{Q\bar{\gamma}_2}{\phi N_0\theta_4}\right) \tag{5.27}$$

where $B_1 = \frac{Q^{\alpha_3}\phi_{11}^{m_1+\alpha_3}\Gamma(\alpha_3+\mu_1)}{\phi_{21}^{m_1}\Gamma(\alpha_3+1)\Gamma(\mu_1)}$, $B_2 = \frac{(\alpha_3+\mu_1)_{j_1}(m_1)_{j_1}}{j_1!(\mu_1)_{j_1}}\left(1-\frac{\phi_{11}}{\phi_{21}}\right)^{j_1}$, $B_3 = \frac{V_0(Q\bar{\gamma}_2)^{\alpha_4}\Gamma(\alpha_4+\Omega)}{\Gamma(\alpha_4+1)}$, $B_4 = \frac{(\alpha_4+\Omega)_{j_3}(m_2M+j)_{j_3}}{j_3!(\Omega)_{j_3}}\left(\frac{e_1}{1+e_1}\right)^{j_3}$, $B_5 = \frac{(1-\mu_1-j_1)_{j_2}(\alpha_3)_{j_2}(Q\phi_{11})^{j_2}}{j_2!(\alpha_3+1)_{j_2}}$, and $B_6 = \frac{(1-\Omega-j_3)_{j_4}(\alpha_4)_{j_4}(Q\bar{\gamma}_2)^{j_4}}{j_4!(\alpha_4+1)_{j_4}}$. The series-form of F_1 function involved in (5.27) converges when $\left|1-\frac{Q\phi_{11}}{N_0\theta_3}\right| < 1$ and $\left|1-\frac{Q\bar{\gamma}_2}{\phi N_0\theta_4}\right| < 1$. This condition may not be satisfied for all values of parameters. In the following cases, we employ some transformations for different cases so that the series-form of F_1 converges.

Case I: When $\left|1-\frac{Q\phi_{11}}{N_0\theta_3}\right| \not< 1$ and $\left|1-\frac{Q\bar{\gamma}_2}{\phi N_0\theta_4}\right| \not< 1$, use a transformation given by [116, Eq. 4.2.4]

$$F_1(a,b_1,b_2;c;x_1,x_2) = (1-x_1)^{-b_1}(1-x_2)^{-b_2}F_1\left(c-a,b_1,b_2;c;\frac{x_1}{x_1-1},\frac{x_2}{x_2-1}\right).$$

The expression for ergodic capacity is obtained as

$$C_{er} = B_1 B_3 \sum_{j_1=0}^{\infty} B_2 \sum_{j_2=0}^{\infty} B_5 \sum_{j=0}^{\infty} U_j \sum_{j_3=0}^{\infty} B_4 \sum_{j_4=0}^{\infty} B_6 \frac{1}{(Q\phi_{11})^{\alpha_3+j_2}(Q\bar{\gamma}_2)^{\alpha_4+j_4}(\alpha_3+\alpha_4+j_2+j_4)} \times F_1\left(1, \alpha_3+j_2, \alpha_4+j_4;\ 1+\alpha_3+\alpha_4+j_2+j_4; 1-\frac{N_0\theta_3}{Q\phi_{11}}, 1-\frac{\phi N_0\theta_4}{Q\bar{\gamma}_2}\right). \tag{5.28}$$

Case II: When $\left|1-\frac{Q\phi_{11}}{N_0\theta_3}\right| \not< 1$ and $\left|1-\frac{Q\bar{\gamma}_2}{\phi N_0\theta_4}\right| < 1$, use a transformation given by [116, Eq. 4.2.4]

$$F_1(a,b_1,b_2;c;x_1,x_2) = (1-x_1)^{-a}F_1\left(a,c-b_1-b_2,b_2;c;\frac{x_1}{x_1-1},\frac{x_1-x_2}{x_1-1}\right).$$

The expression for ergodic capacity is given by

$$\begin{aligned} C_{er} =& B_1 B_3 \sum_{j_1=0}^{\infty} B_2 \sum_{j_2=0}^{\infty} B_5 \sum_{j=0}^{\infty} U_j \sum_{j_3=0}^{\infty} B_4 \sum_{j_4=0}^{\infty} B_6 \\ &\times \left(\frac{\theta_3}{\phi\theta_4}\right)^{\alpha_4+j_4} \frac{1}{(Q\phi_{11})^{\alpha_3+\alpha_4+j_2+j_4}(\alpha_3+\alpha_4+j_2+j_4)} \\ &\times F_1\left(\alpha_3+\alpha_4+j_2+j_4, 1, \alpha_4+j_4; 1+\alpha_3+\alpha_4+j_2+j_4; 1-\frac{N_0\theta_3}{Q\phi_{11}}, 1-\frac{\bar{\gamma}_2\theta_3}{\phi\theta_4\phi_{11}}\right). \end{aligned} \tag{5.29}$$

Case III: When $\left|1-\frac{Q\phi_{11}}{N_0\theta_3}\right| < 1$ and $\left|1-\frac{Q\bar{\gamma}_2}{\phi N_0\theta_4}\right| \not< 1$, use a transformation given by [116, Eq. 4.2.4]

$$F_1(a, b_1, b_2; c; x_1, x_2) = (1-x_1)^{c-a-b_1}(1-x_2)^{-b_2} F_1\left(c-a, c-b_1-b_2, b_2; c; x_1, \frac{x_2-x_1}{x_2-1}\right).$$

The expression for ergodic capacity is obtained as

$$\begin{aligned} C_{er} =& B_1 B_3 \sum_{j_1=0}^{\infty} B_2 \sum_{j_2=0}^{\infty} B_5 \sum_{j=0}^{\infty} U_j \sum_{j_3=0}^{\infty} B_4 \sum_{j_4=0}^{\infty} B_6 \\ &\times \frac{1}{N_0\theta_3(Q\phi_{11})^{\alpha_3+j_2-1}(Q\bar{\gamma}_2)^{\alpha_4+j_4}(\alpha_3+\alpha_4+j_2+j_4)} \\ &\times F_1\left(1, 1, \alpha_4+j_4; 1+\alpha_3+\alpha_4+j_2+j_4; 1-\frac{Q\phi_{11}}{N_0\theta_3}, 1-\frac{\phi\theta_4\phi_{11}}{\bar{\gamma}_2\theta_3}\right). \end{aligned} \tag{5.30}$$

5.4.3 Results and Discussion

In this section, the analytical and the simulation plots are shown for the outage probability and the ergodic capacity with varying Q/N_0 for the dual-hop DF relay-assisted underlay CRN with multiantenna SR. The infinite series involved in the expressions are simulated considering first N finite terms such that the error involved is less than 10^{-5}. From Figs. 5.6 - 5.8, it can be observed that the outage probability and the ergodic capacity improve as Q/N_0 increases. This is because of increased transmission power of ST and relay nodes as Q/N_0 increases. From Figs. 5.6(a) and 5.6(b), it is seen that the outage probability and the ergodic capacity degrade as ρ increases. This is due to the fact that as ρ increases the independent spatial directions at SR decreases. From Figs. 5.7(a) and 5.7(b), it can be seen that both outage probability and

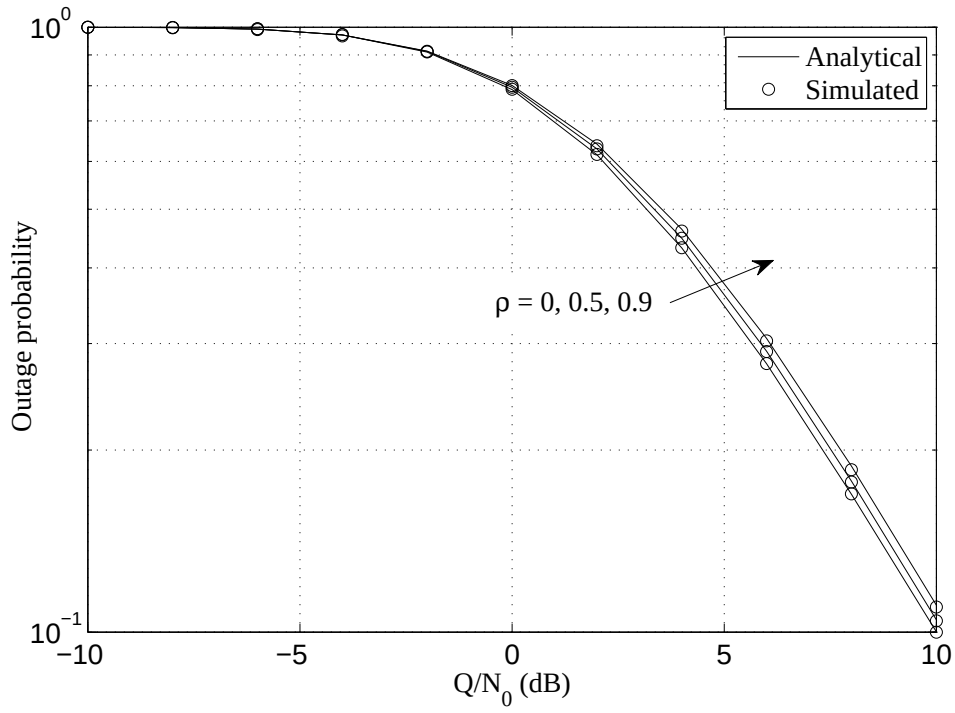

(a) When $\gamma_{th} = 0$ dB

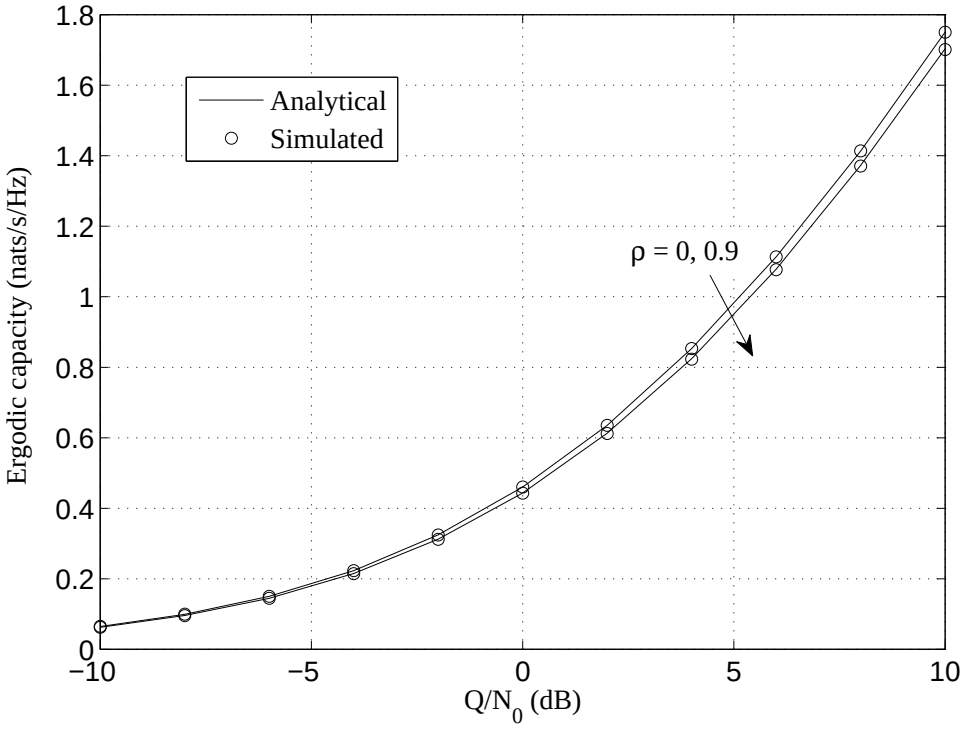

(b)

Figure 5.6: (a) Outage probability and (b) ergodic capacity vs Q/N_0 plots for different ρ when M=2, (κ_1,μ_1,m_1)=(2.5,1.1,1), (κ_{2i},μ_{2i},m_2)= (2.5,1.1,1), $i \in [1, 2]$; (κ_I,μ_I,m_I)= (1.5,3,2), $I \in [3, 4]$; and $\bar{\gamma}_1 = \bar{\gamma}_2 = \bar{\gamma}_3 = \bar{\gamma}_4 = 1$.

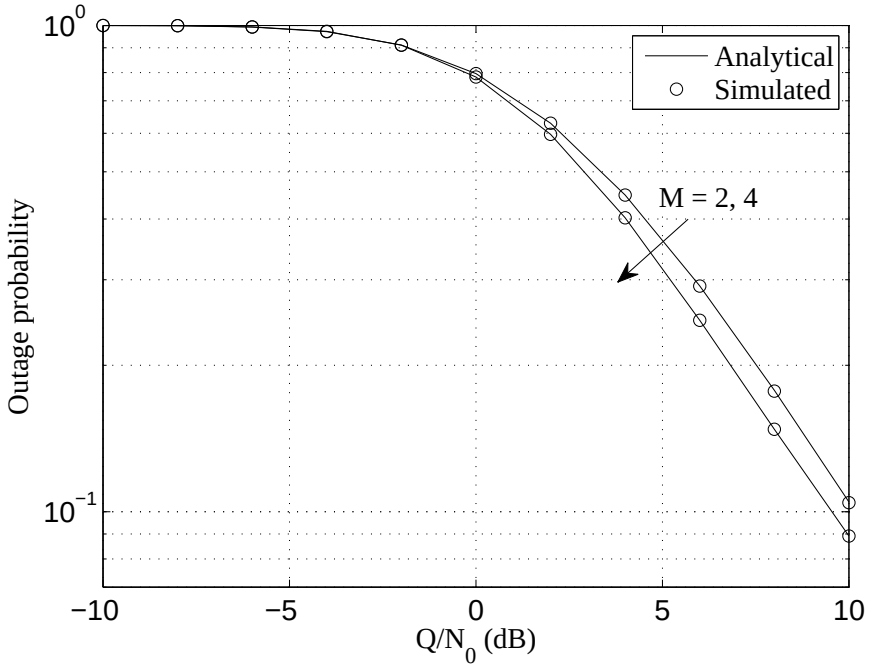

(a) When $\gamma_{th} = 0$ dB

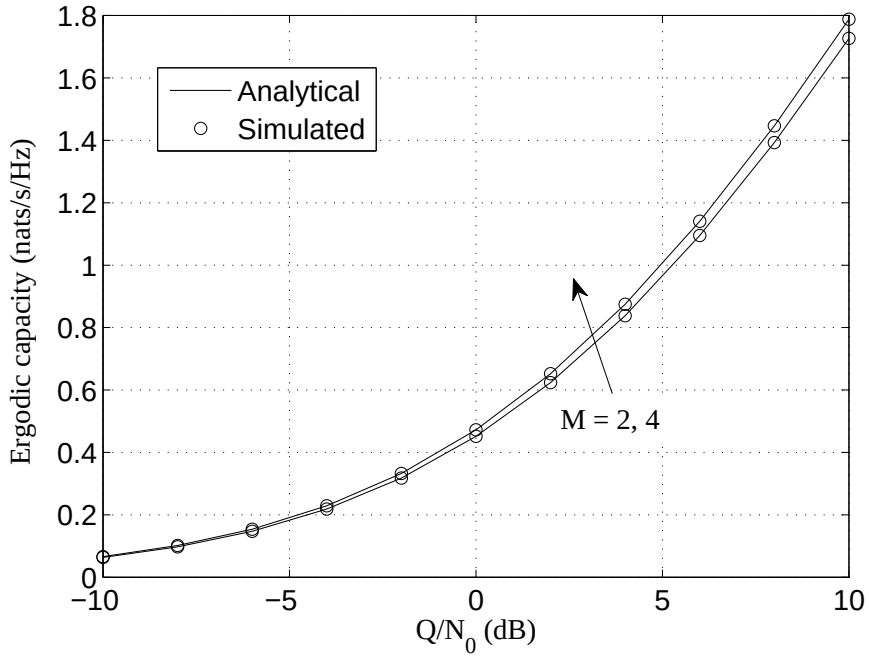

(b)

Figure 5.7: (a) Outage probability and (b) ergodic capacity vs Q/N_0 plots for different M when ρ=0.5, (κ_1,μ_1,m_1)=(2.5,1.1,1), (κ_{2i},μ_{2i},m_2)= (2.5,1.1,1), $i = 1, .., M$; (κ_I,μ_I,m_I)= (1.5,3,2), $I \in [3, 4]$; and $\bar{\gamma}_1 = \bar{\gamma}_2 = \bar{\gamma}_3 = \bar{\gamma}_4 = 1$.

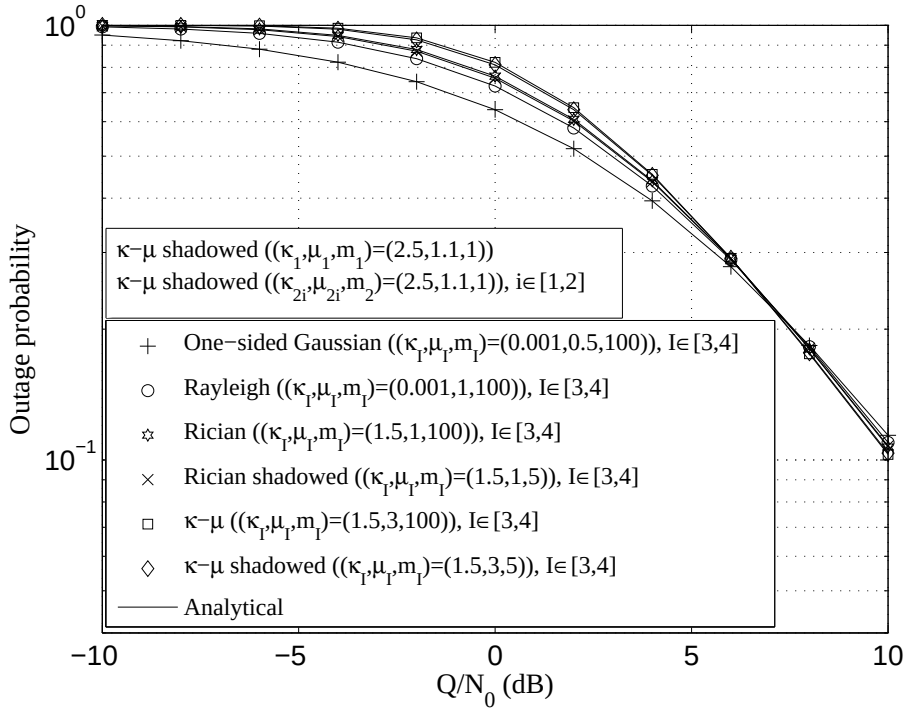

(a) When $\gamma_{th} = 0$ dB

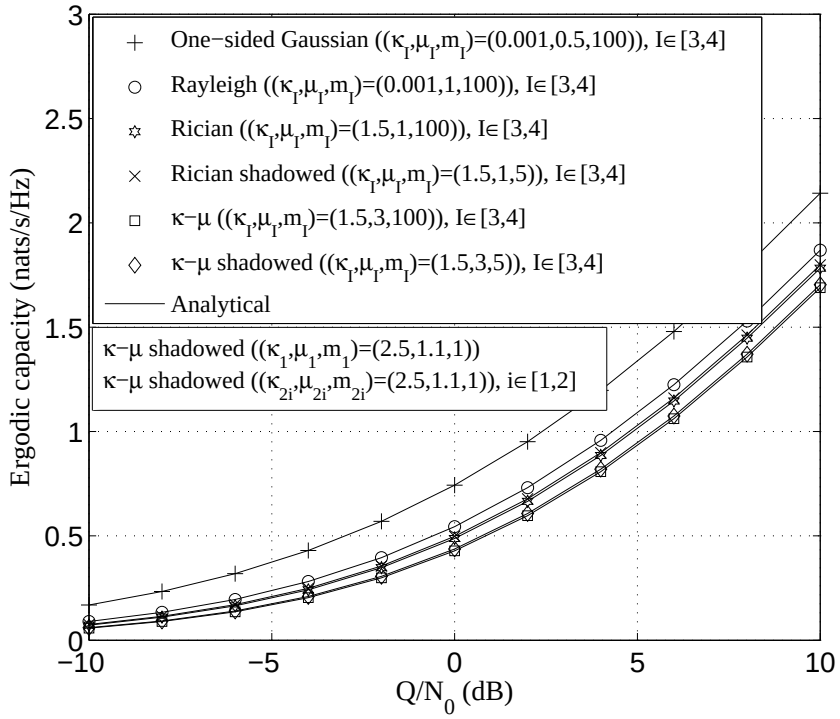

(b)

Figure 5.8: (a) Outage probability and (b) ergodic capacity vs Q/N_0 plots when channels at ST→relay and relay→SR links are κ-μ shadowed distributed and interfering channels at ST→PR and relay→PR links are having various fading/shadowing severities with $M = 2$, $\bar{\gamma}_1 = \bar{\gamma}_2 = \bar{\gamma}_3 = \bar{\gamma}_4 = 1$, and $\rho = 0.5$.

ergodic capacity improve as number of antenna at SR increases which is because of increased spatial diversity of SR.

Figs. 5.8(a) and 5.8(b) show the effect of various fading/shadowing severities of interfering channels at ST→PR and relay→PR links when channels at ST→relay and relay→SR are κ-μ shadowed distributed. From Fig. 5.8(a), it is observed that up to a certain value of Q/N_0, the outage probability improves under severe fading/shadowing at the interfering links. Beyond this value of Q/N_0, the outage probability improves under less severe fading/shadowing at the interfering links. For example, for the lower-region of Q/N_0, the outage probability improves when the interfering channels are one-sided Gaussian (the most severe faded/shadowed link with respect to other channels shown in Fig. 5.8(a)). However, for the upper-region of Q/N_0, the outage probability improves when the interfering channels are κ-μ (the least severe faded/shadowed link with respect to other channels shown in Fig. 5.8(a)). The value of Q/N_0, after which the outage probability shows the opposite trend, depends upon the outage threshold and the channel parameters at various links. The ergodic capacity improves under severe fading/shadowing at the interfering links for the given range of Q/N_0. Thus, the severity of fading/shadowing at the interfering links is favorable to the SUs communication both in terms of outage probability and ergodic capacity only up to a certain value of Q/N_0. This is an important observation which also exists in a dual-hop DF relay-assisted underlay CRN with single antenna users—discussed in Chapter 4, and in a SIMO-based underlay CRN—analyzed in Section 5.3.

5.5 Summary

In this chapter, we have analyzed the performance of a dual-hop DF relay-assisted underlay CRN with multiantenna SR under κ-μ shadowed channels. The channels at SR are considered to be spatially correlated and MRC is employed to combine signals received at different antennas at SR. For the performance analysis, we have derived the analytical expressions for outage probability and ergodic capacity. We have shown that the performance of the system degrades as the spatial correlation at SR increases. This is because of decrease in independent spatial

directions at SR with the increasing correlation among channels. The performance of the system increases as the number of antenna at SR increases which is due to increased spatial diversity of SR. The performance of the system also increases when Q/N_0 increases. This is because of increased transmission power of ST and relay nodes as Q/N_0 increased. Moreover, we have observed that the SUs communication is favorable under severe fading/shadowing at the interfering links only up to a certain value of peak interference power constraint of PR. Beyond this value of peak interference power constraint of PR, the SUs communication improve under less severe fading/shadowing at the interfering links. The analytical results are validated by the simulation results and they are in close agreement.

6

Conclusions and Future Work

Contents

6.1 Research Contributions 100
6.2 Future Directions of Research 101

In this chapter, we summarize the research contributions of our work in Section 6.1 and conclude with some of the future directions of research in Section 6.2.

6.1 Research Contributions

Performance of interweave- and underlay-paradigm based cognitive radio networks (CRNs) with multiantenna and cooperative users have been analyzed in the presence of spatial correlation. For the performance analyses, the analytical expressions for (a) probability of false-alarm and detection for interweave paradigm based CRN and (b) outage probability and ergodic capacity for underlay paradigm based CRN have been derived. The effects of various parameters on analytical performance measures have been studied for the considered systems. The analytical results have been validated by Monte-Carlo simulations and found to be closely matched. The specific contributions of the thesis are enumerated below.

- Spectrum sensing schemes for interweave paradigm based CRNs
  - Two spectrum sensing schemes, weighted cross-correlation absolute value detector and weighted energy detector, have been proposed for interweave paradigm based CRNs. The proposed sensing schemes exploit the knowledge of spatial correlation of noise at the secondary receiver. These schemes are simple, practically implementable, and shown to have improved performance vis-a-vis the existing detectors.
  - For performance analysis, the analytical expressions for decision threshold, probability of false-alarm, and probability of detection have been derived.
- Performance analysis of underlay paradigm based CRN with multiantenna users under prewhitened interfering signals using outdated channel information
  - The effect of outdated channel information based prewhitening of spatially correlated interfering signals has been analyzed. It has been shown that the performance of both primary and secondary systems are susceptible to the outdated channel information.

It has also been shown that, for SU system, the effect of outdated channel information is more harmful than the interference from PU system.

- The analytical expressions for outage probability and channel capacity have been derived.

- Performance analysis of a dual-hop cooperative relay-assisted underlay CRN under κ-μ shadowed channel
  - The performance of a dual-hop DF relay-assisted underlay CRN has been analyzed firstly for single antenna at all users under the κ-μ shadowed channels. Secondly, the analysis has been extended for multiantenna at the secondary receiver with spatially correlated channels.
  - The analytical expressions for outage probability and ergodic capacity have been derived in both scenarios.
  - An important observation that the secondary user communication is favorable under severe fading/shadowing at the interfering links only up to a certain value of peak interference power constraint (PIPC) of primary receiver has been depicted. Beyond this value of PIPC, the performance of the SU system improves under less severe faded/shadowed interfering channels.

The derived analytical expressions for performance measures are in the forms of Q, gamma, incomplete gamma, and hypergeometric functions. The analytical expressions have been evaluated in MATLAB and Mathematica. Wherever the sum of infinite series have been encountered in the analytical expressions, they have been evaluated by truncating to finite number of terms ensuring the sufficient accuracy.

6.2 Future Directions of Research

Some of the future works that can be considered as extensions of this work are suggested as follows.

- Analysis of the effect of impairment in a prior correlation information on spectrum sensing schemes in interweave paradigm based CRN.
- Performance analysis of the DF dual-hop relay-assisted underlay CRN with prewhitened interfering signals using outdated channel information.
- Performance analysis of the DF dual-hop relay-assisted underlay CRN with multiantenna users considering various antenna selections and combining schemes under composite fading and shadowing channel models with/without spatial correlation.
- Performance analysis of the dual-hop relay-assisted underlay CRN assuming amplify-and-forward (AF) protocol at relay node under the scenarios mentioned in second and third points above.
- Analysis of the effect of relay location on the performance of DF/AF dual-hop relay-assisted underlay CRN.
- Performance analysis of the multi-hop relay-assisted underlay CRN under the scenarios mentioned in second and third points above.

A

Appendix

Contents

A.1 Calculation of Mean and Variance of g_{ij} 104
A.2 Calculation of Mean and Variance of Real and Imaginary Parts of g_{ij} for $i \neq j$ 106
A.3 Calculation of Eq. (2.29) 108
A.4 Calculation of Power Margin Factor κ_m 110
A.5 Proof of Lemma 1 112
A.6 Conditions for Interchangeability of Summation and Integration . 115
A.7 Derivation of Eq. (5.27) 116

A.1 Calculation of Mean and Variance of g_{ij}

Linearly transformed received signal vector $\mathbf{z}(n)$ at the SU node is given as

$$\begin{aligned}\mathbf{z}(n) &= \mathbf{U}^H\mathbf{y}(n)\\ &= \mathbf{U}^H(\tilde{\mathbf{h}}s(n)+\hat{\mathbf{w}}(n))\\ &= \mathbf{h}s(n)+\mathbf{w}(n)\end{aligned} \tag{A.1}$$

where $\mathbf{h}=\mathbf{U}^H\tilde{\mathbf{h}}$ and $\mathbf{w}(n)=\mathbf{U}^H\hat{\mathbf{w}}(n)$. It can be determined that $\mathbf{w}(n)\sim\mathcal{CN}(0,\sigma_w^2\Lambda)$. Now, for a large value of N, g_{ij} can be assumed to be Gaussian distributed with mean and variance determined as follows

$$\begin{aligned}\mathrm{E}[g_{ij}] &= \frac{1}{\lambda_i\lambda_j}\mathrm{E}[\mathbf{z}_i^H\mathbf{z}_j e^{\mathbf{j}\phi_{ij}}]\\ &= \frac{1}{\lambda_i\lambda_j}\mathrm{E}[(h_i\mathbf{s}+\mathbf{w}_i)^H(h_j\mathbf{s}+\mathbf{w}_j)e^{\mathbf{j}\phi_{ij}}]\\ &= \frac{1}{\lambda_i\lambda_j}\left(|h_i|\,|h_j|\,\mathrm{E}[\mathbf{s}^H\mathbf{s}]+\mathrm{E}[\mathbf{w}_i^H\mathbf{w}_j e^{\mathbf{j}\phi_{ij}}]\right)\\ &= \frac{N}{\lambda_i\lambda_j}(|h_i|\,|h_j|\,\varepsilon_s+\sigma_w^2\lambda_{i(=j)}\delta_{ij})\end{aligned} \tag{A.2}$$

$$\begin{aligned}\mathrm{var}[g_{ij}] &= \frac{1}{\lambda_i^2\lambda_j^2}\mathrm{var}[\sum_{n=1}^{N}z_i^*(n)z_j(n)e^{\mathbf{j}\phi_{ij}}]\\ &= \frac{1}{\lambda_i^2\lambda_j^2}\sum_{n_1=1}^{N}\sum_{n_2=1}^{N}\mathrm{cov}[z_i^*(n_1)z_j(n_1)e^{\mathbf{j}\phi_{ij}},z_i^*(n_2)z_j(n_2)e^{\mathbf{j}\phi_{ij}}]\\ &= \frac{1}{\lambda_i^2\lambda_j^2}\left(\sum_{n_1=1}^{N}\mathrm{var}[z_i^*(n_1)z_j(n_1)e^{\mathbf{j}\phi_{ij}}]+2\sum_{n_1<n_2}\mathrm{cov}[z_i^*(n_1)z_j(n_1)e^{\mathbf{j}\phi_{ij}},z_i^*(n_2)z_j(n_2)e^{\mathbf{j}\phi_{ij}}]\right).\end{aligned} \tag{A.3}$$

First term in (A.3) can be calculated as

$$\mathrm{var}[z_i^*(n_1)z_j(n_1)e^{\mathbf{j}\phi_{ij}}]=\mathrm{E}[\left|z_i^*(n_1)z_j(n_1)e^{\mathbf{j}\phi_{ij}}\right|^2]-\left|\mathrm{E}[z_i^*(n_1)z_j(n_1)e^{\mathbf{j}\phi_{ij}}]\right|^2. \tag{A.4}$$

The first term in (A.4) can be determined by using an identity [119, 120] $\mathrm{E}[x_1x_2x_3x_4]=\mathrm{E}[x_1x_2]\mathrm{E}[x_3x_4]+\mathrm{E}[x_1x_3]\mathrm{E}[x_2x_4]+\mathrm{E}[x_1x_4]\mathrm{E}[x_2x_3]-2\mathrm{E}[x_1]\mathrm{E}[x_2]\mathrm{E}[x_3]\mathrm{E}[x_4]$ considering $x_1=$

$z_i^*(n_1)$, $x_2 = z_j(n_1)e^{\mathbf{j}\phi_{ij}}$, $x_3 = z_i(n_1)$, and $x_4 = z_j^*(n_1)e^{-\mathbf{j}\phi_{ij}}$ where x_1, x_2, x_3, and x_4 are jointly complex Gaussian distributed. Thus,

$$\begin{aligned}
\mathrm{E}[\left|z_i^*(n_1)z_j(n_1)e^{\mathbf{j}\phi_{ij}}\right|^2] &= \mathrm{E}[z_i^*(n_1)z_j(n_1)e^{\mathbf{j}\phi_{ij}}z_i(n_1)z_j^*(n_1)e^{-\mathbf{j}\phi_{ij}}] \\
&= \mathrm{E}[z_i^*(n_1)z_j(n_1)e^{\mathbf{j}\phi_{ij}}]\mathrm{E}[z_i(n_1)z_j^*(n_1)e^{-\mathbf{j}\phi_{ij}}] + \mathrm{E}[z_i^*(n_1)z_i(n_1)] \\
&\quad \times \mathrm{E}[z_j(n_1)z_j^*(n_1)] + \mathrm{E}[z_i^*(n_1)z_j^*(n_1)e^{-\mathbf{j}\phi_{ij}}]\mathrm{E}[z_j(n_1)z_i(n_1)e^{\mathbf{j}\phi_{ij}}] \\
&\quad - 2\mathrm{E}[z_i^*(n_1)]\mathrm{E}[z_j(n_1)e^{\mathbf{j}\phi_{ij}}]\mathrm{E}[z_i(n_1)]\mathrm{E}[z_j^*(n_1)e^{-\mathbf{j}\phi_{ij}}] \qquad \text{(A.5)} \\
&= \left(|h_i|\,|h_j|\,\varepsilon_s + \sigma_w^2\lambda_{i(=j)}\delta_{ij}\right)^2 + \left(|h_i|^2\,\varepsilon_s + \sigma_w^2\lambda_i\right)\left(|h_j|^2\,\varepsilon_s + \sigma_w^2\lambda_j\right). \qquad \text{(A.6)}
\end{aligned}$$

In (A.5), first and second terms are calculated similar to (A.2), third term vanishes as $\mathrm{E}[(s^*(n_1))^2] = 0$ and $\mathrm{E}[w_i^*(n_1)w_j^*(n_1)] = 0$, and fourth term becomes zero as both signal and noise are zero-mean. Further, second term in (A.4) can be calculated similar to (A.2) as

$$\left|\mathrm{E}[z_i^*(n_1)z_j(n_1)e^{\mathbf{j}\phi_{ij}}]\right|^2 = \left(|h_i|\,|h_j|\,\varepsilon_s + \sigma_w^2\lambda_{i(=j)}\delta_{ij}\right)^2. \qquad \text{(A.7)}$$

From (A.6) and (A.7), (A.4) can be obtained as

$$\mathrm{var}[z_i^*(n_1)z_j(n_1)e^{\mathbf{j}\phi_{ij}}] = \left(|h_i|^2\,\varepsilon_s + \sigma_w^2\lambda_i\right)\left(|h_j|^2\,\varepsilon_s + \sigma_w^2\lambda_j\right). \qquad \text{(A.8)}$$

Second term in (A.3) can be calculated as

$$\begin{aligned}
\mathrm{cov}[z_i^*(n_1)z_j(n_1)e^{\mathbf{j}\phi_{ij}}, z_i^*(n_2)z_j(n_2)e^{\mathbf{j}\phi_{ij}}] &= \mathrm{E}[z_i^*(n_1)z_j(n_1)e^{\mathbf{j}\phi_{ij}}z_i(n_2)z_j^*(n_2)e^{-\mathbf{j}\phi_{ij}}] \\
&\quad - \mathrm{E}[z_i^*(n_1)z_j(n_1)e^{\mathbf{j}\phi_{ij}}]\mathrm{E}[z_i(n_2)z_j^*(n_2)e^{-\mathbf{j}\phi_{ij}}] \\
&= \mathrm{E}[z_i^*(n_1)z_j(n_1)e^{\mathbf{j}\phi_{ij}}]\mathrm{E}[z_i(n_2)z_j^*(n_2)e^{-\mathbf{j}\phi_{ij}}] \\
&\quad - \mathrm{E}[z_i^*(n_1)z_j(n_1)e^{\mathbf{j}\phi_{ij}}]\mathrm{E}[z_i(n_2)z_j^*(n_2)e^{-\mathbf{j}\phi_{ij}}] \\
&= 0. \qquad \text{(A.9)}
\end{aligned}$$

Now, from (A.3), (A.8), and (A.9), we have

$$\mathrm{var}[g_{ij}] = \frac{N\left(|h_i|^2\,\varepsilon_s + \sigma_w^2\lambda_i\right)\left(|h_j|^2\,\varepsilon_s + \sigma_w^2\lambda_j\right)}{\lambda_i^2\lambda_j^2}. \qquad \text{(A.10)}$$

A.2 Calculation of Mean and Variance of Real and Imaginary Parts of g_{ij} for $i \neq j$

The mean of the real part of g_{ij} can be obtained as

$$\mathrm{E}[\Re\{g_{ij}\}] = \mathrm{E}\left[\frac{g_{ij} + g_{ij}^*}{2}\right] = \frac{N\varepsilon_s |h_i| |h_j|}{\lambda_i \lambda_j}. \tag{A.11}$$

$\mathrm{E}[g_{ij}]$ and $\mathrm{E}[g_{ij}^*]$ in (A.11) can be calculated similar to (A.2) considering $i \neq j$. Further, the variance of the real part of g_{ij} can be determined as

$$\begin{aligned}
\mathrm{var}[\Re\{g_{ij}\}] &= \mathrm{var}\left[\frac{g_{ij} + g_{ij}^*}{2}\right] \\
&= \frac{1}{4\lambda_i^2\lambda_j^2}\mathrm{var}[\mathbf{z}_i^H \mathbf{z}_j e^{\mathbf{j}\phi_{ij}} + \mathbf{z}_j^H \mathbf{z}_i e^{-\mathbf{j}\phi_{ij}}] \\
&= \frac{\mathrm{E}[(\mathbf{z}_i^H \mathbf{z}_j e^{\mathbf{j}\phi_{ij}} + \mathbf{z}_j^H \mathbf{z}_i e^{-\mathbf{j}\phi_{ij}})^2] - \mathrm{E}^2[\mathbf{z}_i^H \mathbf{z}_j e^{\mathbf{j}\phi_{ij}} + \mathbf{z}_j^H \mathbf{z}_i e^{-\mathbf{j}\phi_{ij}}]}{4\lambda_i^2\lambda_j^2}.
\end{aligned} \tag{A.12}$$

First term in the numerator of (A.12) can be calculated as

$$\mathrm{E}[(\mathbf{z}_i^H \mathbf{z}_j e^{\mathbf{j}\phi_{ij}} + \mathbf{z}_j^H \mathbf{z}_i e^{-\mathbf{j}\phi_{ij}})^2] = \mathrm{E}[(\mathbf{z}_i^H \mathbf{z}_j e^{\mathbf{j}\phi_{ij}})^2] + \mathrm{E}[(\mathbf{z}_j^H \mathbf{z}_i e^{-\mathbf{j}\phi_{ij}})^2] + 2\mathrm{E}[\mathbf{z}_i^H \mathbf{z}_j e^{\mathbf{j}\phi_{ij}} \mathbf{z}_j^H \mathbf{z}_i e^{-\mathbf{j}\phi_{ij}}]. \tag{A.13}$$

(A.13) can be solved by using an identity given by [120]

$$\begin{aligned}
\mathrm{E}[\mathbf{X}_1\mathbf{X}_2\mathbf{X}_3\mathbf{X}_4] =& \mathrm{E}[\mathbf{X}_1\mathbf{X}_2]\mathrm{E}[\mathbf{X}_3\mathbf{X}_4] + \mathrm{E}[\mathbf{X}_3 \otimes \mathbf{X}_1]\mathrm{E}[\mathbf{X}_4 \otimes \mathbf{X}_2] \\
&+ \mathrm{E}[\mathbf{X}_1\mathrm{E}[\mathbf{X}_2\mathbf{X}_3]\mathbf{X}_4] - 2\mathrm{E}[\mathbf{X}_1]\mathrm{E}[\mathbf{X}_2]\mathrm{E}[\mathbf{X}_3]\mathrm{E}[\mathbf{X}_4]
\end{aligned} \tag{A.14}$$

where $\mathbf{X}_1$, $\mathbf{X}_2$, $\mathbf{X}_3$, and $\mathbf{X}_4$ are matrices of dimensions $p \times q$, $q \times 1$, $1 \times s$, and $s \times t$, respectively. The entries of $\mathbf{X}_1$, $\mathbf{X}_2$, $\mathbf{X}_3$, and $\mathbf{X}_4$ are jointly multivariate complex Gaussian distributed. Thus,

first term in (A.13) can be obtained as

$$\begin{aligned}
\mathrm{E}[(\mathbf{z}_i^H \mathbf{z}_j e^{\mathbf{j}\phi_{ij}})^2] &= \mathrm{E}[\mathbf{z}_i^H \mathbf{z}_j e^{\mathbf{j}\phi_{ij}} \mathbf{z}_i^H \mathbf{z}_j e^{\mathbf{j}\phi_{ij}}] \\
&= \mathrm{E}[\mathbf{z}_i^H \mathbf{z}_j e^{\mathbf{j}\phi_{ij}}]\mathrm{E}[\mathbf{z}_i^H \mathbf{z}_j e^{\mathbf{j}\phi_{ij}}] + \mathrm{E}[\mathbf{z}_i^H \otimes \mathbf{z}_i^H]\mathrm{E}[\mathbf{z}_j e^{\mathbf{j}\phi_{ij}} \otimes \mathbf{z}_j e^{\mathbf{j}\phi_{ij}}] \\
&\quad + \mathrm{E}[\mathbf{z}_i^H \mathrm{E}[\mathbf{z}_j e^{\mathbf{j}\phi_{ij}} \mathbf{z}_i^H]\mathbf{z}_j e^{\mathbf{j}\phi_{ij}}] - 2\mathrm{E}[\mathbf{z}_i^H]\mathrm{E}[\mathbf{z}_j e^{\mathbf{j}\phi_{ij}}]\mathrm{E}[\mathbf{z}_i^H]\mathrm{E}[\mathbf{z}_j e^{\mathbf{j}\phi_{ij}}] \qquad \text{(A.15)} \\
&= (|h_i|\,|h_j|\,N\varepsilon_s)^2 + 0 + |h_i|^2\,|h_j|^2\,N\varepsilon_s^2 + 0 \\
&= N(N+1)\varepsilon_s^2\,|h_i|^2\,|h_j|^2\,. \qquad \text{(A.16)}
\end{aligned}$$

In (A.15), first and third terms are calculated similar to (A.2) considering $i \neq j$, the second term becomes zero as $\mathrm{E}[(s^*(n))^2] = 0$ and $\mathrm{E}[(w_i^*(n))^2] = 0$, and fourth term becomes zero as both signal and noise are zero-mean. Similarly, the second and third terms in (A.13) can be determined as

$$\mathrm{E}[(\mathbf{z}_j^H \mathbf{z}_i e^{-\mathbf{j}\phi_{ij}})^2] = N(N+1)\varepsilon_s^2\,|h_i|^2\,|h_j|^2 \qquad \text{(A.17)}$$

and

$$\mathrm{E}[\mathbf{z}_i^H \mathbf{z}_j e^{\mathbf{j}\phi_{ij}} \mathbf{z}_j^H \mathbf{z}_i e^{-\mathbf{j}\phi_{ij}}] = N^2\varepsilon_s^2\,|h_i|^2\,|h_j|^2 + N(|h_i|^2\,\varepsilon_s + \sigma_w^2\lambda_i)(|h_j|^2\,\varepsilon_s + \sigma_w^2\lambda_j), \qquad \text{(A.18)}$$

respectively. From (A.16), (A.17), and (A.18), (A.13) can be obtained as

$$\mathrm{E}[(\mathbf{z}_i^H \mathbf{z}_j e^{\mathbf{j}\phi_{ij}} + \mathbf{z}_j^H \mathbf{z}_i e^{-\mathbf{j}\phi_{ij}})^2] = N(3N+2)\varepsilon_s^2\,|h_i|^2\,|h_j|^2 + N(|h_i|^2\,\varepsilon_s + \sigma_w^2\lambda_i)(|h_j|^2\,\varepsilon_s + \sigma_w^2\lambda_j). \qquad \text{(A.19)}$$

Using (A.2) and (A.19), (A.12) can be solved to

$$\mathrm{var}[\Re\{g_{ij}\}] = \frac{N}{2\lambda_i^2\lambda_j^2}[\varepsilon_s^2\,|h_i|^2\,|h_j|^2 + (|h_i|^2\,\varepsilon_s + \sigma_w^2\lambda_i)(|h_j|^2\,\varepsilon_s + \sigma_w^2\lambda_j)]. \qquad \text{(A.20)}$$

Similarly, the mean and the variance of the imaginary part of g_{ij} can be obtained as

$$\mathrm{E}[\Im\{g_{ij}\}] = \mathrm{E}\left[\frac{g_{ij} - g_{ij}^*}{2\mathbf{j}}\right] = 0 \qquad \text{(A.21)}$$

and

$$\begin{aligned}\mathrm{var}[\Im\{g_{ij}\}] &= \mathrm{var}\left[\frac{g_{ij}-g_{ij}^{*}}{2\mathbf{j}}\right] \\ &= \frac{\mathrm{E}[\left|\mathbf{z}_i^H\mathbf{z}_j e^{\mathbf{j}\phi_{ij}}-\mathbf{z}_j^H\mathbf{z}_i e^{-\mathbf{j}\phi_{ij}}\right|^2]-\left|\mathrm{E}[\mathbf{z}_i^H\mathbf{z}_j e^{\mathbf{j}\phi_{ij}}-\mathbf{z}_j^H\mathbf{z}_i e^{-\mathbf{j}\phi_{ij}}]\right|^2}{4\lambda_i^2\lambda_j^2} \\ &= \frac{N[-\varepsilon_s^2\left|h_i\right|^2\left|h_j\right|^2+(\left|h_i\right|^2\varepsilon_s+\sigma_w^2\lambda_i)(\left|h_j\right|^2\varepsilon_s+\sigma_w^2\lambda_j)]}{2\lambda_i^2\lambda_j^2}, \end{aligned} \tag{A.22}$$

respectively.

A.3 Calculation of Eq. (2.29)

$$\begin{aligned}\mathrm{var}[T_{WCCAVD}|\mathcal{H}_1,\mathbf{h}] &\approx \sum_{i=1}^{M}\sum_{j=1}^{M}\sum_{k=1}^{M}\sum_{l=1}^{M}\mathrm{cov}[\Re\{g_{ij}\},\Re\{g_{kl}\}] \\ &= \sum_{i=1}^{M}\sum_{j=1}^{M}\sum_{k=1}^{M}\sum_{l=1}^{M}(\mathrm{E}[\Re\{g_{ij}\}\Re\{g_{kl}\}]-\mathrm{E}[\Re\{g_{ij}\}]\mathrm{E}[\Re\{g_{kl}\}]) \\ &= \sum_{i=1}^{M}\sum_{j=1}^{M}\sum_{k=1}^{M}\sum_{l=1}^{M}\left(\mathrm{E}\left[\frac{g_{ij}+g_{ij}^{*}}{2}\frac{g_{kl}+g_{kl}^{*}}{2}\right]-\mathrm{E}\left[\frac{g_{ij}+g_{ij}^{*}}{2}\right]\mathrm{E}\left[\frac{g_{kl}+g_{kl}^{*}}{2}\right]\right) \\ &= \sum_{i=1}^{M}\sum_{j=1}^{M}\sum_{k=1}^{M}\sum_{l=1}^{M}\frac{1}{4}\left(\{\mathrm{E}[g_{ij}g_{kl}]-\mathrm{E}[g_{ij}]\mathrm{E}[g_{kl}]\}+\{\mathrm{E}[g_{ij}^{*}g_{kl}^{*}]-\mathrm{E}[g_{ij}^{*}]\mathrm{E}[g_{kl}^{*}]\}\right. \\ &\quad \left.+\{\mathrm{E}[g_{ij}^{*}g_{kl}]-\mathrm{E}[g_{ij}^{*}]\mathrm{E}[g_{kl}]\}+\{\mathrm{E}[g_{ij}g_{kl}^{*}]-\mathrm{E}[g_{ij}]\mathrm{E}[g_{kl}^{*}]\}\right). \end{aligned} \tag{A.23}$$

First term in (A.23) can be calculated as follows.

$$\begin{aligned}
\mathrm{E}[g_{ij}g_{kl}] &= \frac{1}{\lambda_i\lambda_j\lambda_k\lambda_l}\mathrm{E}[\mathbf{z}_i^H\mathbf{z}_j e^{\mathbf{j}\phi_{ij}}\mathbf{z}_k^H\mathbf{z}_l e^{\mathbf{j}\phi_{kl}}] \\
&= \frac{1}{\lambda_i\lambda_j\lambda_k\lambda_l}\mathrm{E}[(h_i\mathbf{s}+\mathbf{w}_i)^H(h_j\mathbf{s}+\mathbf{w}_j)e^{\mathbf{j}\phi_{ij}}(h_k\mathbf{s}+\mathbf{w}_k)^H(h_l\mathbf{s}+\mathbf{w}_l)e^{\mathbf{j}\phi_{kl}}] \\
&= \frac{1}{\lambda_i\lambda_j\lambda_k\lambda_l}\big(|h_i|\,|h_j|\,|h_k|\,|h_l|\,\mathrm{E}[\mathbf{s}^H\mathbf{s}\mathbf{s}^H\mathbf{s}] + |h_i|\,|h_j|\,\mathrm{E}[\mathbf{s}^H\mathbf{s}]\mathrm{E}[\mathbf{w}_k^H\mathbf{w}_l e^{\mathbf{j}\phi_{kl}}] \\
&\quad + |h_k|\,|h_l|\,\mathrm{E}[\mathbf{w}_i^H\mathbf{w}_j e^{\mathbf{j}\phi_{ij}}]\mathrm{E}[\mathbf{s}^H\mathbf{s}] + \mathrm{E}[\mathbf{w}_i^H\mathbf{w}_j e^{\mathbf{j}\phi_{ij}}\mathbf{w}_k^H\mathbf{w}_l e^{\mathbf{j}\phi_{kl}}] \\
&\quad + |h_i|\,|h_k|\,\mathrm{E}[\mathbf{s}^H\mathbf{w}_j e^{-\mathbf{j}\phi_j}\mathbf{s}^H\mathbf{w}_l e^{-\mathbf{j}\phi_l}] + |h_i|\,|h_l|\,\mathrm{E}[\mathbf{s}^H\mathbf{w}_j e^{-\mathbf{j}\phi_j}\mathbf{w}_k^H\mathbf{s}e^{\mathbf{j}\phi_k}] \\
&\quad + |h_j|\,|h_k|\,\mathrm{E}[\mathbf{w}_i^H\mathbf{s}e^{\mathbf{j}\phi_i}\mathbf{s}^H\mathbf{w}_l e^{-\mathbf{j}\phi_l}] + |h_j|\,|h_l|\,\mathrm{E}[\mathbf{w}_i^H\mathbf{s}e^{\mathbf{j}\phi_i}\mathbf{w}_k^H\mathbf{s}e^{\mathbf{j}\phi_k}]\big) \qquad \text{(A.24)} \\
&= \frac{1}{\lambda_i\lambda_j\lambda_k\lambda_l}\big(|h_i|\,|h_j|\,|h_k|\,|h_l|\,N(N+1)\varepsilon_s^2 + |h_i|\,|h_j|\,N^2\varepsilon_s\sigma_w^2\lambda_{k(=l)}\delta_{kl} \\
&\quad + |h_k|\,|h_l|\,N^2\varepsilon_s\sigma_w^2\lambda_{i(=j)}\delta_{ij} + N^2\sigma_w^4\lambda_{i(=j)}\lambda_{k(=l)}\delta_{ij}\delta_{kl} \\
&\quad + N\sigma_w^4\lambda_{j(=k)}\lambda_{i(=l)}\delta_{jk}\delta_{il} + 0 + |h_i|\,|h_l|\,N\varepsilon_s\sigma_w^2\lambda_{j(=k)}\delta_{jk} \\
&\quad + |h_j|\,|h_k|\,N\varepsilon_s\sigma_w^2\lambda_{i(=l)}\delta_{il} + 0\big)\,. \qquad \text{(A.25)}
\end{aligned}$$

Rest of the terms in (A.24) vanish as channel coefficient, PU signal, and noise are independent and zero-mean. Using (A.14) wherever required, the final form is obtained as in (A.25). Further, using (A.25) and (A.2)

$$\begin{aligned}
\mathrm{E}[g_{ij}g_{kl}] - \mathrm{E}[g_{ij}]\mathrm{E}[g_{kl}] &= \frac{1}{\lambda_i\lambda_j\lambda_k\lambda_l}\big(|h_i|\,|h_j|\,|h_k|\,|h_l|\,N\varepsilon_s^2 + N\sigma_w^4\lambda_{j(=k)}\lambda_{i(=l)}\delta_{jk}\delta_{il} \\
&\quad + N\varepsilon_s\sigma_w^2\big(|h_i|\,|h_l|\,\lambda_{j(=k)}\delta_{jk} + |h_j|\,|h_k|\,\lambda_{i(=l)}\delta_{il}\big)\big)\,. \qquad \text{(A.26)}
\end{aligned}$$

Similarly,

$$\begin{aligned}
\mathrm{E}[g_{ij}^*g_{kl}^*] - \mathrm{E}[g_{ij}^*]\mathrm{E}[g_{kl}^*] &= \frac{1}{\lambda_i\lambda_j\lambda_k\lambda_l}\big(|h_i|\,|h_j|\,|h_k|\,|h_l|\,N\varepsilon_s^2 + N\sigma_w^4\lambda_{j(=k)}\lambda_{i(=l)}\delta_{jk}\delta_{il} \\
&\quad + N\varepsilon_s\sigma_w^2\big(|h_i|\,|h_l|\,\lambda_{j(=k)}\delta_{jk} + |h_j|\,|h_k|\,\lambda_{i(=l)}\delta_{il}\big)\big)\,. \qquad \text{(A.27)}
\end{aligned}$$

$$\begin{aligned}
\mathrm{E}[g_{ij}^*g_{kl}] - \mathrm{E}[g_{ij}^*]\mathrm{E}[g_{kl}] &= \frac{1}{\lambda_i\lambda_j\lambda_k\lambda_l}\big(|h_i|\,|h_j|\,|h_k|\,|h_l|\,N\varepsilon_s^2 + N\sigma_w^4\lambda_{i(=k)}\lambda_{j(=l)}\delta_{ik}\delta_{jl} \\
&\quad + N\varepsilon_s\sigma_w^2\big(|h_i|\,|h_k|\,\lambda_{j(=l)}\delta_{jl} + |h_j|\,|h_l|\,\lambda_{i(=k)}\delta_{ik}\big)\big)\,. \qquad \text{(A.28)}
\end{aligned}$$

$$\mathrm{E}[g_{ij}g_{kl}^*] - \mathrm{E}[g_{ij}]\mathrm{E}[g_{kl}^*] = \frac{1}{\lambda_i\lambda_j\lambda_k\lambda_l}\left(|h_i|\,|h_j|\,|h_k|\,|h_l|\,N\varepsilon_s^2 + N\sigma_w^4\lambda_{i(=k)}\lambda_{j(=l)}\delta_{ik}\delta_{jl}\right.$$
$$\left.+N\varepsilon_s\sigma_w^2\left(|h_i|\,|h_k|\,\lambda_{j(=l)}\delta_{jl} + |h_j|\,|h_l|\,\lambda_{i(=k)}\delta_{ik}\right)\right). \tag{A.29}$$

Using (A.26), (A.27), (A.28), and (A.29), (A.23) can be obtained as (2.29).

A.4 Calculation of Power Margin Factor κ_m

The interference outage probability ε_o is defined as

$$\varepsilon_o \geqslant 1 - \Pr\left(P_S \max_{\{i,j\}\in\{1,..,M\}}\{|(\mathbf{H}_{PS})_{i,j}|^2\} \leqslant Q\right). \tag{A.30}$$

Let us define $z_0 = \max\limits_{\{i,j\}\in\{1,..,M\}}\{|(\mathbf{H}_{PS})_{i,j}|^2\}$ and $\hat{z}_0 = \max\limits_{\{i,j\}\in\{1,..,M\}}\{|(\hat{\mathbf{H}}_{PS})_{i,j}|^2\}$. Using (3.7), the interference outage in (A.30) can be calculated as

$$\begin{aligned}\varepsilon_o &= \Pr\left(\frac{\kappa_m Q z_0}{\hat{z}_0} > Q, P_M z_0 > Q\right)\\ &= \Pr\left(\frac{z_0}{\hat{z}_0} > \frac{1}{\kappa_m}, z_0 > \frac{Q}{P_M}\right)\\ &= \int_{\frac{Q}{P_M}}^{\infty}\int_{0}^{\kappa_m x} f_{z_0,\hat{z}_0}(x,y)\,dy\,dx\end{aligned} \tag{A.31}$$

where $f_{z_0,\hat{z}_0}(x,y)$ is the joint PDF of z_0 and $\hat{z}_0$ and is presented as [67]

$$f_{z_0,\hat{z}_0}(x,y) = \frac{1}{(1-\rho_0^2)\eta_{PS}^2}\exp\left(-\frac{x+y}{(1-\rho_0^2)\eta_{PS}}\right) I_0\left(\frac{2\rho_0\sqrt{xy}}{(1-\rho_0^2)\eta_{PS}}\right), \quad x,y \geqslant 0 \tag{A.32}$$

where $I_0(\cdot)$ is zeroth-order modified Bessel function of the first kind. Now, (A.31) can be calculated as

$$\varepsilon_o = \frac{1}{(1-\rho_0^2)\eta_{PS}^2}\int_{\frac{Q}{P_M}}^{\infty}\exp\left(-\frac{x}{(1-\rho_0^2)\eta_{PS}}\right)\underbrace{\int_{0}^{\kappa_m x}\exp\left(-\frac{y}{(1-\rho_0^2)\eta_{PS}}\right) I_0\left(\frac{2\rho_0\sqrt{xy}}{(1-\rho_0^2)\eta_{PS}}\right)dy}_{I(x)}\,dx. \tag{A.33}$$

In (A.33), $I(x)$ can be calculated using [121, Eq. 10] as

$$I(x) = (1-\rho_0^2)\eta_{PS} \exp\left(\frac{\rho_0^2 x}{(1-\rho_0^2)\eta_{PS}}\right)\left[1 - Q_0\left(\sqrt{\frac{2\rho_0^2 x}{(1-\rho_0^2)\eta_{PS}}}, \sqrt{\frac{2\kappa_m x}{(1-\rho_0^2)\eta_{PS}}}\right)\right] \tag{A.34}$$

where $Q_0(\cdot)$ is the first-order Marcum Q-function defined as [121]

$$Q_0(a,b) = \int_b^\infty t \exp\left(-\frac{t^2+a^2}{2}\right) I_0(at)dt. \tag{A.35}$$

Now, (A.33) can be written as

$$\varepsilon_o = \underbrace{\frac{1}{\eta_{PS}} \int_{\frac{Q}{P_M}}^\infty \exp\left(-\frac{x}{\eta_{PS}}\right)dx}_{I_1} - \underbrace{\frac{1}{\eta_{PS}} \int_{\frac{Q}{P_M}}^\infty \exp\left(-\frac{x}{\eta_{PS}}\right) Q_0\left(\sqrt{\frac{2\rho_0^2 x}{(1-\rho_0^2)\eta_{PS}}}, \sqrt{\frac{2\kappa_m x}{(1-\rho_0^2)\eta_{PS}}}\right) dx}_{I_2}. \tag{A.36}$$

In (A.36), I_1 is calculated as

$$I_1 = \frac{1}{\eta_{PS}} \int_{\frac{Q}{P_M}}^\infty \exp\left(-\frac{x}{\eta_{PS}}\right)dx = \exp\left(-\frac{Q}{P_M\eta_{PS}}\right). \tag{A.37}$$

In (A.36), I_2 can be calculated using [121, Eq. 55] as

$$\begin{aligned} I_2 =& \exp\left(-\frac{Q}{P_M\eta_{PS}}\right) Q_0\left(\sqrt{\frac{2\rho_0^2 Q}{(1-\rho_0^2)P_M\eta_{PS}}}, \sqrt{\frac{2\kappa_m Q}{(1-\rho_0^2)P_M\eta_{PS}}}\right) \\ &+ \frac{t_0}{r_0} Q_0\left(\sqrt{\frac{(l_0-r_0)Q}{2P_M}}, \sqrt{\frac{(l_0+r_0)Q}{2P_M}}\right) - \frac{t_0+r_0}{2r_0} \exp\left(-\frac{l_0 Q}{2P_M}\right) I_0\left(\frac{2\rho_0 Q\sqrt{\kappa_m}}{(1-\rho_0^2)P_M\eta_{PS}}\right) \end{aligned} \tag{A.38}$$

where $l_0 = \frac{2(1+\kappa_m)}{(1-\rho_0^2)\eta_{PS}}$, $r_0 = \frac{2\sqrt{(1+\kappa_m)^2 - 4\kappa_m\rho_0^2}}{(1-\rho_0^2)\eta_{PS}}$, $t_0 = \frac{2(1-\kappa_m)}{(1-\rho_0^2)\eta_{PS}}$. From (A.37), (A.38), and (A.36), the interference outage probability can be obtained as (3.8). The power margin factor κ_m needed to satisfy the prespecified interference outage is not calculated in a closed-form. Hence, the power margin factor κ_m can be calculated numerically for the prespecified value of interference outage probability ε_o.

A.5 Proof of Lemma 1

The channel capacity of the PU system can be obtained using (3.9) as

$$\begin{aligned} C_P &= \log_2 \det \Big(\mathbf{I}_M + \eta_P P_P \mathrm{E}\left[\mathbf{H}_P \mathbf{s}_P \mathbf{s}_P^H \mathbf{H}_P^H\right] \\ &\quad \times \left\{ \mathrm{E}\left[(\sqrt{\eta_{PS}}\sqrt{P_S}\mathbf{H}_{PS}\hat{\mathbf{s}}_S + \mathbf{w}_P)(\sqrt{\eta_{PS}}\sqrt{P_S}\mathbf{H}_{PS}\hat{\mathbf{s}}_S + \mathbf{w}_P)^H \right] \right\}^{-1} \Big) \\ &= \log_2 \det \left(\mathbf{I}_M + \frac{\eta_P P_P}{M} \mathbf{H}_P \mathbf{H}_P^H \left[\eta_{PS} P_S \mathrm{E}\left[\mathbf{H}_{PS}\hat{\mathbf{s}}_S \hat{\mathbf{s}}_S^H \mathbf{H}_{PS}^H\right] + N_0 \mathbf{I}_M \right]^{-1} \right). \end{aligned} \tag{A.39}$$

$\mathrm{E}\left[\mathbf{H}_{PS}\hat{\mathbf{s}}_S\hat{\mathbf{s}}_S^H\mathbf{H}_{PS}^H\right]$ in (A.39) is calculated as

$$\begin{aligned} \mathrm{E}\left[\mathbf{H}_{PS}\hat{\mathbf{s}}_S\hat{\mathbf{s}}_S^H\mathbf{H}_{PS}^H\right] &= \mathrm{E}\left[(\rho_0\hat{\mathbf{H}}_{PS} + \sqrt{1-\rho_0^2}\tilde{\mathbf{H}}_{PS}) \frac{\hat{\mathbf{H}}_{PS}^{-1}\mathbf{u}_S}{\sqrt{T_0}} \frac{\mathbf{u}_S^H \hat{\mathbf{H}}_{PS}^{-H}}{\sqrt{T_0}} (\rho_0\hat{\mathbf{H}}_{PS}^H + \sqrt{1-\rho_0^2}\tilde{\mathbf{H}}_{PS}^H) \right] \\ &= \frac{1}{T_0}\mathrm{E}\left[(\rho_0\mathbf{I}_M + \sqrt{1-\rho_0^2}\tilde{\mathbf{H}}_{PS}\hat{\mathbf{H}}_{PS}^{-1})\mathbf{u}_S\mathbf{u}_S^H(\rho_0\mathbf{I}_M + \sqrt{1-\rho_0^2}\hat{\mathbf{H}}_{PS}^{-H}\tilde{\mathbf{H}}_{PS}^H) \right] \\ &= \frac{1}{T_0}\left\{ \rho_0^2\mathrm{E}\left[\mathbf{u}_S\mathbf{u}_S^H\right] + \rho_0\sqrt{1-\rho_0^2}\mathrm{E}\left[\tilde{\mathbf{H}}_{PS}\hat{\mathbf{H}}_{PS}^{-1}\mathbf{u}_S\mathbf{u}_S^H\right] \right. \\ &\quad \left. + \rho_0\sqrt{1-\rho_0^2}\mathrm{E}\left[\mathbf{u}_S\mathbf{u}_S^H\hat{\mathbf{H}}_{PS}^{-H}\tilde{\mathbf{H}}_{PS}^H\right] + (1-\rho_0^2)\mathrm{E}\left[\tilde{\mathbf{H}}_{PS}\hat{\mathbf{H}}_{PS}^{-1}\mathbf{u}_S\mathbf{u}_S^H\hat{\mathbf{H}}_{PS}^{-H}\tilde{\mathbf{H}}_{PS}^H\right] \right\}. \end{aligned} \tag{A.40}$$

Using an identity given by [120, Eq. (2.3a)]

$$\begin{aligned} \mathrm{E}[\mathbf{X}_1\mathbf{X}_2\mathbf{X}_3\mathbf{X}_4] =& \mathrm{E}[\mathbf{X}_1\mathbf{X}_2]\mathrm{E}[\mathbf{X}_3\mathbf{X}_4] + \sum_{k=1}^{r}\left\{\mathrm{E}[(\mathbf{e}_k^T\mathbf{X}_3)\otimes\mathbf{X}_1]\mathrm{E}[\mathbf{X}_4\otimes(\mathbf{X}_2\mathbf{e}_k)]\right\} \\ &+ \mathrm{E}\left[\mathbf{X}_1\left\{\mathrm{E}[\mathbf{X}_2\mathbf{X}_3]\right\}\mathbf{X}_4\right] - 2\mathrm{E}[\mathbf{X}_1]\mathrm{E}[\mathbf{X}_2]\mathrm{E}[\mathbf{X}_3]\mathrm{E}[\mathbf{X}_4] \end{aligned} \tag{A.41}$$

where $\mathbf{X}_1$, $\mathbf{X}_2$, $\mathbf{X}_3$, and $\mathbf{X}_4$ are matrices of dimensions $p\times q$, $q\times r$, $r\times s$, and $s\times t$. $\mathbf{e}_k$ vector is defined as "1" at the kth position and "0" elsewhere. The dimension of $\mathbf{e}_k$ vector is according to the context.

Using (A.41) and exploiting the independence of $\tilde{\mathbf{H}}_{PS}$, $\hat{\mathbf{H}}_{PS}$, and $\mathbf{u}_S$, the second term in

the right-hand side of (A.40) is calculated as

$$\begin{aligned}\mathrm{E}\left[\tilde{\mathbf{H}}_{PS}\hat{\mathbf{H}}_{PS}^{-1}\mathbf{u}_S\mathbf{u}_S^H\right] &= \mathrm{E}[\tilde{\mathbf{H}}_{PS}\hat{\mathbf{H}}_{PS}^{-1}]\mathrm{E}[\mathbf{u}_S\mathbf{u}_S^H] + \sum_{k=1}^{M}\left\{\mathrm{E}[(\mathbf{e}_k^T\mathbf{u}_S)\otimes\tilde{\mathbf{H}}_{PS}]\mathrm{E}[\mathbf{u}_S^H\otimes(\hat{\mathbf{H}}_{PS}^{-1}\mathbf{e}_k)]\right\} \\ &\quad + \mathrm{E}[\tilde{\mathbf{H}}_{PS}\left\{\mathrm{E}[\hat{\mathbf{H}}_{PS}^{-1}\mathbf{u}_S]\right\}\mathbf{u}_S^H] - 2\mathrm{E}[\tilde{\mathbf{H}}_{PS}]\mathrm{E}[\hat{\mathbf{H}}_{PS}^{-1}]\mathrm{E}[\mathbf{u}_S]\mathrm{E}[\mathbf{u}_S^H] \\ &= \mathbf{0}. \end{aligned} \tag{A.42}$$

Similarly, the third term in the right-hand side of (A.40) can be obtained as

$$\mathrm{E}\left[\mathbf{u}_S\mathbf{u}_S^H\hat{\mathbf{H}}_{PS}^{-H}\tilde{\mathbf{H}}_{PS}^H\right] = \mathbf{0}. \tag{A.43}$$

Further, using (A.14), the fourth term in the right-hand side of (A.40) can be determined by considering $\mathbf{X}_1 = \tilde{\mathbf{H}}_{PS}\hat{\mathbf{H}}_{PS}^{-1}$, $\mathbf{X}_2 = \mathbf{u}_S$, $\mathbf{X}_3 = \mathbf{u}_S^H$, and $\mathbf{X}_4 = \hat{\mathbf{H}}_{PS}^{-H}\tilde{\mathbf{H}}_{PS}^H$ as

$$\begin{aligned}&\mathrm{E}[\tilde{\mathbf{H}}_{PS}\hat{\mathbf{H}}_{PS}^{-1}\mathbf{u}_S\mathbf{u}_S^H\hat{\mathbf{H}}_{PS}^{-H}\tilde{\mathbf{H}}_{PS}^H]\} \\ &= \mathrm{E}[\tilde{\mathbf{H}}_{PS}\hat{\mathbf{H}}_{PS}^{-1}\mathbf{u}_S]\mathrm{E}[\mathbf{u}_S^H\hat{\mathbf{H}}_{PS}^{-H}\tilde{\mathbf{H}}_{PS}^H] + \mathrm{E}[\mathbf{u}_S^H\otimes(\tilde{\mathbf{H}}_{PS}\hat{\mathbf{H}}_{PS}^{-1})]\mathrm{E}[(\hat{\mathbf{H}}_{PS}^{-H}\tilde{\mathbf{H}}_{PS}^H)\otimes\mathbf{u}_S] \\ &\quad + \mathrm{E}[\tilde{\mathbf{H}}_{PS}\hat{\mathbf{H}}_{PS}^{-1}[\mathrm{E}[\mathbf{u}_S\mathbf{u}_S^H]]\hat{\mathbf{H}}_{PS}^{-H}\tilde{\mathbf{H}}_{PS}^H] - 2\mathrm{E}[\tilde{\mathbf{H}}_{PS}\hat{\mathbf{H}}_{PS}^{-1}]\mathrm{E}[\mathbf{u}_S]\mathrm{E}[\mathbf{u}_S^H]\mathrm{E}[\hat{\mathbf{H}}_{PS}^{-H}\tilde{\mathbf{H}}_{PS}^H] \\ &= \mathbf{0} + \mathbf{0} + \mathrm{E}[\tilde{\mathbf{H}}_{PS}\hat{\mathbf{H}}_{PS}^{-1}\hat{\mathbf{H}}_{PS}^{-H}\tilde{\mathbf{H}}_{PS}^H] - \mathbf{0}. \end{aligned} \tag{A.44}$$

To further solve (A.44), we use an identity given by [120, Eq. (2.3b)]

$$\begin{aligned}\mathrm{E}[\mathbf{X}_1\mathbf{X}_2\mathbf{X}_3\mathbf{X}_4] =& \mathrm{E}[\mathbf{X}_1\mathbf{X}_2]\mathrm{E}[\mathbf{X}_3\mathbf{X}_4] + \sum_{l=1}^{q}\sum_{m=1}^{s}\left\{\mathrm{E}[\mathbf{X}_1\mathbf{e}_l\mathbf{e}_m^T\mathbf{X}_3^T]\mathrm{E}[\mathbf{X}_2^T\mathbf{e}_l\mathbf{e}_m^T\mathbf{X}_4]\right\} \\ &+ \mathrm{E}\left[\mathbf{X}_1\left\{\mathrm{E}[\mathbf{X}_2\mathbf{X}_3]\right\}\mathbf{X}_4\right] - 2\mathrm{E}[\mathbf{X}_1]\mathrm{E}[\mathbf{X}_2]\mathrm{E}[\mathbf{X}_3]\mathrm{E}[\mathbf{X}_4] \end{aligned} \tag{A.45}$$

where $\mathbf{X}_1$, $\mathbf{X}_2$, $\mathbf{X}_3$, and $\mathbf{X}_4$ are matrices of dimensions $p\times q$, $q\times r$, $r\times s$, and $s\times t$. $\mathbf{e}_l$ and $\mathbf{e}_m$ vectors are defined as "1" at the lth and the mth positions, respectively, and "0" elsewhere. The dimensions of $\mathbf{e}_l$ and $\mathbf{e}_m$ vectors are according to the context. Now, (A.44) can be calculated

considering $\mathbf{X}_1 = \tilde{\mathbf{H}}_{PS}$, $\mathbf{X}_2 = \hat{\mathbf{H}}_{PS}^{-1}\hat{\mathbf{H}}_{PS}^{-H}$, $\mathbf{X}_3 = \tilde{\mathbf{H}}_{PS}^{H}$, and $\mathbf{X}_4 = \mathbf{I}_M$ as

$$\begin{aligned}
&\mathrm{E}[\tilde{\mathbf{H}}_{PS}\hat{\mathbf{H}}_{PS}^{-1}\hat{\mathbf{H}}_{PS}^{-H}\tilde{\mathbf{H}}_{PS}^{H}] \\
&= \mathrm{E}[\tilde{\mathbf{H}}_{PS}(\hat{\mathbf{H}}_{PS}^{H}\hat{\mathbf{H}}_{PS})^{-1}\tilde{\mathbf{H}}_{PS}^{H}\mathbf{I}_M] \\
&= \mathrm{E}[\tilde{\mathbf{H}}_{PS}(\hat{\mathbf{H}}_{PS}^{H}\hat{\mathbf{H}}_{PS})^{-1}]\mathrm{E}[\tilde{\mathbf{H}}_{PS}^{H}\mathbf{I}_M] + \sum_{l=1}^{M}\sum_{m=1}^{M}\left\{\mathrm{E}[\tilde{\mathbf{H}}_{PS}\mathbf{e}_l\mathbf{e}_m^{T}\tilde{\mathbf{H}}_{PS}^{*}]\mathrm{E}[(\hat{\mathbf{H}}_{PS}^{H}\hat{\mathbf{H}}_{PS})^{-T}\mathbf{e}_l\mathbf{e}_m^{T}\mathbf{I}_M]\right\} \\
&\quad + \mathrm{E}\left[\tilde{\mathbf{H}}_{PS}\left\{\mathrm{E}[(\hat{\mathbf{H}}_{PS}^{H}\hat{\mathbf{H}}_{PS})^{-1}\tilde{\mathbf{H}}_{PS}^{H}]\right\}\mathbf{I}_M\right] - 2\mathrm{E}[\tilde{\mathbf{H}}_{PS}]\mathrm{E}[(\hat{\mathbf{H}}_{PS}^{H}\hat{\mathbf{H}}_{PS})^{-1}]\mathrm{E}[\tilde{\mathbf{H}}_{PS}^{H}]\mathrm{E}[\mathbf{I}_M] \\
&= \mathbf{0} + \mathrm{tr}\{(\hat{\mathbf{H}}_{PS}^{H}\hat{\mathbf{H}}_{PS})^{-1}\}\mathbf{I}_M + \mathbf{0} - \mathbf{0} \\
&= T_0\mathbf{I}_M. \qquad \text{(A.46)}
\end{aligned}$$

By putting the terms calculated in (A.42), (A.43), and (A.46) in (A.40), it is obtained as

$$\mathrm{E}\left[\mathbf{H}_{PS}\hat{\mathbf{s}}_S\hat{\mathbf{s}}_S^{H}\mathbf{H}_{PS}^{H}\right] = \frac{1}{T_0}\left\{\rho_0^2 + (1-\rho_0^2)T_0\right\}\mathbf{I}_M. \qquad \text{(A.47)}$$

Finally, from (A.39) and (A.47), the expression for channel capacity for the PU system can be obtained as in (3.11).

Similarly, the channel capacity for the SU system is derived as

$$\begin{aligned}
C_S &= \log_2\det\Big(\mathbf{I}_M + \eta_S P_S \mathrm{E}\left[\mathbf{H}_S\hat{\mathbf{s}}_S\hat{\mathbf{s}}_S^{H}\mathbf{H}_S^{H}\right] \\
&\quad \times \left\{\mathrm{E}\left[(\sqrt{\eta_{SP}}\sqrt{P_P}\mathbf{H}_{SP}\mathbf{s}_P + \mathbf{w}_S)(\sqrt{\eta_{SP}}\sqrt{P_P}\mathbf{H}_{SP}\mathbf{s}_P + \mathbf{w}_S)^{H}\right]\right\}^{-1}\Big) \\
&= \log_2\det\left(\mathbf{I}_M + \eta_S P_S \mathbf{H}_S \mathrm{E}\left[\frac{\hat{\mathbf{H}}_{PS}^{-1}\mathbf{u}_S}{\sqrt{T_0}}\frac{\mathbf{u}_S^{H}\hat{\mathbf{H}}_{PS}^{-H}}{\sqrt{T_0}}\right]\mathbf{H}_S^{H}\right. \\
&\quad \left.\times \left\{\eta_{SP}P_P\mathbf{H}_{SP}\mathrm{E}\left[\mathbf{s}_P\mathbf{s}_P^{H}\right]\mathbf{H}_{SP}^{H} + N_0\mathbf{I}_M\right\}^{-1}\right) \\
&= \log_2\det\left(\mathbf{I}_M + \frac{\eta_S P_S \mathbf{H}_S\hat{\mathbf{H}}_{PS}^{-1}\hat{\mathbf{H}}_{PS}^{-H}\mathbf{H}_S^{H}}{T_0}\left\{\frac{\eta_{SP}P_P\mathbf{H}_{SP}\mathbf{H}_{SP}^{H}}{M} + N_0\mathbf{I}_M\right\}^{-1}\right) \qquad \text{(A.48)}
\end{aligned}$$

which is also presented as (3.12).

A.6 Conditions for Interchangeability of Summation and Integration

Using Tonelli's theorem for sums and integrals [122], the first summation over j_1 and the integral in (4.22) can be interchanged as $A_6 \geq 0$ for $\frac{\phi_{11}}{\phi_{21}} = \frac{m_1}{\mu_1\kappa_1+m_1} \leq 1$. Similarly, the summation over j_2 can also be interchanged with the integral as $A_7 \geq 0$ for $\frac{\phi_{12}}{\phi_{22}} = \frac{m_2}{\mu_2\kappa_2+m_2} \leq 1$.

In order to interchange the integral with the third and the fourth summations over j_3 and j_4, respectively, we use the Lebesgue's Dominated Convergence Theorem (DCT) [123], [101]. For this, consider $f_{j_3}(x) = \frac{(1-\mu_1-j_1)_{j_3}(\alpha_3)_{j_3}}{j_3!(\alpha_3+1)_{j_3}} \frac{1}{(1+V(e^x-1))^{j_3}}$ where $V = \frac{N_0\theta_3}{Q\phi_{11}} > 0$. It is required to demonstrate that (i) $\sum_{j_3=0}^{\infty} f_{j_3}(x)$ converges and (ii) $\sum_{j_3=0}^{\infty} \int f_{j_3}(x)dx < \infty$.

(i) $\sum_{j_3=0}^{\infty} f_{j_3}(x)$ can be written as

$$\sum_{j_3=0}^{\infty} f_{j_3}(x) = {}_2F_1\left(1-\mu_1-j_1, \alpha_3; \alpha_3+1; \frac{1}{1+V(e^x-1)}\right). \tag{A.49}$$

Since, the series representation of ${}_2F_1(a,b;c;t)$ converges when $|t| < 1$. As $V > 0$, and hence, $\sum_{j_3=0}^{\infty} f_{j_3}(x)$ converges.

(ii) $\int f_{j_3}(x)dx$ can be obtained as

$$\int f_{j_3}(x)dx = \frac{(1-\mu_1-j_1)_{j_3}(\alpha_3)_{j_3} {}_2F_1\left(j_3, 1; j_3+1; \frac{V-1}{V-1-e^xV}\right)}{j_3!(\alpha_3+1)_{j_3} j_3 (1+V(e^x-1))^{j_3}}. \tag{A.50}$$

It can be shown that ${}_2F_1(\cdot)$ involved in (A.50) is bounded when $V \leq 1$ as

$${}_2F_1\left(j_3, 1; j_3+1; z\right) = \sum_{n=0}^{\infty} \frac{(j_3)_n (1)_n z^n}{(j_3+1)_n n!} = \sum_{n=0}^{\infty} \frac{j_3 z^n}{j_3+n} \leq \sum_{n=0}^{\infty} z^n = \frac{1}{1-z} < \infty \tag{A.51}$$

where $z = \frac{V-1}{V-1-e^xV}$ and $|z| < 1$. When $V > 1$, we transform ${}_2F_1(\cdot)$ involved in (A.50) as [116, Eq. 1.2.2.2] ${}_2F_1\left(j_3, 1; j_3+1; \frac{V-1}{V-1-e^xV}\right) = \left(1+e^{-x}\left(\frac{1}{V}-1\right)\right)^{j_3} {}_2F_1\left(j_3, j_3; j_3+1; e^{-x}\left(1-\frac{1}{V}\right)\right)$. It can be easily seen that the expression in the right hand side converges as $V > 1$. Moreover, $\frac{(\alpha_3)_{j_3}}{(\alpha_3+1)_{j_3}} = \frac{\alpha_3}{\alpha_3+j_3} \leq 1$, $\frac{1}{(1+V(e^x-1))^{j_3}} \leq 1$, and $\frac{1}{\Gamma(1-\mu_1-j_1)} < \infty$. Hence, to show that $\sum_{j_3=0}^{\infty} \int f_{j_3}(x)dx < \infty$, it is sufficient to demonstrate that $\sum_{j_3=0}^{\infty} q_{j_3}(x) < \infty$ where $q_{j_3}(x) = \frac{\Gamma(1-\mu_1-j_1+j_3)}{j_3\Gamma(j_3+1)}$. Using the asymptotic expansion of the ratio of two gamma functions [124], $q_{j_3}(x)$ can be written

as

$$q_{j_3}(x) = \frac{1}{j_3^{1+\mu_1+j_1}} \left(1 + \frac{(\mu_1+j_1)(\mu_1+j_1-1)}{2j_3} + O\left(\frac{1}{j_3^2}\right)\right) \tag{A.52}$$

which converges $\forall j_3$ as $\mu_1 > 0$ and $j_1 \geq 0$. Thus, $\sum_{j_3=0}^{\infty} \int f_{j_3}(x)dx < \infty$. Since, both the required conditions for DCT are fulfilled, hence, the integral can be interchanged with the third summation over j_3 in (4.22). Similarly, the integral can also be interchanged with the fourth summation over j_4 in (4.22).

A.7 Derivation of Eq. (5.27)

Ergodic capacity can be obtained as

$$C_{er} = \int_0^{\infty} [1 - P_O(e^x - 1)]dx. \tag{A.53}$$

Using (5.25) and expressing $F_2(\cdot)$ function by the sum of ${}_2F_1(\cdot)$ functions given as [117, Eq. 82]

$$F_2(a, b_1, b_2; c_1, c_2; x_1, x_2) = \sum_{k=0}^{\infty} \frac{(a)_k (b_2)_k}{(c_2)_k k!} x_2^k {}_2F_1(a+k, b_1; c_1; x_1), \quad |x_1| + |x_2| < 1, \tag{A.54}$$

(A.53) can be written as

$$\begin{aligned} C_{er} = \int_0^{\infty} & B_1 \frac{(N_0\theta_3(e^x-1))^{\mu_1}}{(Q\phi_{11} + N_0\theta_3(e^x-1))^{\alpha_3+\mu_1}} \sum_{j_1=0}^{\infty} B_2 \left(\frac{N_0\theta_3(e^x-1)}{Q\phi_{11} + N_0\theta_3(e^x-1)}\right)^{j_1} \\ & \times {}_2F_1\left(\alpha_3+\mu_1+j_1, 1; \alpha_3+1; \frac{Q\phi_{11}}{Q\phi_{11} + N_0\theta_3(e^x-1)}\right) \\ & \times B_3 \frac{(\phi N_0\theta_4(e^x-1))^{\Omega}}{(Q\bar{\gamma}_2 + \phi N_0\theta_4(e^x-1))^{\alpha_4+\Omega}} \sum_{j=0}^{\infty} U_j \sum_{j_3=0}^{\infty} B_4 \left(\frac{\phi N_0\theta_4(e^x-1)}{Q\bar{\gamma}_2 + \phi N_0\theta_4(e^x-1)}\right)^{j_3} \\ & \times {}_2F_1\left(\alpha_4+\Omega+j_3, 1; \alpha_4+1; \frac{Q\bar{\gamma}_2}{Q\bar{\gamma}_2 + \phi\theta_4 N_0(e^x-1)}\right) dx \end{aligned} \tag{A.55}$$

where $B_1 = \frac{Q^{\alpha_3}\phi_{11}^{m_1+\alpha_3}\Gamma(\alpha_3+\mu_1)}{\phi_{21}^{m_1}\Gamma(\alpha_3+1)\Gamma(\mu_1)}$, $B_2 = \frac{(\alpha_3+\mu_1)_{j_1}(m_1)_{j_1}}{j_1!(\mu_1)_{j_1}} \left(1 - \frac{\phi_{11}}{\phi_{21}}\right)^{j_1}$, $B_3 = \frac{V_0(Q\bar{\gamma}_2)^{\alpha_4}\Gamma(\alpha_4+\Omega)}{\Gamma(\alpha_4+1)}$, and $B_4 = \frac{(\alpha_4+\Omega)_{j_3}(m_2M+j)_{j_3}}{j_3!(\Omega)_{j_3}} \left(\frac{e_1}{1+e_1}\right)^{j_3}$. Applying interchange of integration and summation in j_1, as the function involved is convergent, and using a transformation given by [116, Eq. 1.2.2.2]

$${}_2F_1(a, b; c; x) = (1-x)^{c-a-b} {}_2F_1(c-a, c-b; c; x),$$

(A.55) can be simplified as

$$C_{er} = B_1 \sum_{j_1=0}^{\infty} B_2 \int_0^{\infty} \frac{1}{(Q\phi_{11} + N_0\theta_3(e^x-1))^{\alpha_3}} {}_2F_1\left(1-\mu_1-j_1, \alpha_3; \alpha_3+1; \frac{Q\phi_{11}}{Q\phi_{11}+N_0\theta_3(e^x-1)}\right)$$
$$\times B_3 \sum_{j=0}^{\infty} U_j \sum_{j_3=0}^{\infty} B_4 \frac{1}{(Q\bar{\gamma}_2 + \phi N_0\theta_4(e^x-1))^{\alpha_4}}$$
$$\times {}_2F_1\left(1-\Omega-j_3, \alpha_4; \alpha_4+1; \frac{Q\bar{\gamma}_2}{Q\bar{\gamma}_2+\phi\theta_4 N_0(e^x-1)}\right) dx. \quad \text{(A.56)}$$

Now, using the series transform of ${}_2F_1$ function given by [116, Eq. 1.1.2]

$${}_2F_1(a,b;c;x) = \sum_{k=0}^{\infty} \frac{(a)_k (b)_k x^k}{k!(c)_k},$$

(A.56) can be written as

$$C_{er} = B_1 \sum_{j_1=0}^{\infty} B_2 \int_0^{\infty} \frac{1}{(Q\phi_{11} + N_0\theta_3(e^x-1))^{\alpha_3}} \sum_{j_2=0}^{\infty} B_5 \frac{1}{(Q\phi_{11} + N_0\theta_3(e^x-1))^{j_2}}$$
$$\times B_3 \sum_{j=0}^{\infty} U_j \sum_{j_3=0}^{\infty} B_4 \frac{1}{(Q\bar{\gamma}_2 + \phi N_0\theta_4(e^x-1))^{\alpha_4}} \sum_{j_4=0}^{\infty} B_6 \frac{1}{(Q\bar{\gamma}_2 + \phi\theta_4 N_0(e^x-1))^{j_4}} dx \quad \text{(A.57)}$$

where $B_5 = \frac{(1-\mu_1-j_1)_{j_2}(\alpha_3)_{j_2}(Q\phi_{11})^{j_2}}{j_2!(\alpha_3+1)_{j_2}}$ and $B_6 = \frac{(1-\Omega-j_3)_{j_4}(\alpha_4)_{j_4}(Q\bar{\gamma}_2)^{j_4}}{j_4!(\alpha_4+1)_{j_4}}$. Applying interchange of summations with integration, (A.57) can be expressed as

$$C_{er} = B_1 B_3 \sum_{j_1=0}^{\infty} B_2 \sum_{j_2=0}^{\infty} B_5 \sum_{j=0}^{\infty} U_j \sum_{j_3=0}^{\infty} B_4 \sum_{j_4=0}^{\infty} B_6$$
$$\times \int_0^{\infty} \frac{1}{(Q\phi_{11} + N_0\theta_3(e^x-1))^{\alpha_3+j_2} (Q\bar{\gamma}_2 + \phi N_0\theta_4(e^x-1))^{\alpha_4+j_4}} dx. \quad \text{(A.58)}$$

The integration involved in (A.58) can be solved in Mathematica. Thus, the final expression for ergodic capacity is obtained as given by (5.27).

References

[1] FCC, "Spectrum policy task force report," Federal Communications Commission, Tech. Rep. 02-135, Nov. 2002.

[2] M. A. McHenry and D. McCloskey, "Spectrum occupancy measurements," Chicago, Illinois, Tech. Rep., Dec. 2005.

[3] M. H. Islam, C. L. Koh, S. W. Oh, X. Qing, Y. Y. Lai, C. Wang, Y. C. Liang, B. E. Toh, F. Chin, G. L. Tan, and W. Toh, "Spectrum survey in singapore: Occupancy measurements and analyses," in *3rd International Conference on Cognitive Radio Oriented Wireless Networks and Communications (CrownCom)*, May 2008, pp. 1–7.

[4] V. Valenta, R. Marsalek, G. Baudoin, M. Villegas, M. Suarez, and F. Robert, "Survey on spectrum utilization in Europe: Measurements, analyses and observations," in *Proceedings of the Fifth International Conference on Cognitive Radio Oriented Wireless Networks and Communications (CrownCom)*, June 2010, pp. 1–5.

[5] J. Mitola and G. Q. Maguire, "Cognitive radio: making software radios more personal," *IEEE Personal Communications*, vol. 6, no. 4, pp. 13–18, Aug. 1999.

[6] J. M. III, "Cognitive radio: an integrated agent architecture for software defined radio," Ph.D. dissertation, Royal Institute of Technology (KTH), Stockholm, Sweden, 2000.

[7] S. Haykin, "Cognitive radio: Brain-empowered wireless communications," *IEEE Journal on Selected Areas in Communications*, vol. 23, no. 2, pp. 201–220, Feb. 2005.

[8] A. Goldsmith, S. Jafar, I. Maric, and S. Srinivasa, "Breaking spectrum gridlock with cognitive radios: An information theoretic perspective," *Proceedings of the IEEE*, vol. 97, no. 5, pp. 894–914, May 2009.

[9] S. K. Sharma, S. Chatzinotas, and B. Ottersten, "Spectrum sensing in dual polarized fading channels for cognitive SatComs," in *IEEE Global Communications Conference (GLOBECOM)*, Dec. 2012, pp. 3419–3424.

[10] ——, "Exploiting polarization for spectrum sensing in cognitive SatComs," in *7th International ICST Conference on Cognitive Radio Oriented Wireless Networks and Communications (CROWNCOM)*, June 2012, pp. 36–41.

[11] E. Axell, G. Leus, E. Larsson, and H. Poor, "Spectrum sensing for cognitive radio : State-of-the-art and recent advances," *IEEE Signal Processing Magazine*, vol. 29, no. 3, pp. 101–116, May 2012.

[12] A. Ghasemi and E. S. Sousa, "Fundamental limits of spectrum-sharing in fading environments," *IEEE Transactions on Wireless Communications*, vol. 6, no. 2, pp. 649–658, Feb. 2007.

[13] "Establishment of an interference temperature metric to quantify and manage interference and to expand available unlicensed operation in certain fixed, mobile and satellite frequency bands," Federal Commun. Commiss. (FCC), Washington, DC, USA, Tech. Rep. ET Docket No. 03-237, 2003.

[14] M. Costa, "Writing on dirty paper (corresp.)," *IEEE Transactions on Information Theory*, vol. 29, no. 3, pp. 439–441, May 1983.

[15] S. I. Gel'fand and M. S. Pinsker, "Coding for channel with random parameters," *Problems of Control Theory*, vol. 9, no. 1, pp. 19–31, 1980.

[16] V. Chakravarthy, X. Li, Z. Wu, M. A. Temple, F. Garber, R. Kannan, and A. Vasilakos, "Novel overlay/underlay cognitive radio waveforms using SD-SMSE framework to enhance spectrum efficiency- Part I: Theoretical framework and analysis in AWGN channel," *IEEE Transactions on Communications*, vol. 57, no. 12, pp. 3794–3804, Dec. 2009.

[17] V. Chakravarthy, X. Li, R. Zhou, Z. Wu, and M. Temple, "Novel overlay/underlay cognitive radio waveforms using SD-SMSE framework to enhance spectrum efficiency-Part II: Analysis in fading channels," *IEEE Transactions on Communications*, vol. 58, no. 6, pp. 1868–1876, June 2010.

[18] T. M. C. Chu, H. Phan, and H. J. Zepernick, "Hybrid interweave-underlay spectrum access for cognitive cooperative radio networks," *IEEE Transactions on Communications*, vol. 62, no. 7, pp. 2183–2197, July 2014.

[19] T. Yucek and H. Arslan, "A survey of spectrum sensing algorithms for cognitive radio applications," *IEEE Communications Surveys Tutorials*, vol. 11, no. 1, pp. 116–130, First Quarter 2009.

[20] F. F. Digham, M. S. Alouini, and M. K. Simon, "On the energy detection of unknown signals over fading channels," *IEEE Transactions on Communications*, vol. 55, no. 1, pp. 21–24, Jan. 2007.

[21] S. P. Herath, N. Rajatheva, and C. Tellambura, "Energy detection of unknown signals in fading and diversity reception," *IEEE Transactions on Communications*, vol. 59, no. 9, pp. 2443–2453, Sep. 2011.

[22] R. Tandra and A. Sahai, "SNR walls for signal detection," *IEEE Journal of Selected Topics in Signal Processing*, vol. 2, no. 1, pp. 4–17, Feb. 2008.

[23] S. M. Kay, *Fundamentals of statistical signal processing: Detection theory.* Prentice Hall PTR, vol. II.

[24] J. Lunden, V. Koivunen, A. Huttunen, and H. V. Poor, "Spectrum sensing in cognitive radios based on multiple cyclic frequencies," in *2nd International Conference on Cognitive Radio Oriented Wireless Networks and Communications*, Aug. 2007, pp. 37–43.

[25] A. V. Dandawate and G. B. Giannakis, "Statistical tests for presence of cyclostationarity," *IEEE Transactions on Signal Processing*, vol. 42, no. 9, pp. 2355–2369, Sep. 1994.

[26] Y. Zeng and Y. C. Liang, "Robustness of the cyclostationary detection to cyclic frequency mismatch," in *21st Annual IEEE International Symposium on Personal, Indoor and Mobile Radio Communications*, Sep. 2010, pp. 2704–2709.

[27] S. Chaudhari, V. Koivunen, and H. V. Poor, "Autocorrelation-based decentralized sequential detection of OFDM signals in cognitive radios," *IEEE Transactions on Signal Processing*, vol. 57, no. 7, pp. 2690–2700, July 2009.

[28] H. S. Chen, W. Gao, and D. G. Daut, "Spectrum sensing for OFDM systems employing pilot tones," *IEEE Transactions on Wireless Communications*, vol. 8, no. 12, pp. 5862–5870, Dec. 2009.

[29] Y. Zeng, Y. C. Liang, and T. H. Pham, "Spectrum sensing for OFDM signals using pilot induced auto-correlations," *IEEE Journal on Selected Areas in Communications*, vol. 31, no. 3, pp. 353–363, March 2013.

[30] Y. Zeng and Y. C. Liang, "Spectrum-sensing algorithms for cognitive radio based on statistical covariances," *IEEE Transactions on Vehicular Technology*, vol. 58, no. 4, pp. 1804–1815, May 2009.

[31] M. Jin, Q. Guo, J. Xi, Y. Li, Y. Yu, and D. Huang, "Spectrum sensing using weighted covariance matrix in Rayleigh fading channels," *IEEE Transactions on Vehicular Technology*, vol. 64, no. 11, pp. 5137–5148, Nov. 2015.

[32] Y. Zeng and Y.-C. Liang, "Eigenvalue-based spectrum sensing algorithms for cognitive radio," *IEEE Transactions on Communications*, vol. 57, no. 6, pp. 1784–1793, June 2009.

[33] A. Kortun, T. Ratnarajah, M. Sellathurai, C. Zhong, and C. Papadias, "On the performance of eigenvalue-based cooperative spectrum sensing for cognitive radio," *IEEE Journal of Selected Topics in Signal Processing*, vol. 5, no. 1, pp. 49–55, Feb. 2011.

[34] G. Ganesan and Y. Li, "Cooperative spectrum sensing in cognitive radio, Part I: Two user networks," *IEEE Transactions on Wireless Communications*, vol. 6, no. 6, pp. 2204–2213, June 2007.

[35] ——, "Cooperative spectrum sensing in cognitive radio, Part II: Multiuser networks," *IEEE Transactions on Wireless Communications*, vol. 6, no. 6, pp. 2214–2222, June 2007.

[36] A. Taherpour, M. Nasiri-Kenari, and S. Gazor, "Multiple antenna spectrum sensing in cognitive radios," *IEEE Transactions on Wireless Communications*, vol. 9, no. 2, pp. 814–823, Feb. 2010.

[37] P. Wang, J. Fang, N. Han, and H. Li, "Multiantenna-assisted spectrum sensing for cognitive radio," *IEEE Transactions on Vehicular Technology*, vol. 59, no. 4, pp. 1791–1800, May 2010.

[38] J. Luo, J. Wang, Q. Li, and S. Li, "GLRT based spectrum sensing with oversampling," in *International Symposium on Communications and Information Technologies (ISCIT)*, 2012, pp. 284–289.

[39] S. K. Sharma, S. Chatzinotas, and B. Ottersten, "Eigenvalue-based sensing and SNR estimation for cognitive radio in presence of noise correlation," *IEEE Transactions on Vehicular Technology*, vol. 62, no. 8, pp. 3671–3684, Oct. 2013.

[40] ——, "SNR estimation for multi-dimensional cognitive receiver under correlated channel/noise," *IEEE Transactions on Wireless Communications*, vol. 12, no. 12, pp. 6392–6405, Dec. 2013.

[41] X. Chen, H. H. Chen, and W. Meng, "Cooperative communications for cognitive radio networks-From theory to applications," *IEEE Communications Surveys Tutorials*, no. 3, pp. 1180–1192, Third.

[42] S. K. Sharma, T. E. Bogale, S. Chatzinotas, B. Ottersten, L. B. Le, and X. Wang, "Cognitive radio techniques under practical imperfections: A survey," *IEEE Communications Surveys Tutorials*, vol. 17, no. 4, pp. 1858–1884, Fourthquarter 2015.

[43] C. Tepedelenlioglu and R. Challagulla, "Low-complexity multipath diversity through fractional sampling in OFDM," *IEEE Transactions on Signal Processing*, vol. 52, no. 11, pp. 3104–3116, Nov. 2004.

[44] M. Ozdemir, E. Arvas, and H. Arslan, "Dynamics of spatial correlation and implications on MIMO systems," *IEEE Communications Magazine*, vol. 42, no. 6, pp. S14–S19, June 2004.

[45] C. Craeye, "Including spatial correlation of thermal noise in the noise model of high-sensitivity arrays," *IEEE Transactions on Antennas and Propagation*, vol. 53, no. 11, pp. 3845–3848, Nov. 2005.

[46] A. Hedayat, H. Shah, and A. Nosratinia, "Analysis of space-time coding in correlated fading channels," *IEEE Transactions on Wireless Communications*, vol. 4, no. 6, pp. 2882–2891, Nov. 2005.

[47] S. Kumar and S. Chouhan, "Spectrum sensing in MIMO cognitive radio with temporally and spatially correlated signal," in *11th International Symposium on Wireless Communications Systems (ISWCS)*, Aug. 2014, pp. 664–669.

[48] F. Shayegh and F. Labeau, "On signal detection in the presence of weakly correlated noise over fading channels," *IEEE Transactions on Communications*, vol. 62, no. 3, pp. 797–809, Mar. 2014.

[49] S. Kim, J. Lee, H. Wang, and D. Hong, "Sensing performance of energy detector with correlated multiple antennas," *IEEE Signal Processing Letters*, vol. 16, no. 8, pp. 671–674, Aug. 2009.

[50] V. R. S. Banjade, N. Rajatheva, and C. Tellambura, "Performance analysis of energy detection with multiple correlated antenna cognitive radio in Nakagami-m fading," *IEEE Communications Letters*, vol. 16, no. 4, pp. 502–505, April 2012.

[51] R. Zhang, T. J. Lim, Y. C. Liang, and Y. Zeng, "Multi-antenna based spectrum sensing for cognitive radios: A GLRT approach," *IEEE Transactions on Communications*, vol. 58, no. 1, pp. 84–88, Jan. 2010.

[52] L. Luo, P. Zhang, G. Zhang, and J. Qin, "Spectrum sensing for cognitive radio networks with correlated multiple antennas," *Electronics Letters*, vol. 47, no. 23, pp. 1297–1298, Nov. 2011.

[53] J. Sala-Alvarez, G. Vazquez-Vilar, and R. Lopez-Valcarce, "Multiantenna GLR detection of rank-one signals with known power spectrum in white noise with unknown spatial correlation," *IEEE Transactions on Signal Processing*, vol. 60, no. 6, pp. 3065–3078, June 2012.

[54] S. Sedighi, A. Taherpour, and J. Sala, "Spectrum sensing using correlated receiving multiple antennas in cognitive radios," *IEEE Transactions on Wireless Communications*, vol. 12, no. 11, pp. 5754–5766, Nov. 2013.

[55] E. Soltanmohammadi, M. Orooji, and M. Naraghi-Pour, "Spectrum sensing over MIMO channels using generalized likelihood ratio tests," *IEEE Signal Processing Letters*, vol. 20, no. 5, pp. 439–442, May 2013.

[56] M. Orooji, R. Soosahabi, and M. Naraghi-Pour, "Blind spectrum sensing using antenna arrays and path correlation," *IEEE Transactions on Vehicular Technology*, vol. 60, no. 8, pp. 3758–3767, Oct. 2011.

[57] Y. Huang and X. Huang, "Detection of temporally correlated signals over multipath fading channels," *IEEE Transactions on Wireless Communications*, vol. 12, no. 3, pp. 1290–1299, Mar. 2013.

[58] G. Vazquez-Vilar, R. Lopez-Valcarce, and J. Sala, "Multiantenna spectrum sensing exploiting spectral a priori information," *IEEE Transactions on Wireless Communications*, vol. 10, no. 12, pp. 4345–4355, Dec. 2011.

[59] L. Cardoso, M. Debbah, P. Bianchi, and J. Najim, "Cooperative spectrum sensing using random matrix theory," in *3rd International Symposium on Wireless Pervasive Computing*, May 2008, pp. 334–338.

[60] Y. Zeng, Y. C. Liang, E. C. Y. Peh, and A. T. Hoang, "Cooperative covariance and eigenvalue based detections for robust sensing," in *IEEE Global Telecommunications Conference, GLOBECOM*, Nov. 2009, pp. 1–6.

[61] F. Penna, R. Garello, D. Figlioli, and M. A. Spirito, "Exact non-asymptotic threshold for eigenvalue-based spectrum sensing," in *4th International Conference on Cognitive Radio Oriented Wireless Networks and Communications*, June 2009, pp. 1–5.

[62] F. Penna, R. Garello, and M. A. Spirito, "Cooperative spectrum sensing based on the limiting eigenvalue ratio distribution in wishart matrices," *IEEE Communications Letters*, vol. 13, no. 7, pp. 507–509, July 2009.

[63] M. Gastpar, "On capacity under receive and spatial spectrum-sharing constraints," *IEEE Transactions on Information Theory*, vol. 53, no. 2, pp. 471–487, Feb. 2007.

[64] R. Zhang and Y. C. Liang, "Exploiting multi-antennas for opportunistic spectrum sharing in cognitive radio networks," *IEEE Journal of Selected Topics in Signal Processing*, vol. 2, no. 1, pp. 88–102, Feb. 2008.

[65] A. Jovicic and P. Viswanath, "Cognitive radio: An information-theoretic perspective," *IEEE Transactions on Information Theory*, vol. 55, no. 9, pp. 3945–3958, Sep. 2009.

[66] L. Musavian and S. Aissa, "Fundamental capacity limits of cognitive radio in fading environments with imperfect channel information," *IEEE Transactions on Communications*, vol. 57, no. 11, pp. 3472–3480, Nov. 2009.

[67] H. Suraweera, P. Smith, and M. Shafi, "Capacity limits and performance analysis of cognitive radio with imperfect channel knowledge," *IEEE Transactions on Vehicular Technology*, vol. 59, no. 4, pp. 1811–1822, May 2010.

[68] H. Kim, H. Wang, S. Lim, and D. Hong, "On the impact of outdated channel information on the capacity of secondary user in spectrum sharing environments," *IEEE Transactions on Wireless Communications*, vol. 11, no. 1, pp. 284–295, Jan. 2012.

[69] X. Zhang, J. Xing, Z. Yan, Y. Gao, and W. Wang, "Outage performance study of cognitive relay networks with imperfect channel knowledge," *IEEE Communications Letters*, vol. 17, no. 1, pp. 27–30, Jan. 2013.

[70] Y. Huang, F. Al-Qahtani, C. Zhong, Q. Wu, J. Wang, and H. Alnuweiri, "Cognitive MIMO relaying networks with primary user's interference and outdated channel state information," *IEEE Transactions on Communications*, vol. 62, no. 12, pp. 4241–4254, Dec. 2014.

[71] M. S. Kang, B. C. Jung, D. K. Sung, and W. Choi, "A pre-whitening scheme in a MIMO-based spectrum-sharing environment," *IEEE Communications Letters*, vol. 12, no. 11, pp. 831–833, Nov. 2008.

[72] J. Kim, W. Choi, S. Nam, and Y. Han, "An efficient prewhitening scheme for MIMO cognitive radio systems," *IEEE Transactions on Vehicular Technology*, vol. 63, no. 4, pp. 1934–1939, May 2014.

[73] M. Xia and S. Aissa, "Spectrum-sharing multi-hop cooperative relaying: Performance analysis using extreme value theory," *IEEE Transactions on Wireless Communications*, vol. 13, no. 1, pp. 234–245, Jan. 2014.

[74] Y. Guo, G. Kang, N. Zhang, W. Zhou, and P. Zhang, "Outage performance of relay-assisted cognitive-radio system under spectrum-sharing constraints," *Electronics Letters*, vol. 46, no. 2, pp. 182–184, Jan. 2010.

[75] J. Si, Z. Li, X. Chen, B. Hao, and Z. Liu, "On the performance of cognitive relay networks under primary user's outage constraint," *IEEE Communications Letters*, vol. 15, no. 4, pp. 422–424, April 2011.

[76] L. Luo, P. Zhang, G. Zhang, and J. Qin, "Outage performance for cognitive relay networks with underlay spectrum sharing," *IEEE Communications Letters*, vol. 15, no. 7, pp. 710–712, July 2011.

[77] J. Lee, H. Wang, J. G. Andrews, and D. Hong, "Outage probability of cognitive relay networks with interference constraints," *IEEE Transactions on Wireless Communications*, vol. 10, no. 2, pp. 390–395, Feb. 2011.

[78] C. Zhong, T. Ratnarajah, and K.-K. Wong, "Outage analysis of decode-and-forward cognitive dual-hop systems with the interference constraint in Nakagami- m fading channels," *IEEE Transactions on Vehicular Technology*, vol. 60, no. 6, pp. 2875–2879, July 2011.

[79] W. Xu, J. Zhang, P. Zhang, and C. Tellambura, "Outage probability of decode-and-forward cognitive relay in presence of primary user's interference," *IEEE Communications Letters*, vol. 16, no. 8, pp. 1252–1255, Aug. 2012.

[80] T. Duong, P. L. Yeoh, V. N. Q. Bao, M. Elkashlan, and N. Yang, "Cognitive relay networks with multiple primary transceivers under spectrum-sharing," *IEEE Signal Processing Letters*, vol. 19, no. 11, pp. 741–744, Nov. 2012.

[81] X. Zhang, Y. Zhang, Z. Yan, J. Xing, and W. Wang, "Performance analysis of cognitive relay networks over Nakagami- m fading channels," *IEEE Journal on Selected Areas in Communications*, vol. 33, no. 5, pp. 865–877, May 2015.

[82] T. Q. Duong, V. N. Q. Bao, H. Tran, G. C. Alexandropoulos, and H. J. Zepernick, "Effect of primary network on performance of spectrum sharing AF relaying," *Electronics Letters*, vol. 48, no. 1, pp. 25–27, Jan. 2012.

[83] T. Duong, D. Benevides da Costa, M. Elkashlan, and V. N. Q. Bao, "Cognitive amplify-and-forward relay networks over Nakagami-m fading," *IEEE Transactions on Vehicular Technology*, vol. 61, no. 5, pp. 2368–2374, Jun. 2012.

[84] T. Q. Duong, V. N. Q. Bao, and H. j. Zepernick, "Exact outage probability of cognitive AF relaying with underlay spectrum sharing," *Electronics Letters*, vol. 47, no. 17, pp. 1001–1002, Aug. 2011.

[85] M. M. Shurman, M. F. Al-Mistarihi, and M. M. Alhulayil, "Performance analysis of amplify-and-forward cognitive relay networks with interference power constraints over Nakagami-m fading channels," *IET Communications*, vol. 10, no. 5, pp. 594–605, 2016.

[86] P. Sharma, S. Solanki, and P. Upadhyay, "Outage analysis of cognitive opportunistic relay networks with direct link in Nakagami-m fading," *IEEE Communications Letters*, vol. 19, no. 5, pp. 875–878, May 2015.

[87] L. Fan, X. Lei, T. Duong, R. Hu, and M. Elkashlan, "Multiuser cognitive relay networks: Joint impact of direct and relay communications," *IEEE Transactions on Wireless Communications*, vol. 13, no. 9, pp. 5043–5055, Sep. 2014.

[88] P. L. Yeoh, M. Elkashlan, T. Duong, N. Yang, and D. da Costa, "Transmit antenna selection for interference management in cognitive relay networks," *IEEE Transactions on Vehicular Technology*, vol. 63, no. 7, pp. 3250–3262, Sep. 2014.

[89] P. L. Yeoh, M. Elkashlan, T. Q. Duong, N. Yang, and D. B. da Costa, "Transmit antenna selection in cognitive relay networks with Nakagami-m fading," in *IEEE International Conference on Communications (ICC)*, June 2013, pp. 2775–2779.

[90] P. L. Yeoh, M. Elkashlan, K. J. Kim, T. Q. Duong, and G. K. Karagiannidis, "Cognitive MIMO relaying with multiple primary transceivers," in *IEEE Global Communications Conference (GLOBECOM)*, Dec. 2013, pp. 1956–1961.

[91] P. L. Yeoh, M. Elkashlan, T. Q. Duong, N. Yang, and C. Leung, "Cognitive MIMO relaying in Nakagami-m fading," in *IEEE 77th Vehicular Technology Conference (VTC Spring)*, June 2013, pp. 1–5.

[92] P. Yeoh, M. Elkashlan, K. Kim, T. Duong, and G. Karagiannidis, "Transmit antenna selection in cognitive MIMO relaying with multiple primary transceivers," *IEEE Transactions on Vehicular Technology*, vol. 65, no. 1, pp. 483–489, Jan. 2016.

[93] Y. Deng, M. Elkashlan, P. L. Yeoh, N. Yang, and R. K. Mallik, "Cognitive MIMO relay networks with generalized selection combining," *IEEE Transactions on Wireless Communications*, vol. 13, no. 9, pp. 4911–4922, Sep. 2014.

[94] Y. Deng, L. Wang, M. Elkashlan, K. J. Kim, and T. Duong, "Generalized selection combining for cognitive relay networks over Nakagami- m fading," *IEEE Transactions on Signal Processing*, vol. 63, no. 8, pp. 1993–2006, April 2015.

[95] A. H. A. El-Malek, F. Al-Qahtani, S. A. Zummo, and H. Alnuweiri, "TAS/MRC in cognitive relay networks over Rayleigh fading channels with correlated antennas," in *2014 IEEE International Conference on Communications (ICC)*, Jun. 2014, pp. 1520–1524.

[96] ——, "MIMO multiuser cognitive relay network in spectrum sharing environment with antenna correlation over Rayleigh fading channels," in *2015 IEEE Wireless Communications and Networking Conference (WCNC)*, Mar. 2015, pp. 504–509.

[97] J. Yang, L. Chen, X. Lei, K. P. Peppas, and T. Q. Duong, "Dual-hop cognitive amplify-and-forward relaying networks over η-μ fading channels," *IEEE Transactions on Vehicular Technology*, vol. 65, no. 8, pp. 6290–6300, Aug. 2016.

[98] J. Paris, "Statistical characterization of κ-μ shadowed fading," *IEEE Transactions on Vehicular Technology*, vol. 63, no. 2, pp. 518–526, Feb. 2014.

[99] M. Aloqlah, "Performance analysis of energy detection-based spectrum sensing in $\kappa-\mu$ shadowed fading," *Electronics Letters*, vol. 50, no. 25, pp. 1944–1946, Dec. 2014.

[100] G. Chandrasekaran and S. Kalyani, "Performance analysis of cooperative spectrum sensing over κ-μ shadowed fading," *IEEE Wireless Communications Letters*, vol. 4, no. 5, pp. 553–556, Oct. 2015.

[101] S. Kumar, "Approximate outage probability and capacity for κ-μ shadowed fading," *IEEE Wireless Communications Letters*, vol. 4, no. 3, pp. 301–304, Jun. 2015.

[102] M. R. Bhatnagar, "On the sum of correlated squared $\kappa-\mu$ shadowed random variables and its application to performance analysis of MRC," *IEEE Transactions on Vehicular Technology*, vol. 64, no. 6, pp. 2678–2684, Jun. 2015.

[103] P. Hansen and S. Jensen, "Prewhitening for rank-deficient noise in subspace methods for noise reduction," *IEEE Transactions on Signal Processing*, vol. 53, no. 10, pp. 3718–3726, Oct. 2005.

[104] J. P. C. da Costa, K. Liu, H. C. So, S. Schwarz, M. Haardt, and F. Romer, "Multidimensional prewhitening for enhanced signal reconstruction and parameter estimation in colored noise with kronecker correlation structure," *Signal Processing*, vol. 93, no. 11, pp. 3209–3226, 2013.

[105] S. Kumar and S. Chouhan, "Performance analysis of MIMO spectrum-sharing networks with pre-whitened interfering signals under outdated channel information," *IEEE Wireless Communications Letters*, vol. 5, no. 2, pp. 156–159, April 2016.

[106] W. Hager, "Updating the inverse of a matrix," *SIAM Review*, vol. 31, no. 2, pp. 221–239, June 1989.

[107] J. Hayya, D. Armstrong, and G. N., "A note on the ratio of two normally distributed variables," *Management Science*, vol. 21, no. 11, pp. 1338–1341, July 1975.

[108] J. G. Proakis and M. Salehi, *Digital communications*, 5th ed. McGraw Hill Education (India) Private Limited, 2014.

[109] L. Li, C. Xu, and M. Tao, "Resource allocation in open access OFDMA femtocell networks," *IEEE Wireless Communications Letters*, vol. 1, no. 6, pp. 625–628, Dec. 2012.

[110] A. Attar, V. Krishnamurthy, and O. Gharehshiran, "Interference management using cognitive base-stations for UMTS LTE," *IEEE Communications Magazine*, vol. 49, no. 8, pp. 152 –159, Aug. 2011.

[111] D. Tse and P. Viswanath, *Fundamentals of wireless communication*. Cambridge University Press, 2005.

[112] Y. S. Cho, J. Kim, W. Y. Yang, and C. G. Kang, *MIMO-OFDM wireless communications with MATLAB*. John Wiley and Sons (Asia) Pte Ltd, 2010.

[113] R. Heath, M. Kountouris, and T. Bai, "Modeling heterogeneous network interference using poisson point processes," *IEEE Transactions on Signal Processing*, vol. 61, no. 16, pp. 4114–4126, Aug. 2013.

[114] S. Cotton, "Human body shadowing in cellular device-to-device communications: Channel modeling using the shadowed $\kappa - \mu$ fading model," *IEEE Journal on Selected Areas in Communications*, vol. 33, no. 1, pp. 111–119, Jan. 2015.

[115] H. Ding, J. Ge, D. da Costa, and Z. Jiang, "Asymptotic analysis of cooperative diversity systems with relay selection in a spectrum-sharing scenario," *IEEE Transactions on Vehicular Technology*, vol. 60, no. 2, pp. 457–472, Feb. 2011.

[116] H. Exton, *Multiple hypergeometric functions and applications*. Chichester, U.K.: Ellis Horwood, 1976, ser. Ellis Horwood Series in Mathematics and its Applications.

[117] Y. A. Brychkov and N. Saad, "On some formulas for the Appell function F2(a,b,b';c,c';w;z)," *Integral Transforms and Special Functions*, vol. 25:2, pp. 111–123, 2014.

[118] H. M. Srivastava and P. W. Karlsson, *Multiple Gaussian hypergeometric series*. Ellis Horwood Limited, 1985.

[119] J. S. Bendat and A. G. Piersol, *Measurement and alnalysis of random data*. New York: Wiley, 1966.

[120] P. H. M. Janssen and P. Stoica, "On the expectation of the product of four matrix-valued Gaussian random variables," *IEEE Transactions on Automatic Control*, vol. 33, no. 9, pp. 867–870, Sep. 1988.

[121] A. H. Nuttall, "Some integrals involving the Q-function," Naval Underwater Systems Center, Tech. Rep. 4297, April 1971.

[122] T. Tao, "An introduction to measure theory," American Mathematical Soc. vol. 126, 2011.

[123] T. M. Apostol, *Mathematical analysis*, 2nd ed. Addison-Wesley, 1974.

[124] F. G. Tricomi and A. Erdlyi, "The asymptotic expansion of a ratio of gamma functions," *Pacific Journal of Mathematics*, vol. 1, no. 1, pp. 133–142, 1951.